CHAPTER 1

Introduction

1.1 Overview

The dissertation of so called nano-structures is currently attracting worldwide interest among scientists and engineers. It has the potential for revolutionizing the ways in which materials and products are created and the range and nature of functionalities that can be accessed. The term “nano-structures” is applied in the context that one or more dimensions have been restricted to lengths in the order of the mean free path of charge carriers or excitons in the material. A worldwide study of research and development status and trends in nanoparticles, nanostructured materials, and nanodevices (or more concisely, nanostructure science and technology) was carried out in recent years.

The gallium nitride (GaN)-based material with a direct wide bandgap offers a range of optical emission from the red to the ultraviolet (UV) when alloyed with In or Al. Therefore, wurtzitic polytypes of GaN, AlN, and InN, and their ternary and quaternary alloys have attracted a great deal of attention since the successful commercialization of blue/UV light emitting diodes (LEDs) and laser diodes (LDs) [1-3]. Since wurtzite polytypes of III-nitrides form a continuous alloy system whose direct bandgap ranging from 0.7 eV for InN [4], to 3.4 eV for GaN, and to 6.2 eV for AlN [5]. In addition, the III-nitrides are superior materials for high-temperature and high-power applications. [6-8].

Nitride-based green and blue Light Emitting Diodes (LEDs) with efficiency, brightness, and longevity that are well in excess of those required for outdoor applications are already commercially available. In addition, blue LEDs are employed to pump integrated inorganic and organic media to produce colors reaching red, on the one hand, and white light on the other. In addition to the traditional displays, these LEDs have applications in traffic lights, moving signs, indicator lights, spot lights, and possibly light sources for accelerated photosynthesis, and medicine for diagnosis and treatment. Potentially, further improvement in LEDs would expand the applications to lighting with large energy savings, as LEDs are more efficient than incandescent bulbs.

Injection lasers operating at short wavelengths have been coveted for years for digital data reading and storage applications. Semiconductor nitrides have the bandgaps required to reach these short wavelengths. Unlike display and lighting applications, digital information storage and reading requires coherent light sources, namely lasers. The output of these coherent light sources can be focused into a diffraction-limited spot, paving the way for an optical system in which bits of information can be recorded and read with ease and uncommon accuracy. As the wavelength of the light gets shorter, the focal diameter becomes smaller. Using a two-layer scheme in what has been named as the Digital Versatile Disk: (DVD), the storage density is predicted to go up from today's 1 Gb to about 40 Gb per compact disk when blue lasers are used. For consumer applications, Continuous Wave (CW) operating lifetimes on the order of 10,000 hours at 60^{o}C are required. Currently, the extrapolated room-temperature lifetimes of InGaN/GaN/AlGaN injection lasers exceed that a low power levels [9].

Due to quantum confinement effects, fabrication and studies of nano structures have attracted considerable interest for potential application to electronic and optoelectronic devices. Therefore, reducing the dimension of semiconductor structures not only saves space and increases the capacity of a single chip, but also brings the benefits of quantum effects. Confining the electrons in such a low-dimensional structure will quantize the allowed energies of the electrons. It has been proven that these quantization effects in a semiconductor structure can make an electronic device more efficient and allow it to be operated at lower voltages and/or higher speeds. For example, some devices utilizing quantum wells, in which electrons are confined to a plane, are already at work in our daily life. We have already enjoyed the benefits of the so-called quantum-well laser, which have been used to read the information on a compact disk. The next level of confinement is to restrict the motion of electrons to a line, or a so-called quantum wire. If the electrons are further confined three-dimensionally, i.e., trapping the electrons in a small volume, it will form a system called quantum dot.

In fact, the InGaN/GaN MQW nanorods are tiny semiconductor structures (of the order of nanometers or tens of nanometers in diameter) surrounded by a material of wider bandgap. Electrons and holes are confined within these structures in all three spatial dimensions, and into a few numbers of confined energy levels, depending on their size.

1.2 Outline of this dissertation

The development of new semiconductor devices seems to be limited only by the imagination of the designer. This dissertation provides a nano-size structure of III-nitride materials. It covers their fabrication, electronic, optical, and transport properties, their role in exploring new physical phenomena, and their application in devices. This dissertation is classified into four subjects. The first subject is concerned with GaN-based top surface nano-roughened LED, including the process, electric and light output performance of the nano-scale GaN-based LED. In the following, the GaN-based sidewalls nano-roughened LED are studied in this chapter. The process, electric and light output performance of the sidewalls nano-roughened LEDs are also investigated in the chapter 3. In chapter 4, one-dimensional structure of InGaN/GaN multi-quantum-well (MQW) nanorods fabricated by induced coupled plasma etching with Ni nano-masks from bulk MQW samples are present, including fabrication technique and optical properties. Then, a process technique to improve emission output of InGaN/GaN MQW nanorods LEDs by photo-enhanced chemical etching process is proposed and demonstrated experimentally. Finally, a conclusion and a brief description in the future works are presented.

REFERENCE

[1] S. Nakamura, T. Mukai, and M. Senoh, Appl. Phys. Lett. 64, 1687 (1994).

[2] S. Nakamura, M. Senoh, N. Iwasa, and S. Nagahama, Jpn. J. Appl. Phys.34, L797 (1995).

[3] G. Y. Xu, A. Salvador, W. Kim, Z. Fan, C. Lu, H. Tang, H. Markoc, G. Smith, M. Estes, B. Goldberg, W. Yank, and S. Krishnankutty, Appl. Phys. Lett. 71, 2154 (1997).

[4] T. Matsuoka, H. Okamoto, M. Nakao, H. Harima, and E. Kurimoto, Appl. Phys. Lett. 81, 1246 (2002).

[5] L. J. Schowalter, G. A. Slack, J. B. Whitlock, K. Morgan, S. B. Schujman, B. Raghothamachar, M. Dudley, and K. R. Evans, Phys. Stat. Sol. (c) 0, No. 7, 1997 (2003).

[6] T. G. Zhu, D. J. H. Lambert, B. S. Shelton, M. N. Wong, U. Chowdhury, H. K. Kwon, and R. D. Dupuis, Electron Lett. 36, 1971 (2000).

[7] B. S. Shelton, D. J. H. Lambert, H. J. Jang, M. M. Wong, U. Chowdhury, Z. T. Gang, H. K. Kwon, Z. Liliental-Weber, M. Benarama, M. Feng, and R. D. Dupuis, IEEE Trans Electron Devices 48, 490 (2001).

[8] A. P. Zhang, J. Han, F. Ren, K. E. Waldrio, C. R. Abernathy, B. Luo, G. Dang, J. W. Johnson, K. P. Lee, and S. J. Pearton, Electronchem. Solid-State Lett. 4, G39 (2001).

[9] H. Morkoc, Nitride Semiconductors and Devices, (Springer-Verlag, Berlin, 1999).

CHAPTER 2

GaN-Based Top-Surface Nano-Roughened Light-Emitting Diodes

2.1 Progress in GaN-based top-surface nano-roughened LED device using self-assembled Ni nano-mask and wet etching.

Recent progress in electro-optical systems demands drastic increases in the degree of integration of photonic and electronic devices for large-capacity and ultrahigh-light output and information processing. GaN-based materials have attracted considerable interest in relation to their potential use in optoelectronic devices, such as light emitting diodes (LEDs) and laser diodes (LDs) [1]-[4]. However, the internal quantum efficiency of GaN-based LEDs is much less than 100% at room temperature because of non-radiative defects. Furthermore, the external quantum efficiency of GaN-based LEDs is low because the refractive index of the nitride epitaxial layer differ greatly from that of the air. The refractive indexes of GaN and air are 2.5 and 1.0, respectively. Thus, the critical angle at which light generated in the InGaN–GaN active region can escape, is approximately $[\theta_c = \sin^{-1}(n_{air}/n_{GaN})]$ ~23^{o}, which limits the external quantum efficiency of conventional GaN-based LEDs to only a few percent [5]. The light from LEDs can be enhanced either through the sample surface or through the side walls of the chip. Research into improving the light extraction efficiency (external quantum efficiency) and brightness in the LEDs [5]-[11] has been intense. Recently, Chang *et al.* reported that cap layers grown at low temperature (800^{o}C) increased the power output by InGaN–GaN MQW LEDs by 10% [12]. T. Fujii reported an increase in the extraction efficiency of GaN-based light-emitting diodes by surface roughening [13]. These processes all allow the photons generated within the LEDs to find the escape cone, by multiply scattering from a rough surface. Huh *et al.* reported that micro-roughening the top surface of an InGaN/GaN LED using metal clusters as a wet etching mask increased the wall-plug efficiency by 62% [5] as shown in Fig. 2.1. Huh *et al.* showed a large improvement in the light output power, indicating that the use of metal clusters to fabricate a roughened p-GaN surface is an excellent means of making a high-power LED. However, higher treatment temperature of 900^{o}C is necessary to form Pt clusters. Therefore, higher temperature maybe increase the Indium segregation probability in the InGaN/GaN quantum well region and reduce the internal quantum efficiency [14]-[16]. Pt has a high melting point and chemical stability [17], [18]. Therefore, specific wet chemical etching should be necessary to remove Pt metal clusters by dipping into a boiling aqua-regia solution [5]. This investigation report the production of GaN LED with a nano-roughened p-GaN surface using a self-assembled Ni metal cluster as the wet etching mask. The dimensions and density of the self-assembled Ni cluster can be controlled by rapid thermal annealing at temperatures from 750^{o}C to 850^{o}C, details of which have been recently reported [19].

2.2 Fabrication of GaN-Based top-surface nano-roughened LED device using self-assembled Ni nano-mask and wet etching.

Nano-roughened LEDs were formed by depositing Ni thin film with a thickness of 5 nm on a p-GaN surface by electron beam evaporation. Rapid thermal annealing (RTA) was then performed at 850^{o}C for 1min to change the Ni layer to the metal Ni nano-mask on the top p-GaN surface. Then, wet etching was performed to produce nano-roughened LEDs, using a boiling 85% phosphoric acid (H_3PO_4) solution for 4min etching (Fig. 2.2). The etching rate of the p-GaN layer in boiling 85% H_3PO_4 solution was determined to be approximately 15nm/mim at 200^{o}C. The nano-roughened LED was dipped into a nitric acid solution (HNO_3) for 5min to remove the Ni nano-mask from a nano-roughened LED after the wet etching process. Afterwards, the conventional LED and the LED with a nano-roughened surface were fabricated using the standard process (four mask steps) with a mesa area (300×300 μm^2). Firstly, the 0.5 um SiO_2 was deposited onto the sample surface by plasma enhanced chemical vapor deposition (PECVD). Photo-lithography was used to define the mesa pattern after wet etching of SiO_2 by a buffer oxide etching solution. The mesa etching was then performed with Cl_2/Ar as the etching gas in an ICP-RIE system (SAMCO ICP-RIE 101iPH) which the ICP source power and bias power were operated at 13.56 MHz. The metal contact layers, including transparent contact and pad layers, were patterned by a lift-off procedure and deposited onto samples by electron beam evaporation. Ni/Au (3/5 nm) was used for the transparent electrode and Ti/Al/Ni/Au (20/150/20/200 nm) was used for the n-type electrode. Finally, Ni/Au (20/150 nm) was deposited onto the p-type electrode. (Fig. 2.3)

2.3 Characteristics of GaN-Based top-surface nano-roughened LED device using self-assembled Ni nano-mask and wet etching.

Figure 2-4(a)-(c) show the AFM images that describe the change of the surface morphology of the p-GaN surface during surface-roughening. Figure 2-4(a) shows that the conventional p-GaN cap has a root mean-square (RMS) roughness of 0.7 nm, and a surface depth of approximately 2 nm. The surface of the conventional LED was smooth. Figure 2-4(b) shows a nano-mask AFM image RMS roughness of 5.9 nm before wet etching was performed. The self-assembled Ni mask dimension size and density were approximately 250 nm and $2x10^9$ cm^{-2}, and the height of the Ni clusters was approximately 30 nm when the original Ni thickness was 50 Å under RTA conditions of 850^oC for 1min. Figure 2-4(c) displays the AFM image that shows that RMS roughness of p-GaN surface increased drastically to 3.6 nm, and the surface depth was approximately 15 nm after wet etching and the removal of the Ni nano-mask.

The I-V characteristics of the conventional and nano-roughened LEDs were also measured. Figure 2-5(a) plots the I-V characteristics of conventional and nano-roughened LEDs. The forward voltages of the conventional and nano-roughened LEDs were 3.65V and 3.5V at a driving current of 20 mA, respectively. Furthermore, the dynamic resistance (R=dV/dI) of the nano-roughened LED (32 Ω) was 20% lower than that of the conventional LED (40 Ω). The reduction in the series resistance of the LED with wet etching on a top nano-roughened LED surface can be attributed to the improvement in the Ohmic contact resistance caused by the increase in the contact area [5]. A 1μm-thick p-GaN sample (hole carrier concentration of 5.0×10^{17} cm^{-3} and hole mobility of 10.2 cm^2/V-s) and both nano-roughened and conventional p-GaN samples were deposited with the same metallization of Ni（20nm）/Au（150nm）and rapid thermal annealing (RTA) 450^oC for 1min, to investigate the electric characteristics of the Ohmic contact of nano-roughened and conventional LEDs on the p-GaN layer. Figure 2-5(b) plots the I-V characteristics of the nano-roughened and conventional p-GaN as measured by the Circular Transmission Line Method (CTLM). The nano-roughened p-GaN sample has better linearity than the conventional p-GaN sample. The total resistance (Y) measured by CTLM is linearly related to the pad distance (X), as shown in Figure 2(c). The specific contact resistance ρ_c was determined from the linear equation $Y=2Rc+\rho_s/2\pi R\times X$, and the relationship between the specific resistance and the sheet resistance was $\rho_c=\rho_s\times L_T^2$, where R_c is the contact resistance; ρ_s is the sheet resistance, and L_T is the transfer length. The data were fitted to obtain a lower specific contact resistance value of $2.5\times10^{-4}\Omega cm^2$ for the nano-roughened p-GaN than the value $7.2\times10^{-3}\Omega cm^2$ for the conventional p-GaN sample. The results indicated that nano-roughening facilitates p-type contact, resulting in an Ohmic contact with a low specific resistance. In Figure 2-5(a) shows that the rough surface of the LED nano-roughened using an Ni nano-mask and wet etching did not induce a larger leakage current than that in the conventional LED. Furthermore, two devices, based on conventional and nano-roughened LEDs, in HBM (human body mode) were observed in an electrostatic discharge (ESD) test at a reverse voltage of >300V.

Electroluminescence (EL) was measured by injecting a continuous current into a device at room temperature. The light output was detected using a calibrated large-area Si photodiode placed 5 mm from the top of the device. This detecting condition covers almost all of the power emitted from the LEDs. Figures 2-6(a) and (b) plot the spectra and intensity–current (*L–I*) characteristics of conventional and nano-roughened LEDs. The EL intensity of the nano-roughened LED exceeds that observed from the conventional LED (as shown in Figure 2-6(a)). At an injection current of 20 mA, all of the MQW emission peaks of these two were at approximately 450 nm and the light output power of the conventional and nano-roughened LEDs were approximately 4.5 mW and 6.3 mW, respectively (as shown in Figure 2-6(b)). Restated, nano-roughening the p-GaN surface increased the output power of the InGaN–GaN MQW LEDs by a factor of 1.4, indicating that the LED with the nano-roughened surface had larger light extraction efficiency. The wall-plug efficiency (output power/input power) was also calculated: it was 45% higher than that of the conventional LED at an injection current of 20 mA, because of enhanced light output power and a lower forward voltage.

The intensity distributions of conventional and nano-roughened LEDs were measured to investigate further the influence of surface roughness on the light output performance of an LED. Figures 2-7(a) and (b) show the photons of conventional and nano-roughened LEDs when a 20 mA dc current is injected into these two devices. Intensity distributions are also shown. The EL intensities observed from the nano-roughened LED clearly exceeded those from the conventional LED at the same injection current, especially on the LED top surface. Such an enhancement could be attributed to the top surface roughness and the fact that photons were more likely to be emitted from the surface-roughed device, resulting in an increase in the light output power of the nano-roughened LED, as shown in Figure 2-6.

In summary, this investigation describes the improvement of an InGaN/GaN MQW light emitting diode by nano-roughening the p-GaN surface using Ni nano-mask and wet etching. The nano-roughened surface improved the escape probability of photons inside the LED structure, increasing by 40% the light output of InGaN/GaN LED at 20 mA. The operating voltage of the InGaN/GaN LED was reduced from 3.65 to 3.5V at 20 mA and the series resistance was reduced by 20% by the increase in the contact area of the nano-roughened surface. The wall-plug efficiency of the InGaN/GaN LED was increased by 45% by nano-roughening the top p-GaN surface using the Ni nano-mask and wet etching.

2.4 Fabrication of GaN-Based top-surface nano-roughened LED device using self-assembled Ni nano-mask and excimer laser etching.

2.4.1 Thermal Model of Excimer Laser Interactions

Laser light treatments serve a wide range of purpose in processing of semiconductor materials. Examples include softening or hardening of metals, annealing of crystals, dopant diffusion in semiconductors, compound formation in mixtures or thin-film couples, oxide-layer growth, and many others. The use of lasers as heat sources in place of furnaces is being adopted or explored in growing number of heat-treatment processes. The main advantage, obviously, is that the laser heating can be done in a localized mode, both in space and in time. By matching the wavelength and the beam power to the optical and thermal material properties, the amount of heating can be chosen accurately to suit the needs of process. If surface heating is required and/or volume heating is to be avoided, a large absorption coefficient and a short interaction time can be selected. Sharply delimited areas can be heated to high temperature while the remainder of the work-piece stays virtually cold. Rapid cooling of the heated material can be achieved by using short pulses or rapidly mobbing beams. Apart from localization, laser beams are chemically “pure and free of inertia, can be moved easily and passes through windows to reach remote or inaccessible parts of a work-piece.

The energy of laser light is typically transported the hot carriers to the semiconductor material. When the lattice of semiconductor absorbs the laser energy, the heat flow begins within the material. The mathematical theory of heat conduction is based on the assumption that the heat flux across a plane in a solid is proportional to the local temperature gradient: [20]

$$\psi(z_0) = -K\left(\frac{dT}{dz}\right)_{z_0} \qquad (2\text{-}1)$$

where K is the thermal conductivity of the material. Accepting this for the moment; we can express the energy balance of a slab of material bounded by plane at z and z+Δz in terms of its volumetric heat capacity C_p/V [20-21]

$$\Delta t\left[\psi(z) - \psi(z+\Delta z)\right] = \Delta T \frac{C_p}{V}\Delta z \qquad (2\text{-}2)$$

Here ΔT is the change in temperature brought about by a net heat flux across the boundaries. Letting $\Delta z \to 0$, the bracketed term on the Left-Hand Side (LHS) can be expressed as $\left(\partial\psi / \partial z\right)\Delta z$. Replacing the finite difference by differentials and using (2-1) then yields

[20-21]

$$\frac{\partial}{\partial z}\left[K\frac{\partial T}{\partial z}\right]=\frac{C_p}{V}\frac{\partial T}{\partial t} \tag{2-3}$$

which is the usual form of the heating-flow equation in one dimension. If heat is produced in the material, the power density of heat source is added to the LHS.

To solve, first, we assume the power density of heat production to equal that of the absorbed laser light, as given by [20-21]

$$I_a(z,t)=I_0(t)(1-R)\exp(-\alpha z) \tag{2-4}$$

where $I_a(z,t)$ is the power density [J/cm^2] of the incident laser light at a depth z and time. $I_0(t)$ is the output laser power density and R is the reflectance and α is the absorption coefficient determine the amount of beam power absorbed within the material. In this equation, we assume the thin film is homogenous absorbing medium.

The material is taken to be at zero initial temperature: a uniform initial temperature is simply added to the calculated temperature. The GaN thin film is assumed to be thermally insulated, ie., not heat flow across the boundaries is allowed. This means that the temperature distribution $T(x,y,z,t)$ must satisfy the condition

$$\frac{\partial T}{\partial z}=0 \qquad \text{for z=0} \quad \text{and z=L at all times.} \quad \text{(where for GaN, L=}\infty\text{)}$$

The laser beam is incident onto to a plane $z=0$ and taken to be of cylindrical symmetry. The heat-flow equation can now be rewritten as [20-21]

$$\frac{\partial T}{\partial t}=D\nabla^2 T+\frac{\alpha I_a(x,y,t)}{\rho C_p}\exp(-\alpha z) \tag{2-5}$$

where $D=K/\rho C_p$ is the heat diffusivity.

Green's function [4.2] is used to obtain the analytical solution to the heat equation. For notational convenience, we introduce the diffusion length $\xi=\sqrt{2Kt}$.

For a uniform surface source of incident power density, we have: [20-21]

$$T(z,t)=\frac{I_a\xi}{K}\sum_{n=-\infty}^{\infty} ierfc\left[\frac{2nL-z}{\xi}\right](1-R) \tag{2-6}$$

In particular, for the semi-infinite solid (for $L=\infty$), the temperature at the irradiated surface is: [20]

$$T(0.t)=I_a\frac{\xi}{K\sqrt{\pi}}(1-R) \tag{2-7}$$

The general expression for the uniform penetrating source is: [20-21]

$$T(z,t)=\frac{I_a(1-R)}{4K}\int_0^{\xi}\exp\left[-\left(\alpha\beta/2\right)^2\right]\gamma_2 d\beta \qquad (2\text{-}8)$$

where $\gamma_2=\sum\exp[\alpha(2nL-z)]\times\left[erfc\left(\frac{(2n+1)L-z}{\beta}+\frac{\alpha\beta}{2}\right)-erfc\left(\frac{2nL-z}{\beta}+\frac{\alpha\beta}{2}\right)\right]$ and $\beta=2\sqrt{K|t-t'|}$.

The closed from solutions is obtained for semi-infinite solid: [20-21]

$$T(z,t)=\frac{I_a(1-R)}{K}\left\{\begin{array}{l}\xi\cdot ierfc\left(\frac{z}{\xi}\right)-\left(\frac{1}{\alpha}\right)e^{-\alpha z}+\left(\frac{1}{2\alpha}\right)e^{\left(\frac{\alpha\xi}{2}\right)^2}\\ \times\left[e^{-\alpha z}erfc\left(\frac{\alpha\xi}{2}-\frac{z}{\xi}\right)+e^{\alpha z}erfc\left(\frac{\alpha\xi}{2}+\frac{z}{\xi}\right)\right]\end{array}\right\} \qquad (2\text{-}9)$$

For the temperature at the surface (*z=0*) of the irradiated target, the solution is: [20-21]

$$T(0,t)=\frac{I_a(1-R)}{K}\left\{\frac{\xi}{\sqrt{\pi}}-\frac{1}{\alpha}\left[1-e^{\left(\alpha\xi/2\right)^2}erfc\left(\frac{\alpha\xi}{2}\right)\right]\right\} \qquad (2\text{-}10)$$

In the next section, the experiment of laser etching for top-surface of LEDs will be investigated using different laser energy condition. The material and optical properties of laser irradiated GaN LEDs will be characterized.

2.4.2 Experiment for Laser Etching using Ni nano-masks

Fig. 2-8 depicts a schematic diagram of the LED with nano-roughened surface. We simulated light propagation and reflection using the ray tracing method provided by Advanced System Analysis Program (ASAP). For simplicity, we employed a two-dimensional model which is similar on GaN-based LED structures. The top mesa area is 300 × 300 μm^2 and depth is 1μm with and without rough top surface. Fig. 2-9 shows light extraction efficiency of conventional and rough top surface LED structures as a function of absorption coefficient of the p-GaN layer. The light extraction efficiency here was defined as the ratio of the collected power outside the LED structure and the total power generated from the active region. The result clearly shows that by adding a rough top surface, the extraction efficiency can be greatly enhanced. The extraction efficiency can be enhanced about a factor of 1.29-1.67 times compared with conventional and rough top surface LED structures considering the absorption coefficient of p-GaN layer changed from 10000 to 100 cm^{-1}.

Figure 2-10 shows the schematic diagram of the setup for conducting the laser etching experiment. A KrF excimer laser (Lambda Physick LPX210) operated at wavelength of λ =

248 nm with a pulse width of 25 ns was used for laser etching technique. The laser output energy can be varied from 10 nJ to 25 mJ. The laser beam was reshaped and homogenized using a special optical system to form a highly uniform (±5% RMS) beam profile of 12 × 12 mm^2 after the mask plane. A beam splitter then splits the laser beam into a laser etching beam and a monitor beam. The laser etching beam passed through a projection system of 10× magnification with a 0.2 numerical aperture, and then focused on the LED sample with a squared spot size of 1.0 × 1.0 mm^2. The monitor beam was incident on a beam analyzer for real-time monitoring of the laser beam quality. The LED samples were placed on the top of a working station which can be moved 1.0 mm step by step to scan a typical sample size of 2 × 2 cm^2 by using the computer controlled stepper motor. The CCD camera was used to in-situ monitor the laser etching process.

The GaN LED samples were grown by metal-organic chemical vapor deposition (MOCVD) with a rotating-disk reactor (Emcore D75^{TM}) on a c-axis sapphire (0001) substrate at a growth pressure of 200 mbar. Trimethylgallium, Trimethylaluminum, ammonia, CP_2Mg and Si_2H_6 were used as sources of Ga, Al, N, Mg and Si. The LED structure includes a 30nm-thick GaN low-temperature buffer layer, a 4.0um-thick highly conductive Si-doped GaN layer (grown at 1050^{o}C), an active region of undoped multiple quantum wells (MQW) that includes five periods of 2/5nm-thick $In_{0.21}Ga_{0.79}N$/GaN (grown at 750^{o}C), a 50nm-thick Mg-doped AlGaN layer (grown at 1050^{o}C) and finally a 0.1um-thick Mg-doped GaN layer (grown at 1050^{o}C). The top surface of LED, which is a p-GaN surface, was roughened by the laser etching after the formation of Ni nano-mask on the top surface. The surface roughness of the LED cap layer was measured by the tapping mode atomic force microscopy (Veeco).

The nano-masks were formed by depositing a Ni thin film with a thickness of 5 nm on a p-GaN surface by electron beam evaporation. RTA was then performed at 750^{o}C for 1 min to change the Ni layer to the metal Ni nano-masks on the top p-GaN surface. Then, a KrF excimer laser at wavelength of 248 nm with a pulse width of 25 ns and the incident laser fluence were from 250 mJ/cm^2 to 800 mJ/cm^2 was used to etch the p-GaN surface in the air atmosphere. In this process, the beam size of KrF laser (1mm × 1mm) was larger than the size of LEDs (300 × 300um^2) to avoid non-uniformity of the laser irradiation on the surface of p-GaN. Figure 2-11 shows the etching rate of the p-GaN layer as a function of laser fluence in the air atmosphere. The etching rate increased with the increasing laser fluence. The etching rate of the p-GaN layer from 250 mJ/cm^2 to 800 mJ/cm^2 were determined to be approximately 15 nm/pulse to 50 nm/pulse. After the laser etching process, the nano-roughened LED samples were dipped into HCl solution for 5 min to remove the residual Ga and Ga oxide on the p-GaN and then dipped into a nitric acid solution (HNO_3) for 5 min to remove the Ni nano-mask from a nano-roughened LED. Afterwards, the conventional LED and the LED with a nano-roughened surface were fabricated using the standard process (four mask steps) having a mesa area of 300 × 300 μm^2. First, the 0.5 um SiO_2 was deposited onto the sample surface by plasma enhanced chemical vapor deposition. Photo-lithography was used to define the mesa pattern after wet etching of SiO_2 by a buffer oxide etching solution. The mesa etching was then performed with Cl_2/Ar as the etching gas in an ICP-RIE system (SAMCO ICP-RIE 101iPH) which the ICP source power and bias power were operated at the frequency of 13.56 MHz. The metal contact layers, including transparent contact and pad layers, were patterned by a lift-off procedure and deposited onto samples by electron beam evaporation. Ni/Au (3/5 nm) was used for the transparent electrode and Ti/Al/Ni/Au (20/150/20/200 nm) was used for the n-type electrode. Finally, Ni/Au (20/150 nm) was deposited onto the p-type electrode.

2.5 Characteristics of GaN-Based top-surface nano-roughened LED device using self-assembled Ni nano-mask and excimer laser etching.

Figure 2-12 show the (a) SEM and (b) AFM images of the Ni nano-mask on p-GaN surface morphology of a nano-roughened LED sample. The SEM image in Fig. 2-12(a) shows that the dimension and density of the self-assembled Ni masks under RTA conditions of 750^oC for 1 min were approximately 250 nm and $3x10^9$ cm^{-2}, and the height of the Ni clusters was approximately 30 nm when the original Ni thickness was 50 Å. The AFM image in Fig. 2-12(b) shows a Ni nano-mask with a root mean-square (RMS) roughness of 7.4 nm before the laser etching was performed.

Figure 2-13(a) and (b) show the AFM images depicting the change of the surface morphology of the p-GaN surface during the surface-roughening. Figure 2-13(a) shows that the conventional p-GaN cap has a RMS roughness of 0.7 nm, and a surface depth of approximately 2 nm, demonstrating a rather smooth p-GaN surface in the conventional LED. Figure 2-13(b), (c) and (d) show the AFM images of the p-GaN surface roughened by the laser etching energy of 300, 400 and 800 mJ/cm^2, respectively. The RMS roughness of p-GaN surface increased drastically to 8.7 nm as the energy of excimer laser increased from 300 mJ/cm^2 to 800 mJ/cm^2.

The I-V characteristics of the conventional and nano-roughened LEDs were also measured. Figure 2-14 plots the I-V characteristics of conventional and nano-roughened LEDs. The forward voltages of the conventional and nano-roughened LEDs etched by the laser energy of 300 mJ/cm^2 were 3.54V and 3.27V at a driving current of 20 mA, respectively. Furthermore, the dynamic resistance (R=dV/dI) of the nano-roughened LED (27 Ω) was 32% lower than that of the conventional LED (40 Ω). The results indicated that the nano-roughening surfaces could facilitate the p-type contact to form an Ohmic contact with a low specific resistance when the energy of laser etching ranged from 250 mJ/cm^2 to 400 mJ/cm^2. However, the energy of laser etching over 600 mJ/cm^2 could result in a Schottky contact with a high specific resistance, which might be due to that the surface morphology was too rough to form good contacts on the top p-GaN surface.

Electroluminescence (EL) was measured by injecting a continuous current into a chip device at room temperature. The light output was detected using a calibrated large-area Si photodiode placed 5 mm from the top of the device. This detecting condition covers almost all of the power emitted from the top of the LEDs. Figures 2-15(a) shows the spectra of the conventional and nano-roughened LEDs. Figure 2-15(b) plot the intensity–current (*L–I*) characteristics versus the RMS roughness of the surfaces in nano-roughened LEDs. As shown in Fig. 2-15(a), the EL intensity of the nano-roughened LED exceeds the conventional LED. At an injection current of 20 mA, the MQW emission peak was at approximately 452 nm and the light output power of the conventional and nano-roughened LEDs etched by laser energy of 300 mJ/cm^2 were approximately 5.3 mW and 8.3 mW, respectively (as shown in Fig. 2-15(b)). Nano-roughening the p-GaN surface with the laser etching energy of 300 mJ/cm^2 increased the output power of the conventional InGaN–GaN MQW LEDs by a factor of 1.55. The enhancement of the wall-plug efficiency of the nano-roughened LEDs over the conventional LED was 68% at 20 mA. The nano-roughened LEDs with energy of laser etching over 600 mJ/cm^2 shows slightly lower light output than the conventional LED. This could be due to a Schottky contact with a high specific resistance (shows the Figure 2-14) and generation of non-radiative defects and slight deterioration in the InGaN/GaN MQW active regions during the high energy laser etching [22]-[23]. The etched surface morphology was also obtained by AFM measurement with a scan area of 5 μm^2. The RMS roughness of the nano-roughed surface morphology were increase from 0.7 nm to 8.4 nm as the laser fluence increase from 0 to 800 mJ/cm^2.

In summary, InGaN/GaN MQW LEDs fabricated by nano-roughening the p-GaN surface using Ni nano-masks and laser etching were demonstrated. The nano-roughened surface could improve the escape probability of photons inside the LED structure and has increased the maximum light output and wall-plug efficiency of 55% and 68% respectively over the conventional InGaN/GaN LEDs at 20 mA when the energy of laser etching was 300 mJ/cm^2. The operating voltage of the InGaN/GaN LED was reduced from 3.54 to 3.27V at 20 mA and the series resistance was reduced by 32% by the increase in the contact area of the nano-roughened surface.

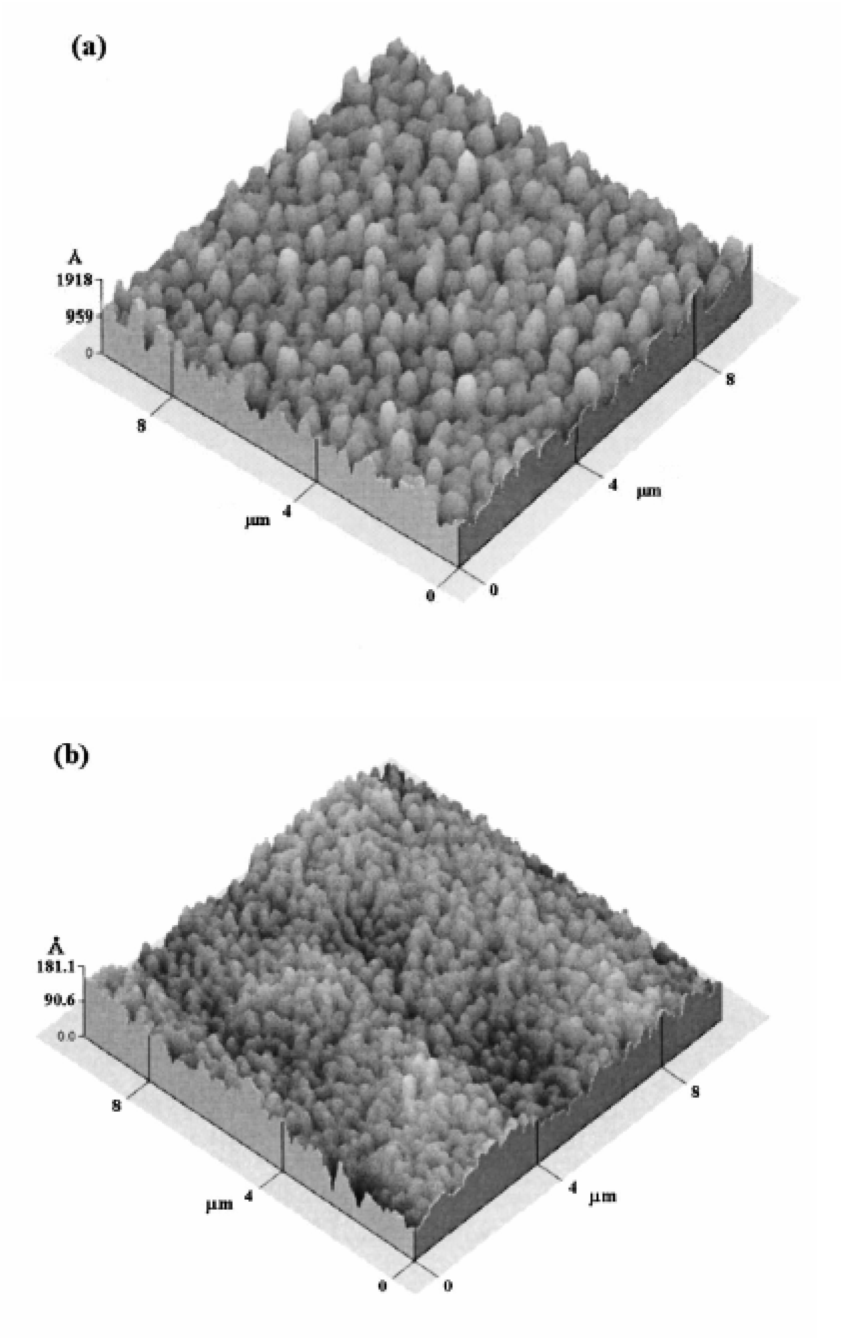

Fig. 2-1 AFM images presenting the top surface morphology of a LED sample. (a) Image taken from the top surface of a LED sample after the formation of Pt clusters. (b) Image taken from the top surface of a LED spectrum, respectively.

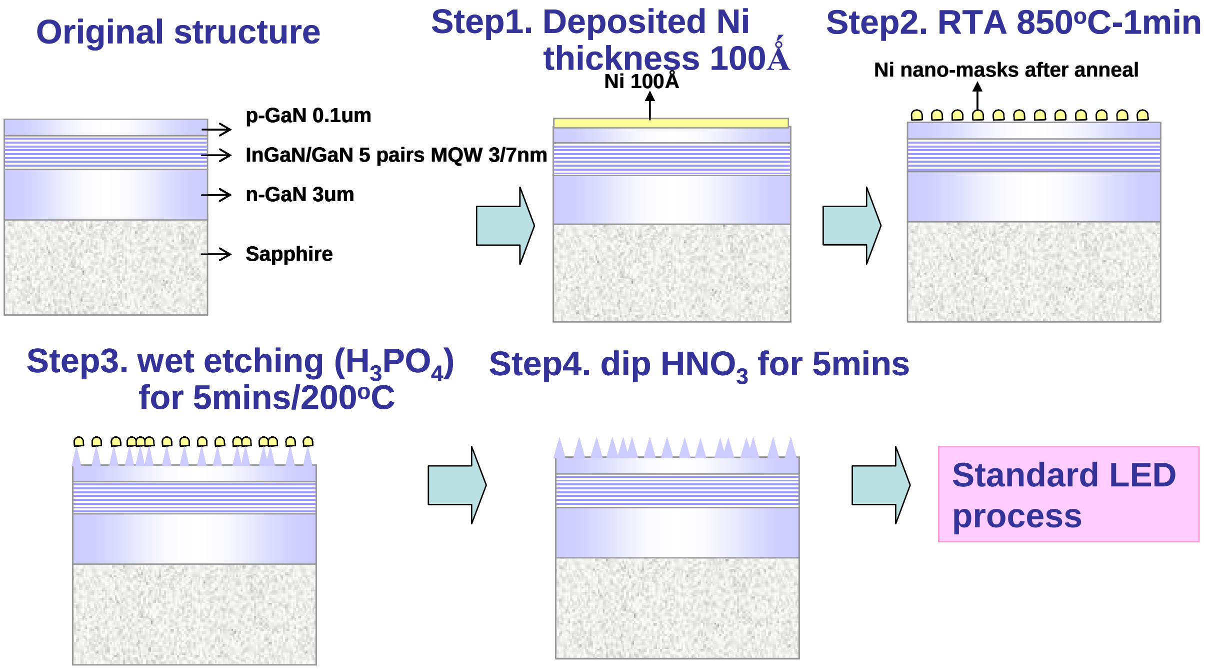

Fig. 2-2 Showing the process flowchart of the GaN-based top-surface nano-roughened LEDs using wet etching.

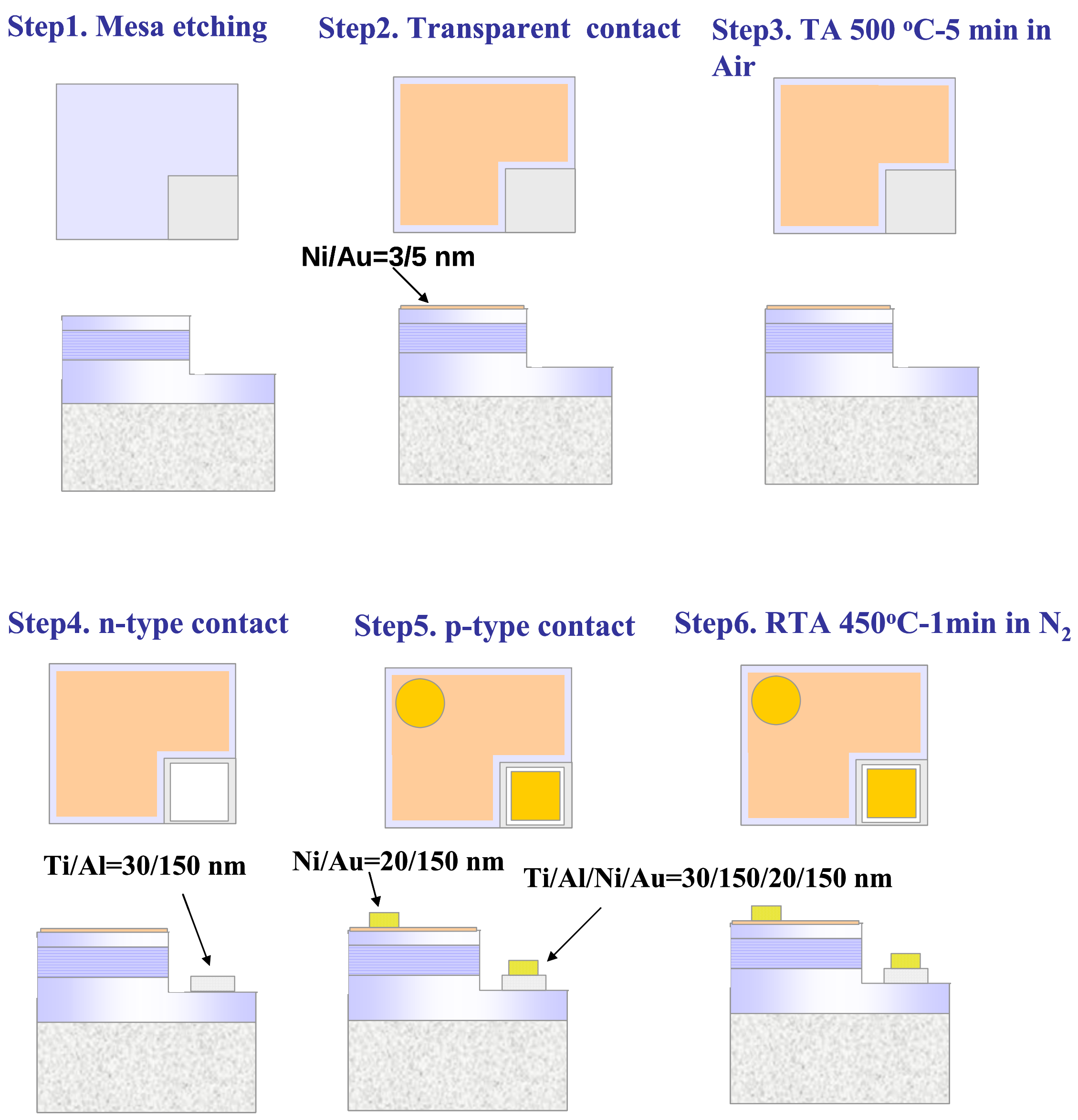

Fig. 2-3 Showing the standard process flowchart of GaN-based LEDs.

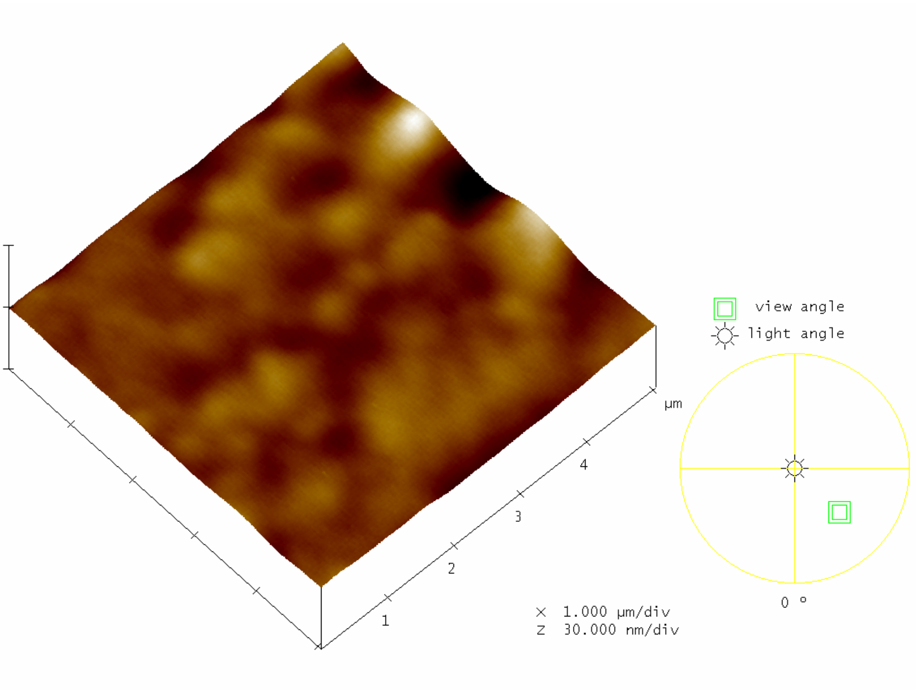

RMS roughness=0.7 nm

(a)

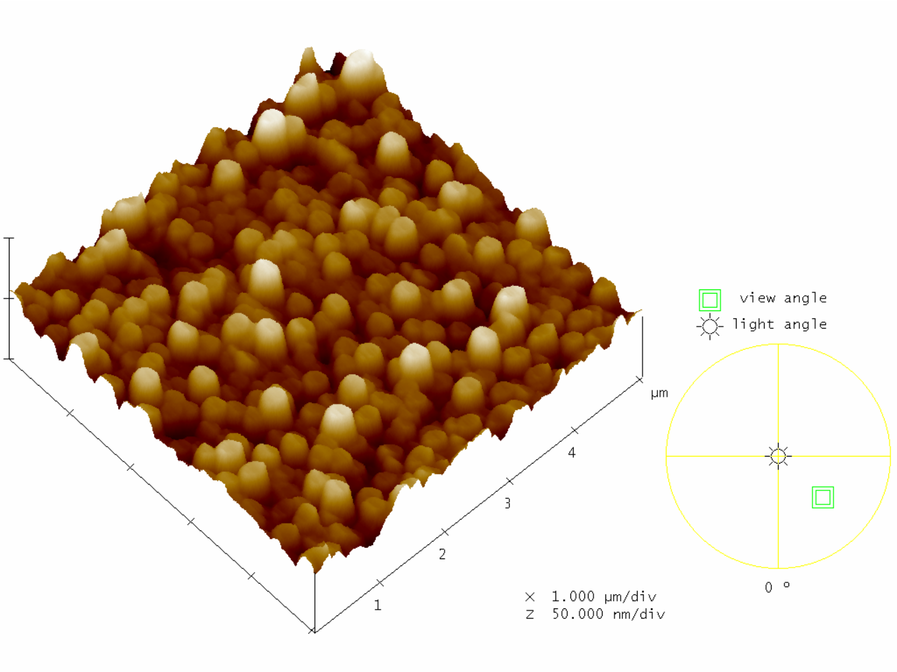

RMS roughness=5.9 nm

(b)

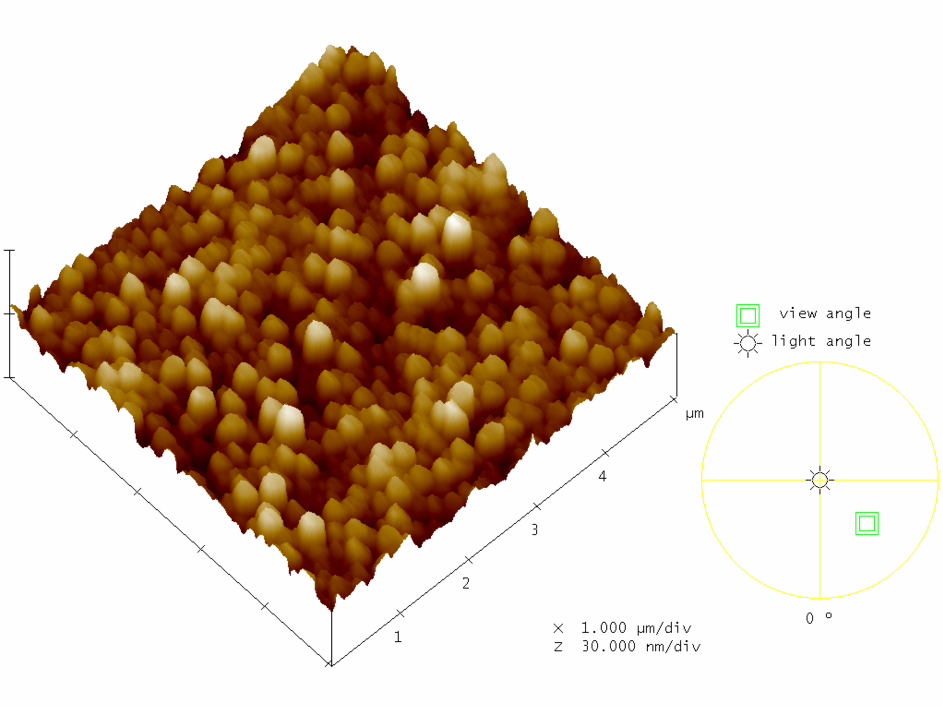

RMS roughness=3.6 nm

(c)

Fig. 2-4 AFM images of the top surface morphology of a LED sample. (a) Conventional LED p-GaN surface image. (b) Ni nano-mask on p-GaN surface image. (c) Nano-roughened LED top p-GaN surface image.

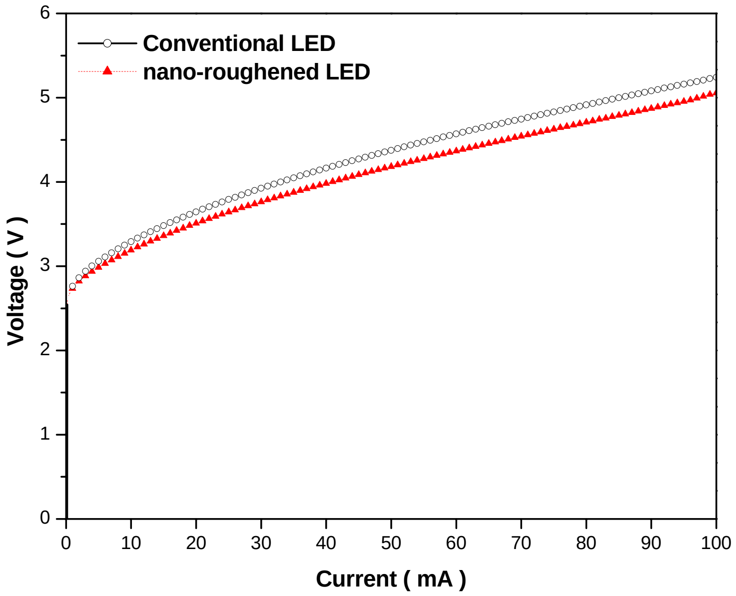

(a)

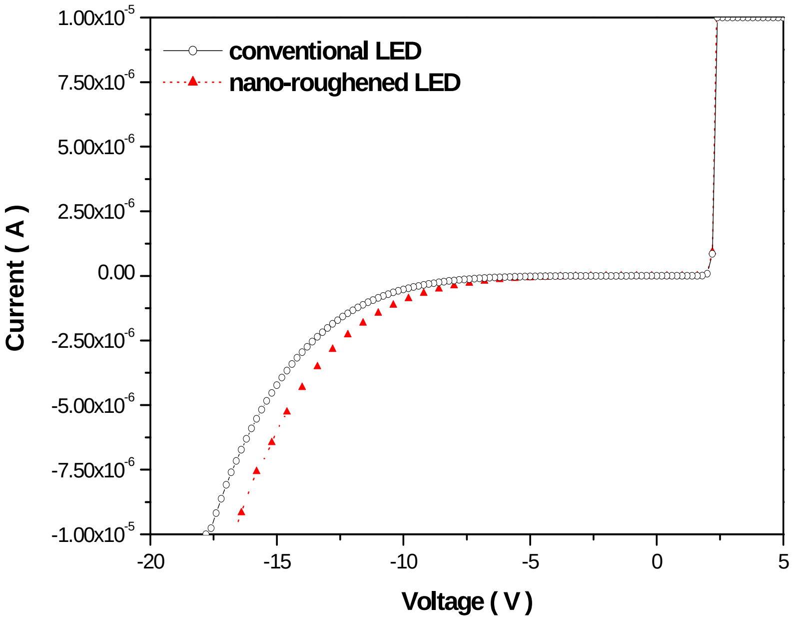

(b)

Fig. 2-5 I-V (a) forward (b) reverse curves of conventional and nano-roughened LEDs fabricated in this investigation.

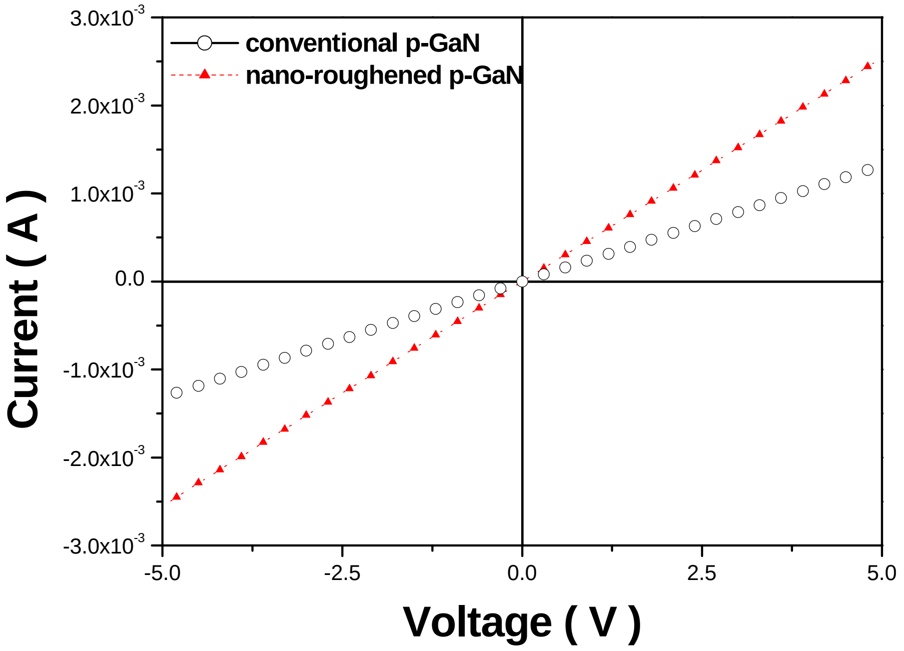

(c)

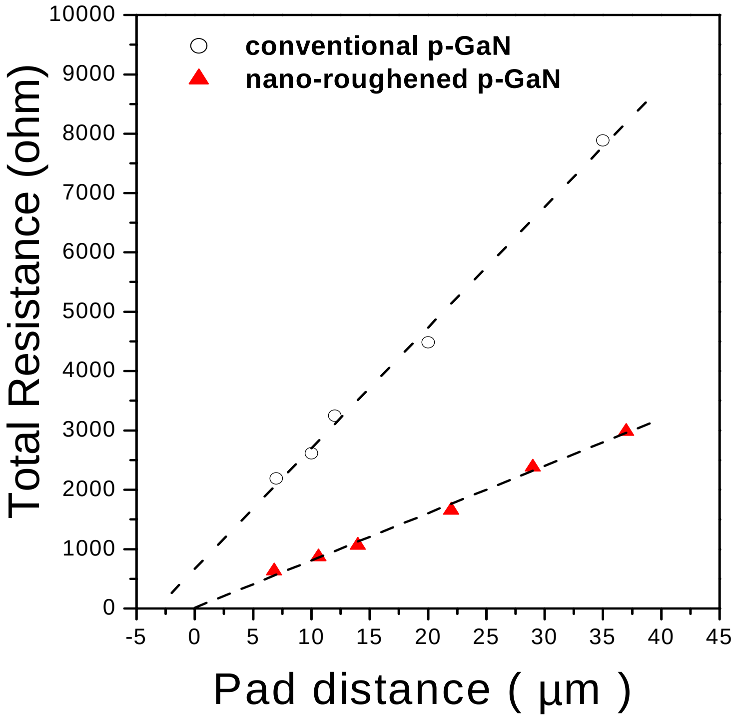

(d)

Fig. 2-5 (c) I-V characteristics of the nano-roughened and conventional p-GaN measured by the Circular Transmission Line Method (CTLM). (d) Total resistance (Y) measured by CTLM is linearly related to the pad distance (X).

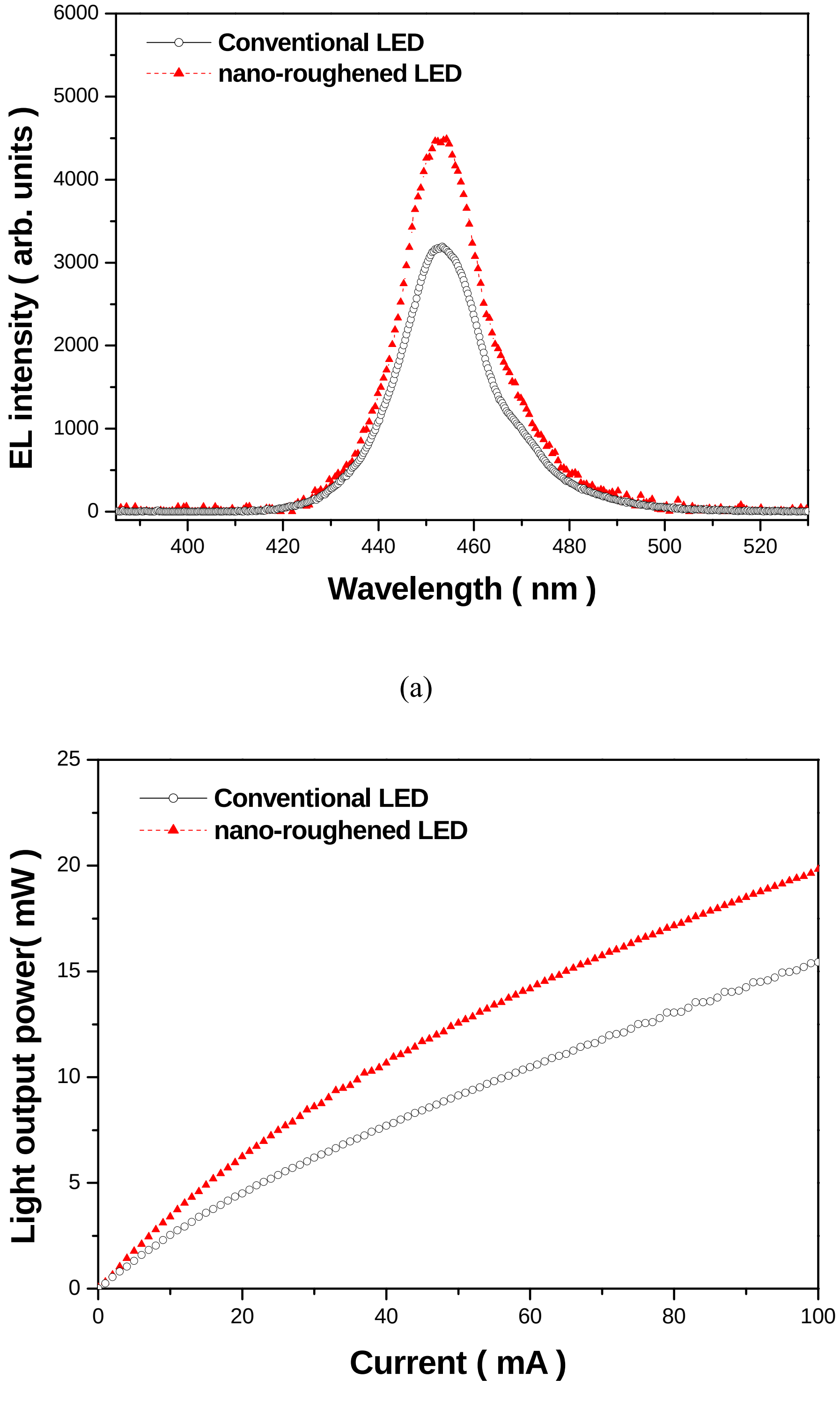

(a)

(b)

Fig. 2-6 (a) Room temperature EL spectrum of conventional and nano-roughened LED at a current of 20 mA. (b) Light output power-current (L-I) characteristics of conventional and nano-roughened LEDs.

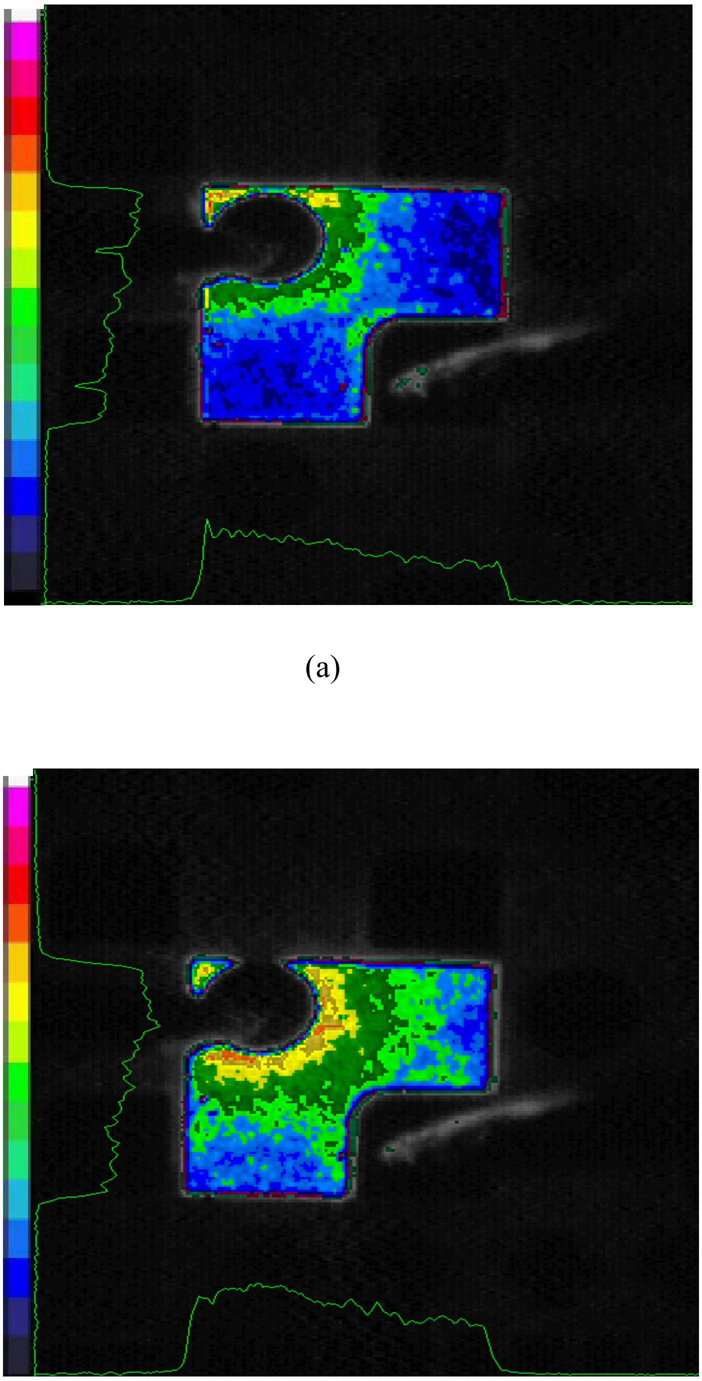

(a)

(b)

Fig. 2-7 Photos of (a) conventional LED and (b) nano-roughened LED at a dc injection current of 20 mA.

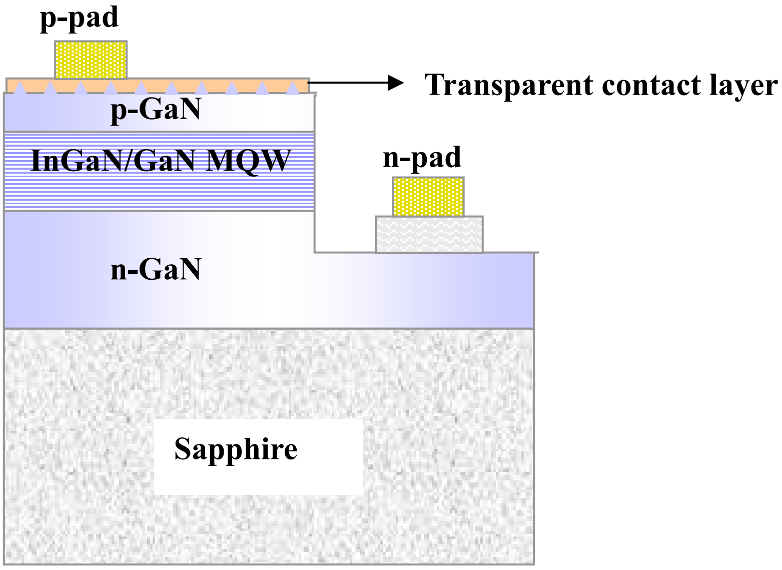

Fig. 2-8 Schematic diagram of the nano-roughed LED structure.

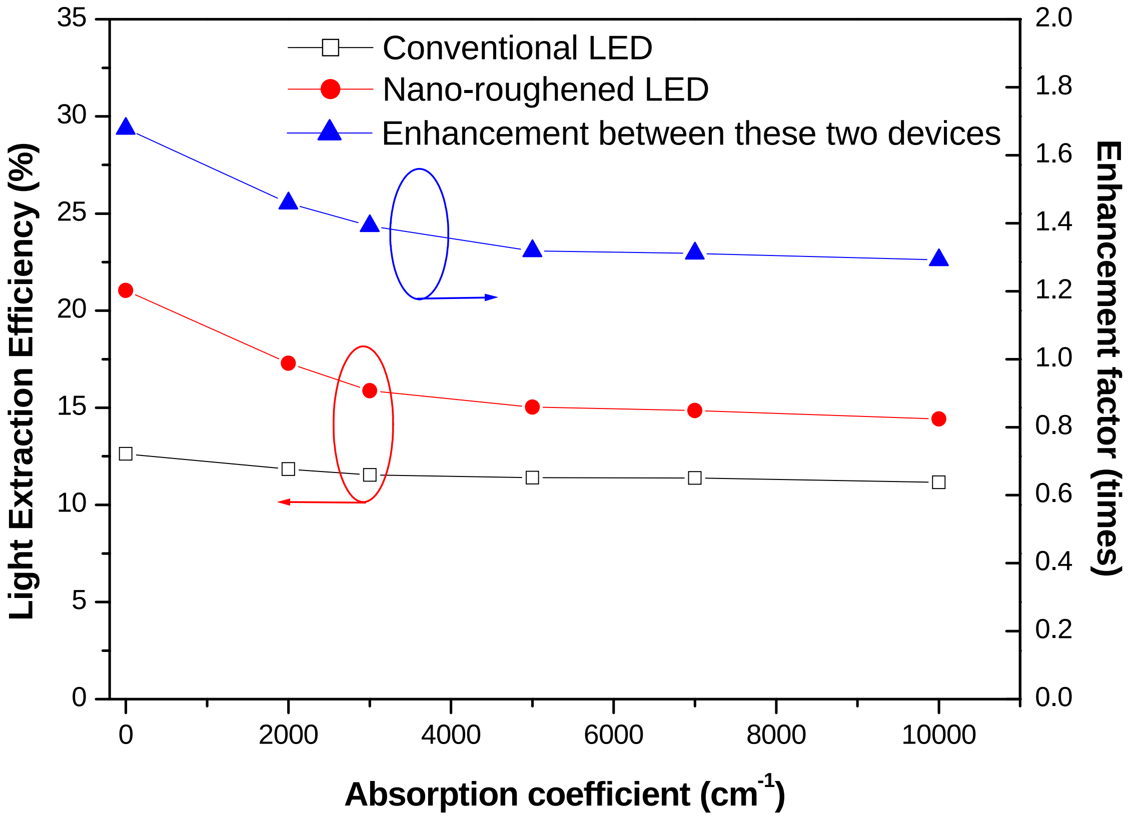

Fig. 2-9 Simulation describes the light extraction efficiency of LEDs with and without rough top surface as a function of absorption coefficient of the p-GaN.

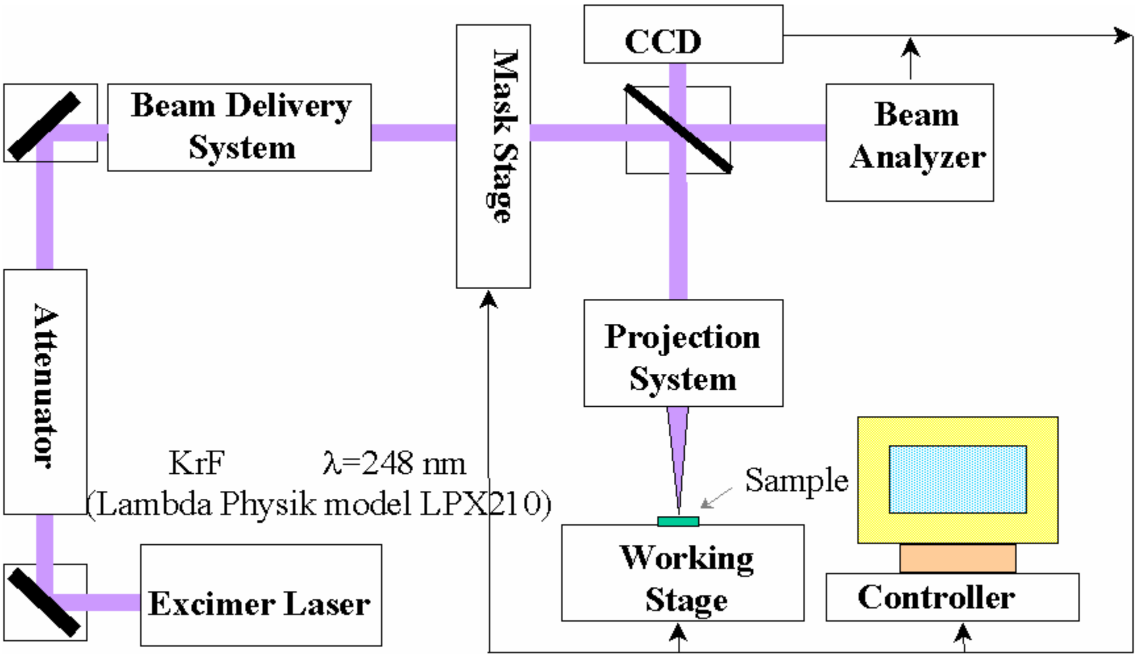

Fig. 2-10 The schematic diagram of laser etching process setup.

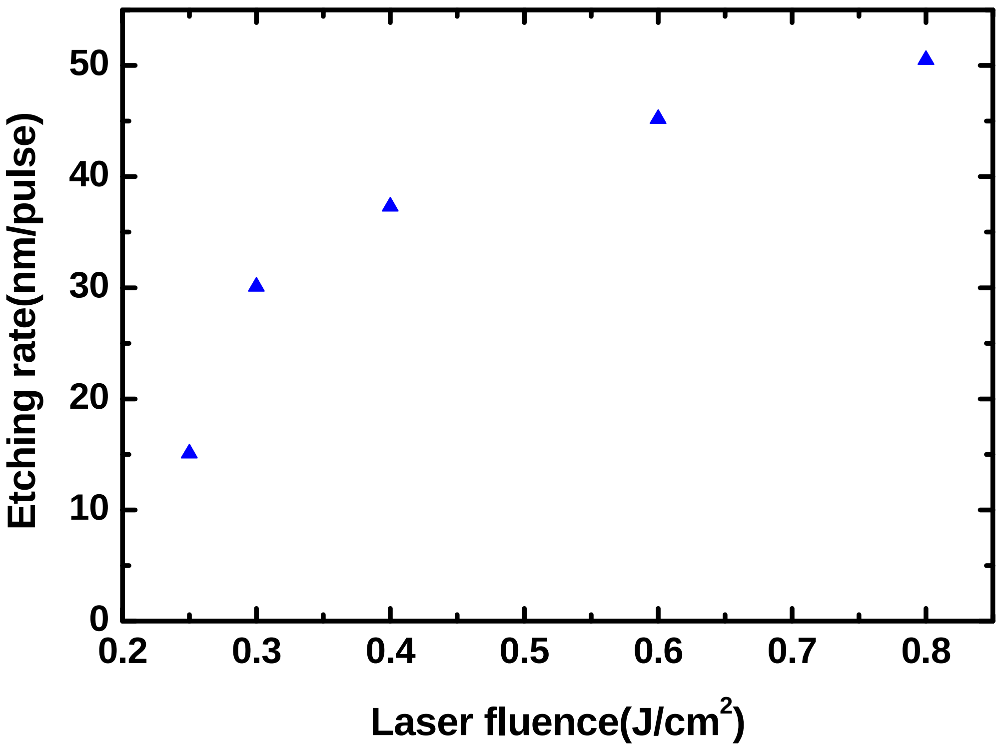

Fig. 2-11 The etching rate as a function of laser fluence.

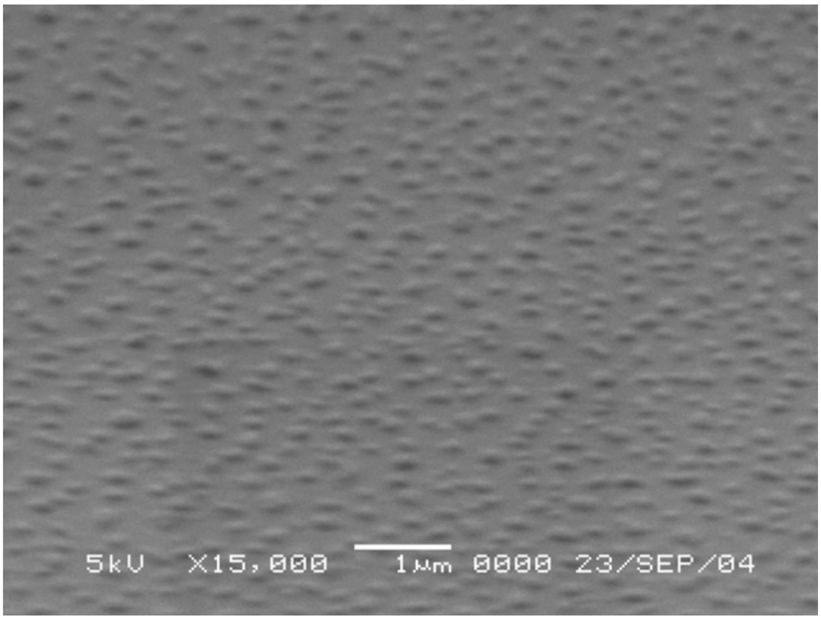

(a)

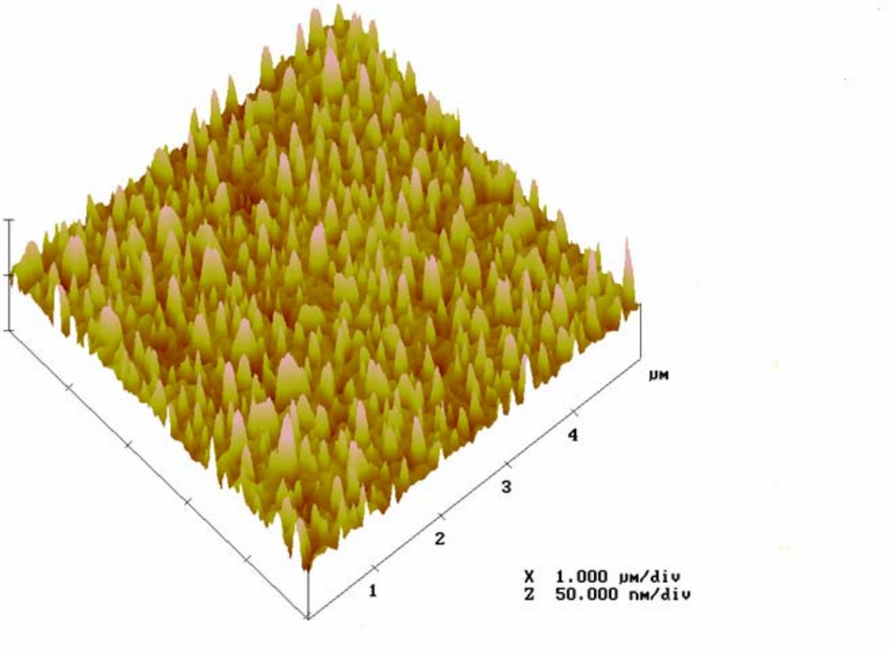

RMS roughness=7.4 nm

(b)

Fig. 2-12 (a) SEM and (b) AFM images of the Ni nano-mask on p-GaN surface morphology of a nano-roughened LED sample.

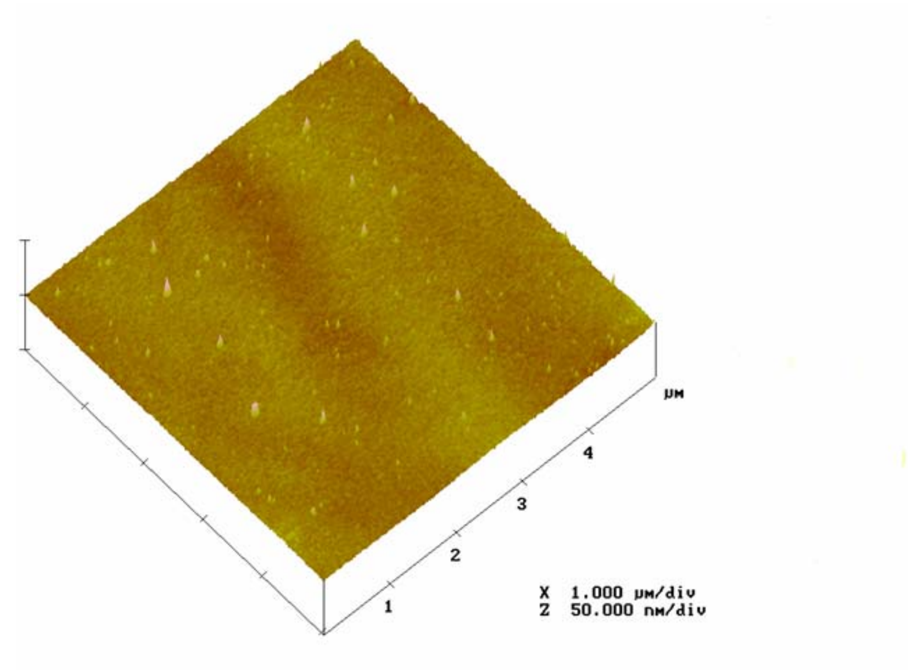

RMS roughness=0.7 nm

(a)

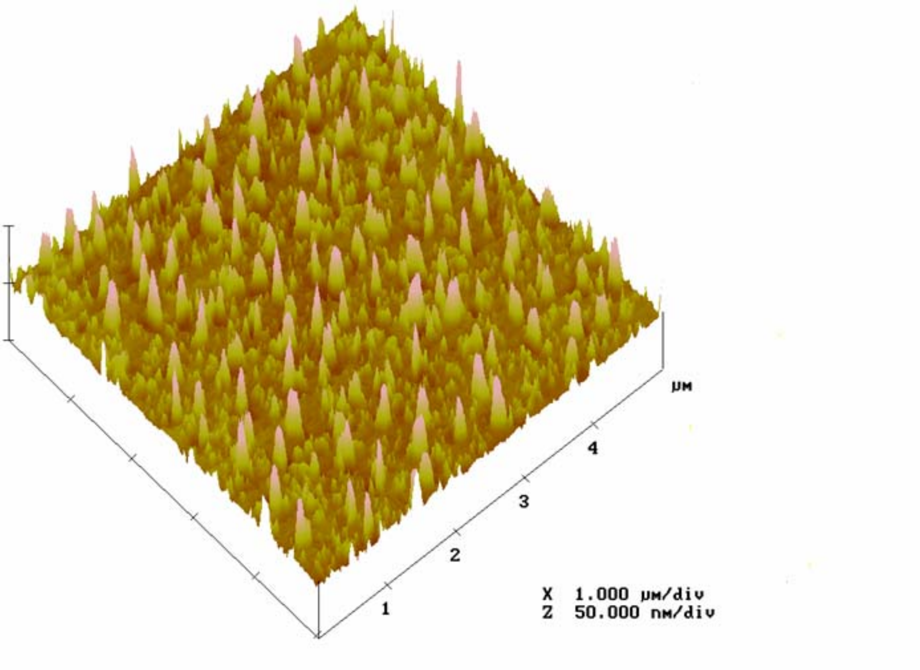

RMS roughness=5.8 nm

(b)

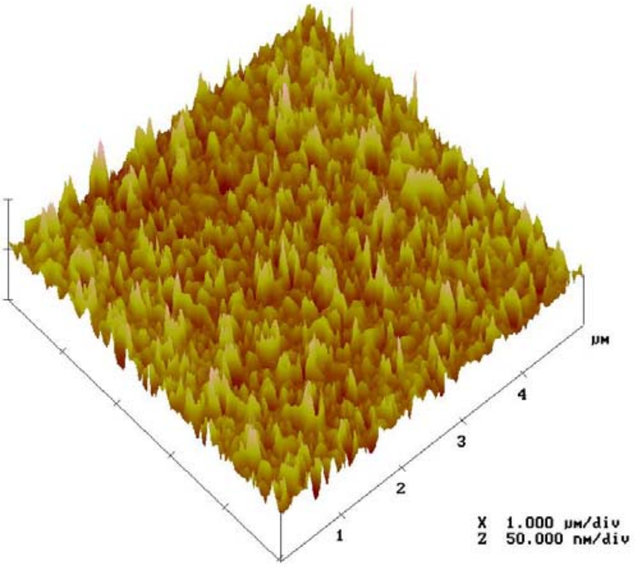

RMS roughness=6.5 nm

(c)

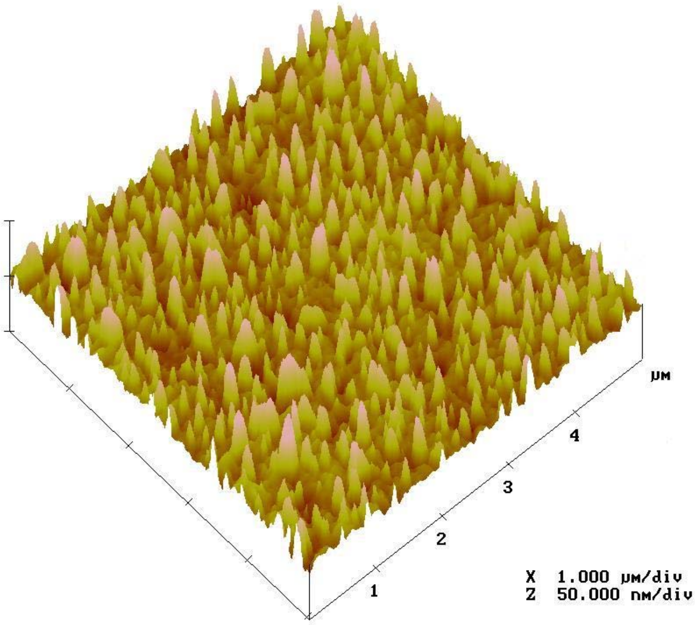

RMS roughness=8.7 nm

(d)

Fig. 2-13 AFM images of the top surface morphology of a LED sample. (a) Conventional LED p-GaN surface image. Nano-roughened LED top p-GaN surface applied laser etching energy of : (b) 300 mJ/cm^2, (c) 400mJ/cm^2, (d) 800mJ/cm^2.

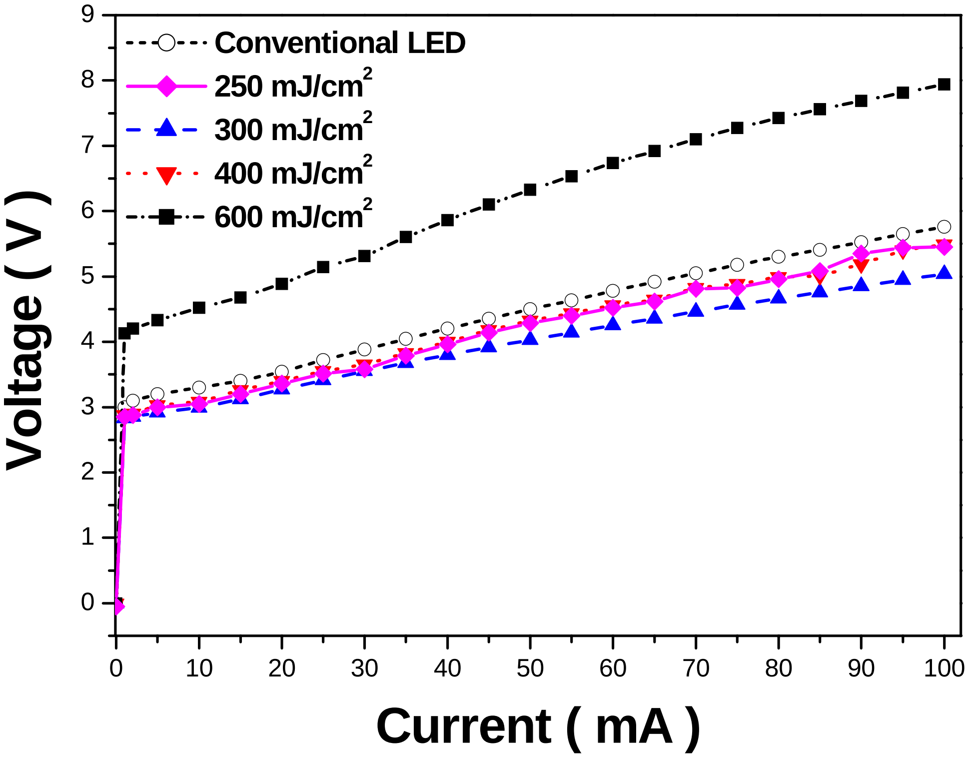

Fig. 2-14 Forward I-V curves of conventional and nano-roughened LEDs.

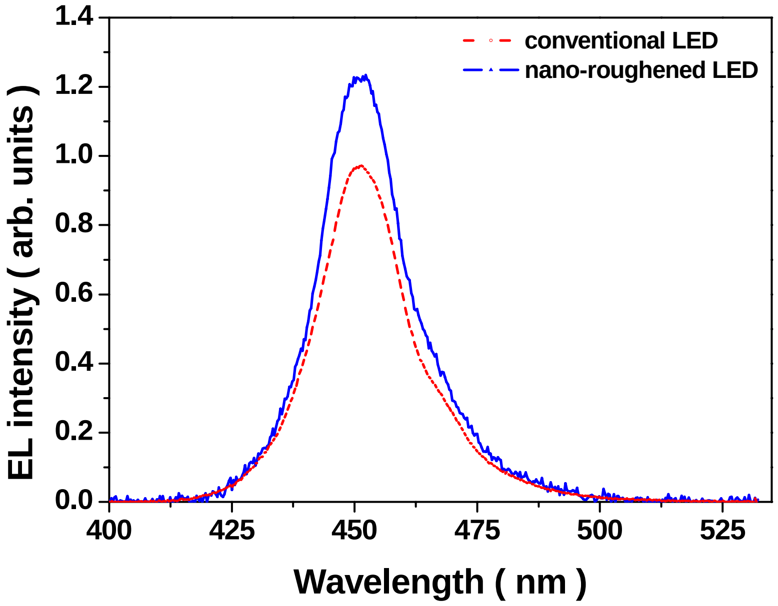

(a)

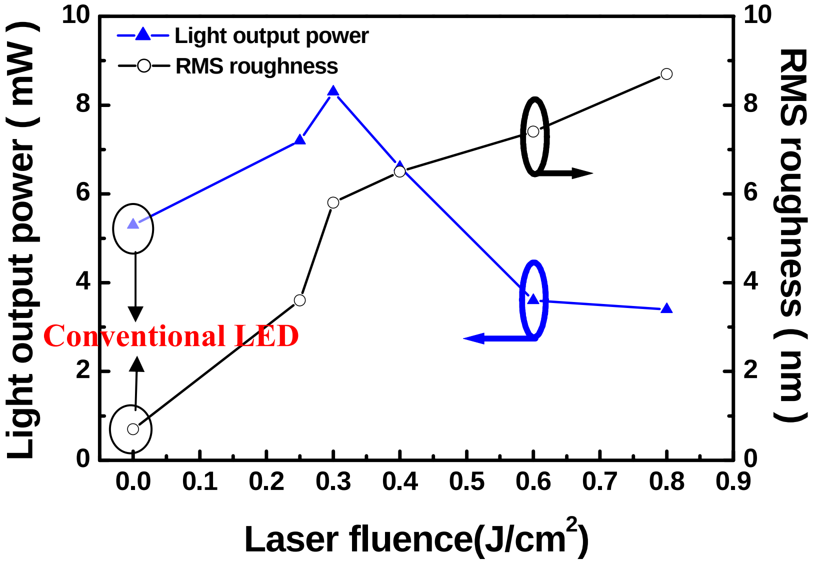

(b)

Fig. 2-15 (a) Room temperature EL spectra of conventional and nano-roughened LEDs with laser etching energy of 300 mJ/cm^2 at a current of 20 mA. (b) Light output power-current (L-I) and RMS surface roughness characteristics of conventional and nano-roughened LEDs.

REFERENCE

[1] S. Nakamura, M. Senoh, S. Nagahama, N. Iwasa, T. Yamada, T. Matsushita, Y. Sugimoto and H. Kiyoku, Appl. Phys. Lett., Vol. 70, pp. 868 (1997).

[2] S. Nakamura, M. Senoh, N. Iwasa and S. Nagahama, Jpn. J. Appl. Phys., Vol. 34, pp. L797 (1995).

[3] S. Nakamura, T. Mukai, and M. Senoh, Appl. Phys. Lett., Vol. 64, pp. 1687 (1994).

[4] T. Mukai and S. Nakamura, Jpn. J. Appl. Phys., Vol. 38, pp. 5735 (1999).

[5] C. Huh, K. S. Lee, E. J. Kang, and S. J. Park, J. Appl. Phys., Vol. 93, pp. 9383, (2003).

[6] J. J. Wierer, D. A. Steigerwald, M. R. Krames, J. J. O'shea, M. J. Ludowise, G. Christenson, Y. C. Shen, C. Lowery, P. S. Martin, S. Subramanya, W. Gotz, N. F. Gradner, R. S. Kern, and S. A. Stockman, Appl. Phys. Lett., Vol. 78, pp. 3379 (2001).

[7] S. X. Jin, J. Li, J. Y. Lin, and H. X. Jiang, Appl. Phys. Lett., Vol. 77, pp. 3236 (2000).

[8] T. N. Oder, J. Shakya, J. Y. Lin, and H. X. Jiang, Appl. Phys. Lett., Vol. 83, pp. 1231, (2003).

[9] T. N. Oder, K. H. Kim, J. Y. Lin, and H. X. Jiang, Appl. Phys. Lett., Vol. 84, pp. 466, (2004).

[10] H. W. Choi, M. D. Dawson, P. R. Edwards, and R. W. Martin, Appl. Phys. Lett., Vol. 83, pp. 4483 (2003).

[11] T. Fujii, Y. Gao, R. Sharma, E. L. Hu, S. P. DenBaars, and S. Nakamura, Appl. Phys. Lett., Vol. 84, pp. 855 (2004).

[12] S. J. Chang, L. W. Wu, Y. K. Su, Senior Member, IEEE, Y. P. Hsu, W. C. Lai, J. M. Tsai, J. K. Sheu, and C. T. Lee, Senior Member, IEEE, IEEE Photo. Technol. Lett., Vol. 16, NO. 6, pp. 1447 (2004).

[13] T. Fujii, Y. Gao, R. Sharma, E. L. Hu, S. P. DenBaars, and S. Nakamura, Appl. Phys, Lett., 84, 855 (2004).

[14] M. D. McCluskey, L. T. Romano, B. S. Krusor, D. P. Bour, Appl. Phys, Lett. 72, 1730 (1998).

[15] Y. S. Lin, K. J. Ma, C. C. Yang, and T. E. Weirich, J. Cryst. Growth 242, 35 (2002).

[16] C. J. Youn, T. S. Jeong, M. S. Han, J. W. Yang, K. Y. Lim, and H. W. Yu, J. Cryst. Growth 250, 331 (2003).

[17] H. Ishikawa, S. Kobayashi, Y. Koide, S. Yamasaki, S. Nagai, J. Umezaki, M. Koike, and M. Murakami, J. Appl. Phys., Vol. 81 (3), pp. 1315 (1997).

[18] H. D. Tong, R. A. F. Zwijze, J. W. Berenschot, R. J. Wiegerink, G. J. M. Krijnen, and M.

C. Elwenspoek, Proceedings of the SeSens workshop, pp. 697 (2000).

[19] H. W. Huang, C. C. Kao, T. H. Hsueh, C. C. Yu, C. F. Lin, J. T. Chu, H. C. Kuo, and S. C. Wang, Mater. Sci. & Eng. B, Vol. 113/2, pp. 125 (2004).

[20] Martin Von Allmen and Andreas Blastter, *Laser-Beam Interactions with Materials, Physical Principles and Applications (Second Edition)*, Springer-Verlag, Berlin (1995).

[21] C. F. Chu, "*Study of GaN Light Emitting Devices Fabricated by Laser Lift-Off Technique*" Ph. D. Thesis by National Chiao Tung University, Taiwan (2003).

[22] C. J. Youn, T. S. Jeong, M. S. Han, J. W. Yang, K. Y. Lim, and H. W. Yu, J. Cryst. Growth 250, 331 (2003).

[23] H. W. Huang, C. C. Kao, J. T. Chu, C. C. Yu, C. F. Lin, H. C. Kuo, and S. C. Wang, Mater. Sci. & Eng. B, Vol. 113, pp. 19 (2004).

CHAPTER 3

GaN-Based Sidewalls Roughened Light-Emitting Diodes

3.1 Progress in GaN-based sidewalls roughened LED device by natural lithography

The light from LEDs can be enhanced either through the sample surface or through the side walls of the chip. Research into improving the light extraction efficiency (external quantum efficiency) and brightness in the LEDs [3]-[8], [10]-[15] has been intense. These processes all allow the photons generated within the LEDs to find the escape cone, by multiply scattering from a rough surface. A similar concept should also be applied to chip sidewalls. In other words, more photons should be able to escape from LEDs with textured chip sidewalls as compared to LEDs with conventional flat chip sidewalls.

By using plasma-enhanced chemical vapor deposition SiO_2 layer as the etching mask, Chang *et al.* successfully demonstrated a 10% output power enhancement of nitride-based LEDs with μm-scale wavelike textured sidewalls [8]. Due to the lithography limits of their instruments, they used a mask with a large period to fabricate μm-scale wavelike textured sidewalls. Further enhance the light output can be achieved if sidewall roughness can be reduced to the sub-micrometer or nano-scale range. Therefore, Deckman *et al.* described to application of textured surfaces prepared using “natural lithography” technique are currently being investigated [9]. Recently, Horng *et al.* demonstrated the power enhancement of surface-textured ITO/GaN LEDs using a combination of natural lithography and dry etching techniques [10]. In this paper, nitride-based LEDs with nano-scale textured chip sidewalls were fabricated by natural lithography and and dry etching techniques. As a result, the light output efficiency of LED with nano-scale textured sidewalls was significantly increased compared to that of the conventional LED. Furthermore, the nano-scale textured sidewalls will not result in any degradation in the electrical properties of nitride-based LEDs.

3.2 Fabrication of GaN-Based sidewalls roughened LED device by natural lithography

The GaN-based LED samples were grown by metal-organic chemical vapor deposition (MOCVD) with a rotating-disk reactor (Emcore) on a c-axis sapphire (0001) substrate at the growth pressure of 200 mbar. The LED structure consists of a 50-nm-thick GaN nucleation layer grown at 550 ^{o}C, a 3 μm-thick Si-doped n-GaN buffer layer grown at 1050 ^{o}C, an unintentionally doped InGaN/GaN multiple quantum well (MQW) active region grown at 770 ^{o}C, a 50-nm-thick Mg-doped p-AlGaN electron blocking layer grown at 1050 ^{o}C, a

0.25um-thick Mg-doped p-GaN contact layer grown at 1050 ^{o}C and a Si-doped n $In_{0.23}Ga_{0.77}N$/GaN SPS structure. The MQW active region consists of five periods of 3-nm/7nm-thick $In_{0.21}Ga_{0.79}N$/GaN well layers and barrier layers. After annealing to activate Mg in the p-type layers, a 0.5 um SiO_2 layer was then deposited on top the LED samples by plasma-enhanced chemical vapor deposition (PECVD). Photolithography was subsequently performed to define the mesa mask pattern. The boundary of SiO_2 mask (300 μm x 300 μm) and mesa edge is about 10um. A combination of natural lithography and dry etching techniques were used to form a nano-scale textured sidewalls where the TiO_2 polystyrenes (PSs) were spun randomly onto the top as the natural mask around the boundary of SiO_2 mask and mesa edge, the process flowchart of sidewalls roughened is shown in Fig. 3-1. The LED sample was then subjected to the ICP process using the Cl_2 /Ar mixture. A schematic diagram of the GaN LED structure with textured sidewalls is shown in Fig. 3-2. An 300-nm-thick indium–tin oxide (ITO) layer was subsequently evaporated onto the LED sample surfaces to serve as the upper contact at 300^{o}C. Since ITO is electrically conductive with a high transparency, we could achieve a much larger light output from the LED surface [4], [10]. On the other hand, Ti/Al/Ti/Au contact was deposited onto the exposed n-type GaN layer to serve as the n-type electrode. Finally, Ni/Au was deposited onto the p-type electrode. The wafers were then lapped down to about 90 um. We then used scribe and break to fabricate InGaN–GaN LED chips. Fig. 3-3 (a) and (b) shows the scanning electron microscopy (SEM) picture of the side wall. It can be seen clearly that this device indeed has nano-scale textured side walls. The SEM images in Fig. 3-3(a) and (b) shows the nano-rods dimension and density of the nano-scale textured sidewalls were approximately 200 nm and $2x10^{9}$ cm^{-2}, and the height of the nano-rods was approximately 1.28 μm. The tilt sidewall can be greatly enhanced the nano-roughness sidewall effect than conventional LED [17].

3.3 Characteristics of GaN-Based sidewalls roughened LED device by natural lithography

A prime concern of these LED samples is their leakage current characteristics. Figure 3-4 (a) shows the reverse I–V curves of the ITO/GaN LEDs with and without nano-scale textured sidewalls. The nano-scale textured sidewalls of LEDs did not induce a larger leakage current than that in the conventional LED. At reverse voltage -5 V, the leakage current were both approximately similar. Therefore, to avoid ITO being residual at sidewall is also very important (remove ITO at sidewalls) to reduce I_R. Furthermore, it was found that the results indicate that the dry etching process does not adversely affect the LED performance because the plasma does not destroy the *p*-GaN layer. The forward voltages of the LED with nano-scale textured sidewalls and conventional LED were both approximately 3.42 V at a driving current of 20 mA. Such an observation indicates that the nano-scale textured sidewalls will not result in any degradation in the electrical properties of nitride-based LEDs. Fig. 3-4(b) L–I characteristics of the LED with nano-scale textured sidewalls and conventional LED. At an injection current of 20 mA, the light output power of the LED with nano-scale textured sidewalls and conventional LED were approximately 9.5 mW and 7.2 mW, respectively. The LED with nano-scale textured sidewalls increased the output power of the InGaN–GaN MQW LEDs by a factor of 1.3, indicating that the LED with nano-scale textured sidewalls had larger light extraction efficiency. The wall-plug efficiency (output power/input power) was also calculated: it was 30% higher than that of the conventional LED at an injection current of 20 mA because of enhanced light output power with nano-scale textured sidewalls.

To further investigate the influence of sidewall roughness on light output performance of LED chip, intensity distribution measurements were performed on conventional LED and LED with nano-scale textured sidewalls in Fig. 3-5. During these measurements, we injected a 20 mA dc current into these two different kinds of LEDs. It can be seen clearly that the LEDs with nano-scale textured sidewalls shows higher extraction efficiency with wider view angle compare to conventional LEDs. The higher light extraction efficiency can be attributed to the increase of photons scattering from sidewalls roughness of InGaN/GaN LED [8]. Further, the slight enhancement in the near vertical directions can be attributed to tilt angle of sidewalls [17] and we simulated light propagation and reflection using the ray tracing method provided by Advanced System Analysis Program(ASAP). For simplicity, we employed a two-dimensional model which is similar on GaN-based LED structures: The top mesa width is 300 μm and depth is 1.3 μm with vertical sidewall and 42^{o} over-cut sidewall. Fig. 3-6(a) and (b) shows the top-view ray tracing images of conventional LED and LED with nano-scale textured sidewalls. The result also can be greatly enhanced to light extraction efficiency. Such an enhancement could have a larger probability to be emitted from the nano-scale textured sidewalls and, thus, achieve even brighter LEDs.

In summary, InGaN/GaN LEDs with nano-scale textured sidewalls have been fabricated. By using PSs as the etching mask and ICP-etched the epitaxial layers of LEDs to achieve nano-scale textured sidewalls. The LED with nano-scale textured sidewalls increased the output power of the InGaN–GaN MQW LEDs by a factor of 1.3, indicating that the LED with nano-scale textured sidewalls had larger light extraction efficiency. The wall-plug efficiency of nitride-based LED was increased by 30% with textured sidewalls.

3.4 Fabrication of GaN-Based sidewalls roughened power chip LED device by natural lithography

A 0.5 um SiO_2 layer was then deposited on top the LED samples by plasma-enhanced chemical vapor deposition (PECVD). Photolithography was subsequently performed to define the mesa mask pattern. The boundary of SiO_2 mask (1 mm x 1 mm) and mesa edge is about 10um. A combination of natural lithography and dry etching techniques were used to form a sidewalls roughness where the PSs were spun randomly onto the top as the natural mask around the boundary of SiO_2 mask and mesa edge. The power chip LED sample was then subjected to the ICP process using the Cl_2 /Ar mixture. Top-view of power-chip LEDs and a schematic diagram of the GaN LED structure with a sidewalls roughness are shown in Fig. 3-7 and 3-3(a)-(b). A 300-nm-thick indium–tin oxide (ITO) layer was subsequently evaporated onto the LED sample surfaces to serve as the upper contact at 300^{o}C. Since ITO is electrically conductive with a high transparency, we could achieve a much larger light output from the power chip LED surface [4], [10]. On the other hand, Ti/Al/Ti/Au contact was deposited onto the exposed n-type GaN layer to serve as the n-type electrode. Finally, Ni/Au was deposited onto the p-type electrode. The wafers were then lapped down to about 90 um. We then used scribe and break to fabricate GaN-based LED power chips. The scanning electron microscopy (SEM) picture of the sidewall roughness is shown in Fig. 3-3(a)-b). The SEM image in Fig. 3-3(b) shows the nano-rods dimension of the nano-scale sidewalls was approximately 200 nm, and the height of the nano-rods was approximately 1 μm.

3.5 Characteristics of GaN-Based sidewalls roughened power chip LED device by natural lithography

A prime concern of these power chip LED samples is their forward current characteristics. Figure 3-8(a) shows the forward I–V curves of the ITO/GaN LEDs with and without sidewall roughness. The forward voltages of the power chip LEDs with sidewall roughness and conventional LED were both approximately 3.22 V at a driving current of 350 mA. Such an observation indicates that the sidewalls roughness will not result in any degradation in the electrical properties of GaN-based power chip LEDs. Fig. 3-8(b) L–I characteristics of the LED with sidewall roughness and conventional LED were not encapsulated for LIV measurement. During light output intensity testing, the GaN-based LEDs were put onto a copper plate with the collection angle at about 27 degree. At an injection current of 350 mA, the light output intensity of the power chip LED with sidewall roughness and conventional power chip LED were approximately 2.34 cd and 1.85 cd, respectively. The power chip LED with sidewall roughness increased the light output intensity of the InGaN/GaN MQW LEDs by a factor of 1.26, indicating that the LED with sidewall roughness had larger light extraction efficiency. The wall-plug efficiency (output power/input power) was also calculated: it was 26.5% higher than that of the conventional power chip LED at an injection current of 350 mA because of enhanced light output intensity with sidewall roughness.

As shown in Fig. 3-9, when the dc drive current increased from 20 to 200 mA, the Electroluminescence (EL) emission peak wavelengths of the GaN-based power-chip LEDs blue-shifted from 462.7 to 460.7 nm, and is then saturated over I_f = 350 mA. This blue-shift is due to the band filling effect and screening effect in a piezoelectric filed QW. Then, it is continuously red-shifted over I_f = 1300 mA. This red-shift can be explained by the effect of band shrinkage due to joule heating. The emission peak wavelength of conventional LED is similar to sidewall roughened LEDs.

To further investigate the influence of sidewalls roughness and 42 degree over-cut sidewall on light output performance of power-chip LED, intensity distribution measurements were performed on conventional LED and LED with sidewalls roughness and 42 degree over-cut sidewall in Fig. 3-10. During these measurements, we injected a 350 mA dc current into these two different kinds of LEDs. It can be seen clearly that the LEDs with sidewalls roughness and 42 degree over-cut sidewall shows higher extraction efficiency with wider view angle compare to conventional LEDs. The higher light extraction efficiency can be attributed to the increase of photons scattering from sidewalls roughness of InGaN/GaN LED [8].We simulated light propagation and reflection using the ray tracing method provided by Advanced System Analysis Program(ASAP). For simplicity, we employed a two-dimensional model which is similar on GaN-based power-chip LED structures. The structure layer of the simulated GaN-based power-chip LEDs is described in Table 3.1. The chip size is 1mm × 1mm. The top mesa width is 1 mm and depth is 1.3 μm with vertical sidewall and 42 degree over-cut sidewall. The light extraction efficiency of the inclination angle between 40~70 degree is enhanced about 15% over the conventional LED in stimulation results. However, the simulation structure neglected sidewalls roughness and the absorption coefficient. Only the tile angle is 42 degree LED is enhanced to light extraction efficiency around ~17% than conventional LED from simulation. Fig. 3-11(a) and (b) shows the top-view ray tracing images of the conventional power-chip LED and the power-chip LED with 42 degree over-cut sidewalls. The result also can be greatly enhanced to light extraction efficiency. The higher light extraction efficiency can be attributed to the increase of photons scattering from 42 degree over-cut sidewalls of InGaN/GaN LED in fig 3-11(a) and (b).During life test, all five power chip LEDs with sidewall roughness were driven by 350 mA current injection at room temperature in Fig. 3-12. After 1000 h, it was found that normalized output power of power chip LED with sidewall roughness only decreased by 7-11%, respectively. The power-chip LEDs with sidewall roughness could also achieve the same performance in lifetime testing compared without sidewall roughness.

In summary, InGaN/GaN LEDs with sidewalls roughness have been fabricated. By using PSs as the etching mask and ICP-etched the epitaxial layers of power chip LEDs to achieve sidewalls roughness. The LED with sidewalls roughness increased the light output intensity of the InGaN/GaN MQW LEDs by a factor of 1.26, indicating that the power chip LED with sidewalls roughness had larger light extraction efficiency at an injection current of 350 mA. The wall-plug efficiency of GaN-based power chip LED was increased by 26.5% with sidewalls roughness at an injection current of 350 mA. After 1000 h life test, it was found that normalized output intensity of power chip LED with sidewall roughness only decreased by 7-11%.

Table 3.1. Parameters of structure layer in the stimulated power-chip LEDs.

Layer	Sapphire	n-GaN	MQW	p-GaN	ITO
Thickness (μm)	350	4.0	0.1	0.1	0.3
Refractive Index	1.78	2.5	2.5	2.5	2.0

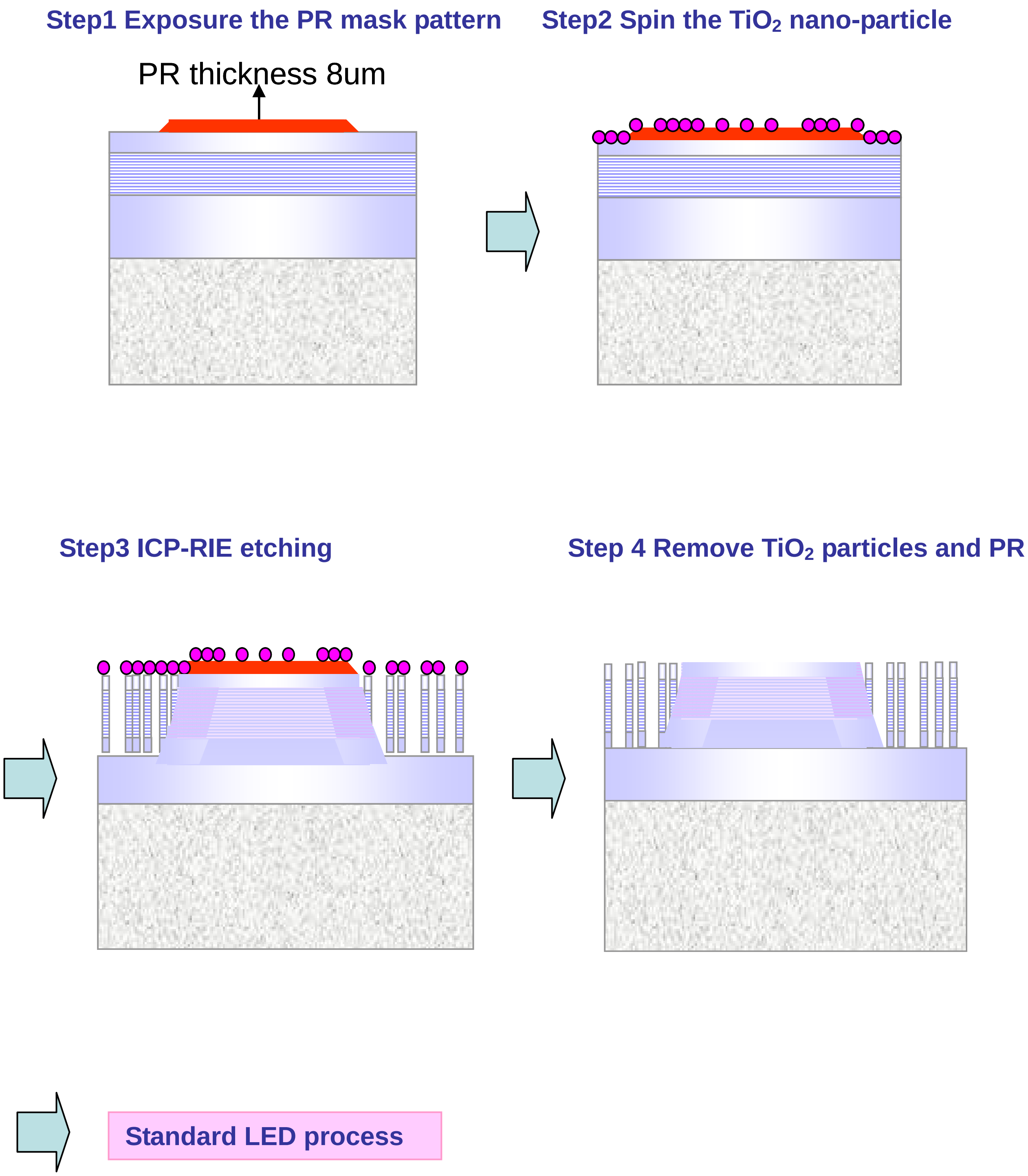

Fig. 3-1 Showing the process flowchart of the GaN-based sidewalls roughened LEDs by ICP-RIE using TiO_2 polystyrenes.

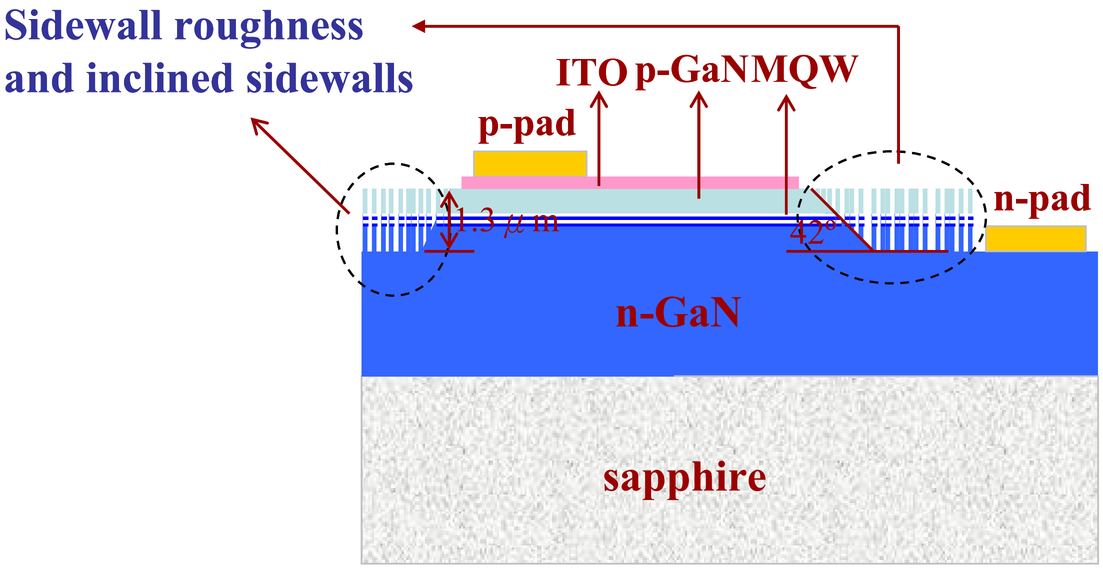

Fig. 3-2 A schematic diagram of InGaN-GaN MQW LED structure with sidewalls roughened.

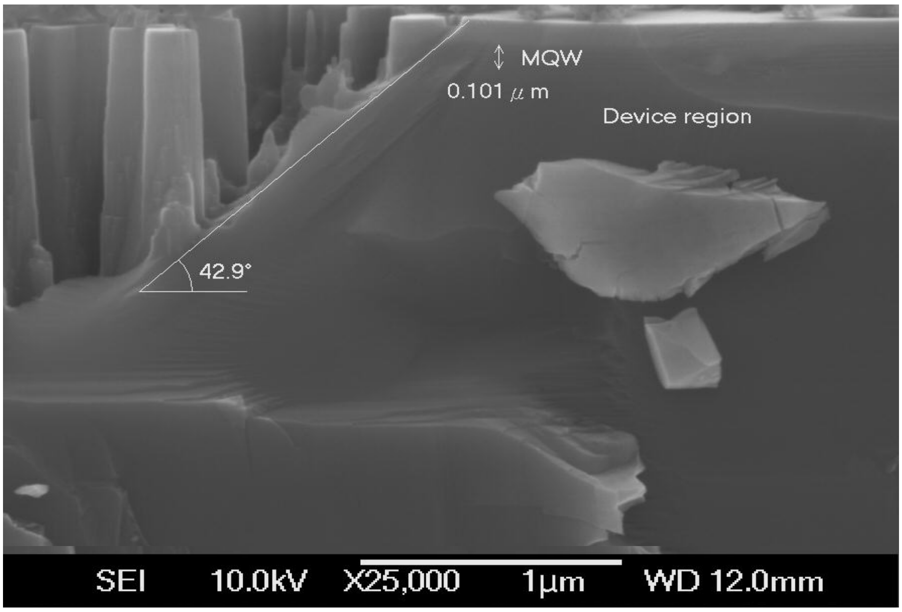

(a)

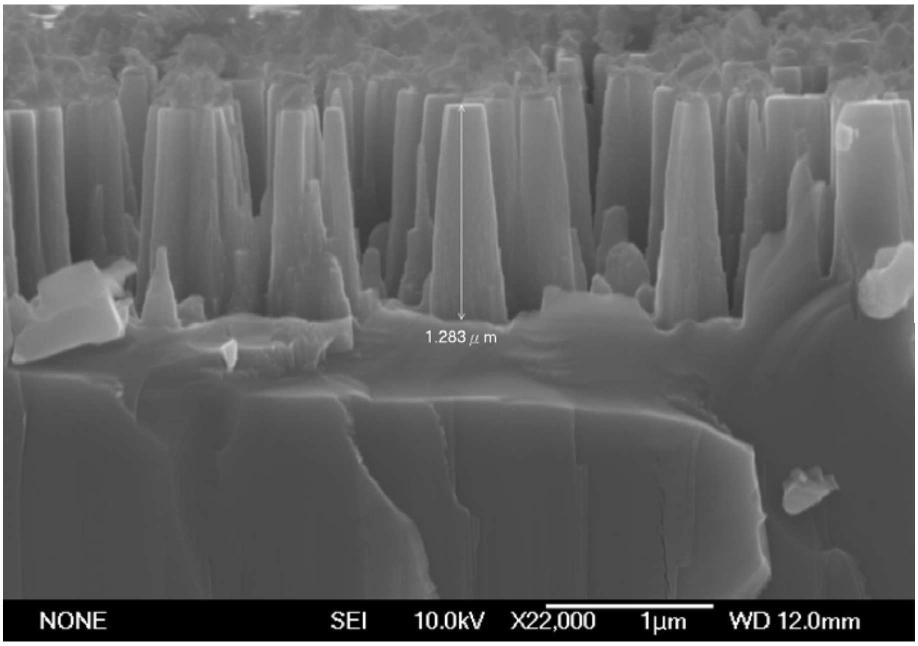

(b)

Fig. 3-3 SEM images of InGaN-GaN MQW LED structure with nano-scale textured sidewalls. (a) cross-section of nano-scale textured sidewalls and (b) nano-rods density of nano-scale textured sidewalls.

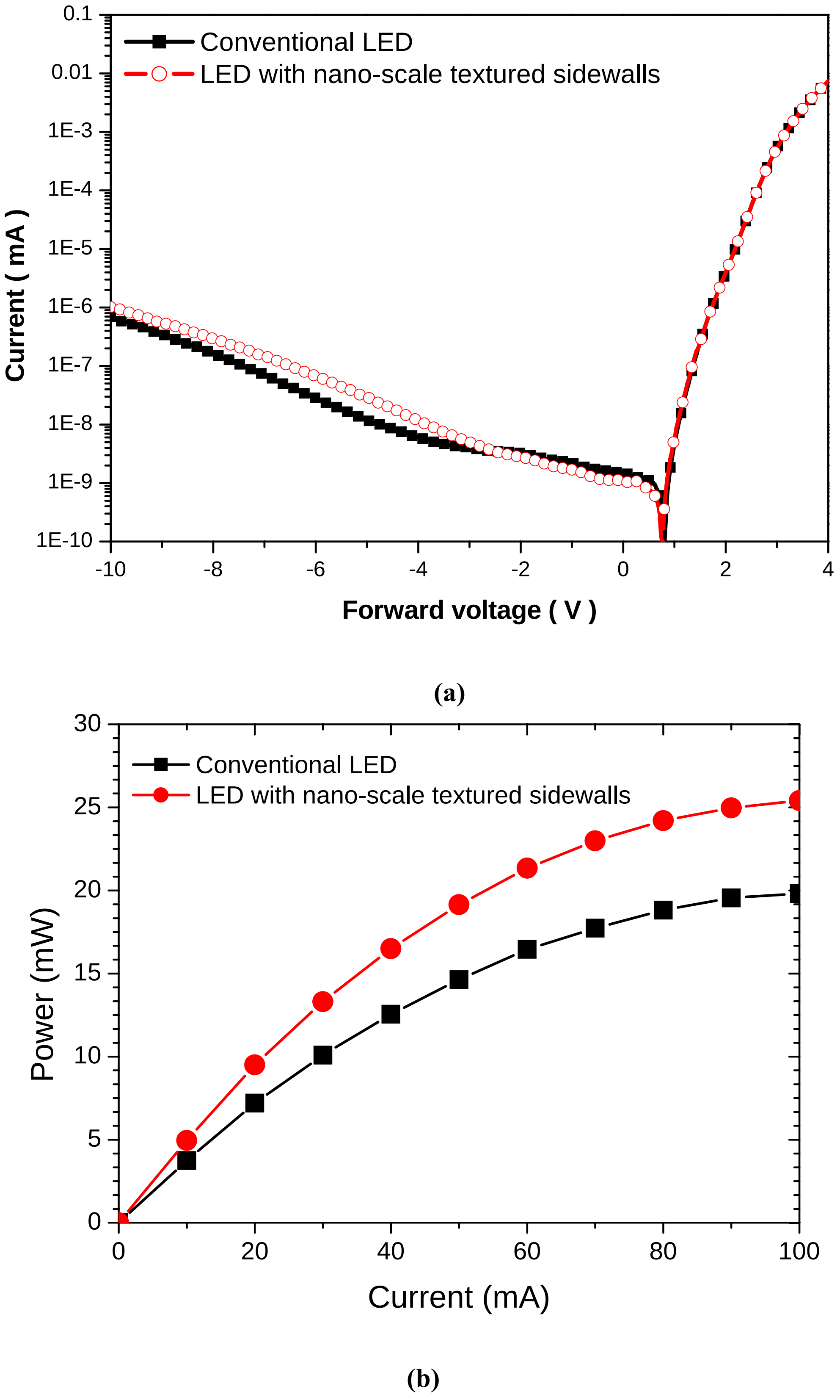

(a)

(b)

Fig. 3-4(a) Current-voltage (I-V) and (b)intensity–current (L–I) characteristics of conventional and LED with nano-scale textured sidewalls LEDs fabricated in this investigation.

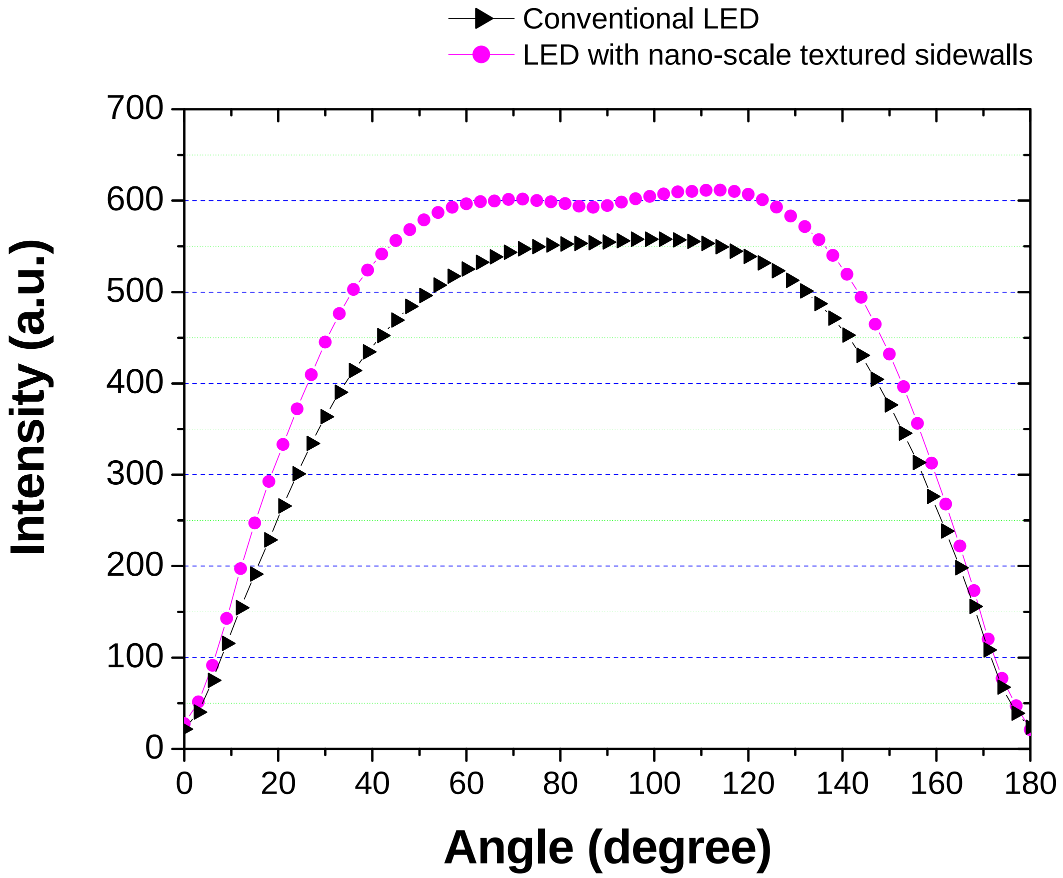

Fig. 3-5 Light output patterns of the LED with nano-scale textured sidewalls and the conventional LED.

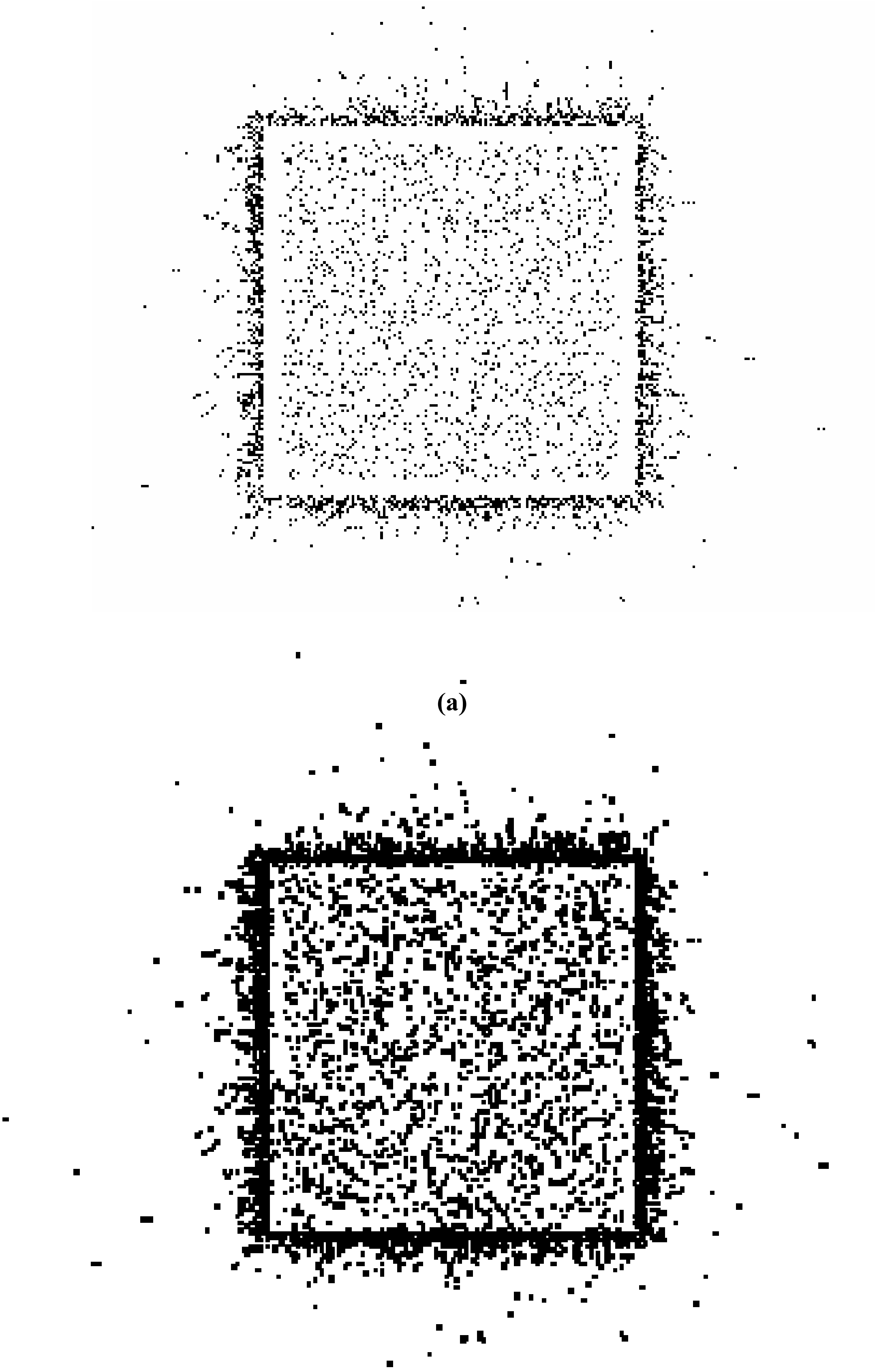

(a)

(b)

Fig. 3-6 Top-view ray tracing images of the (a) conventional LED and the (b) LED with nano-scale textured sidewalls.

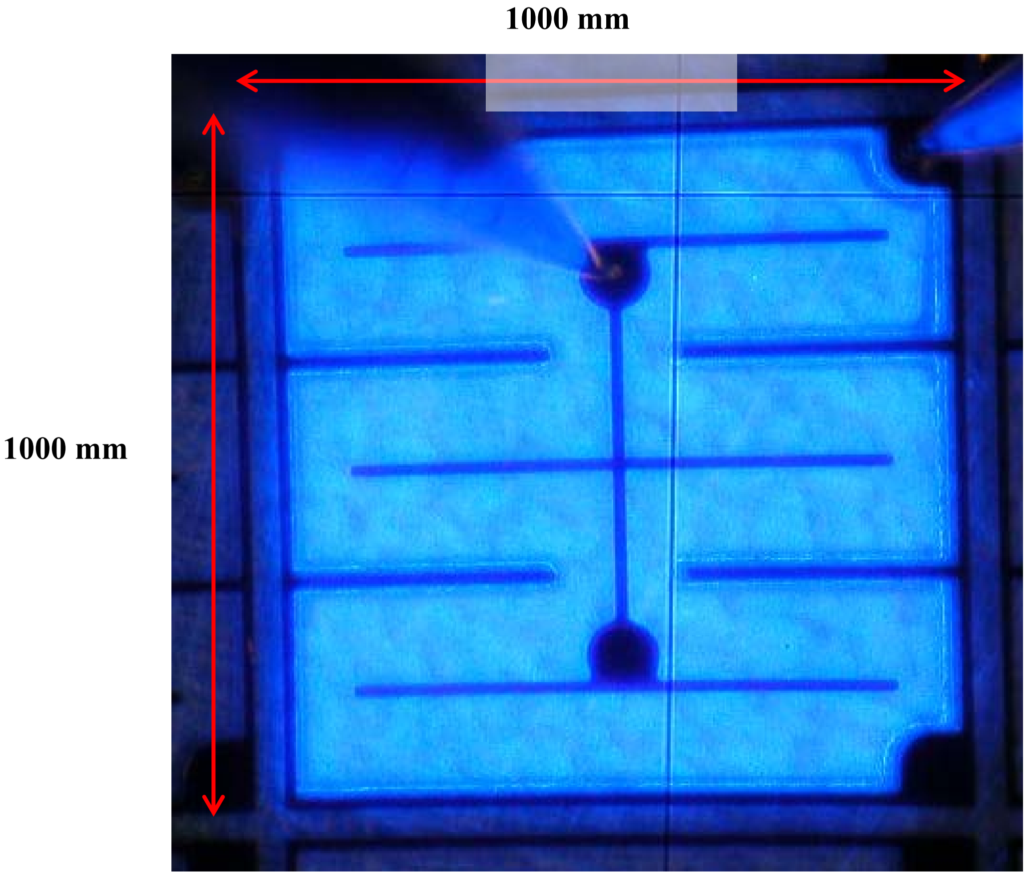

Fig. 3-7 Top-view image of power chip LED.

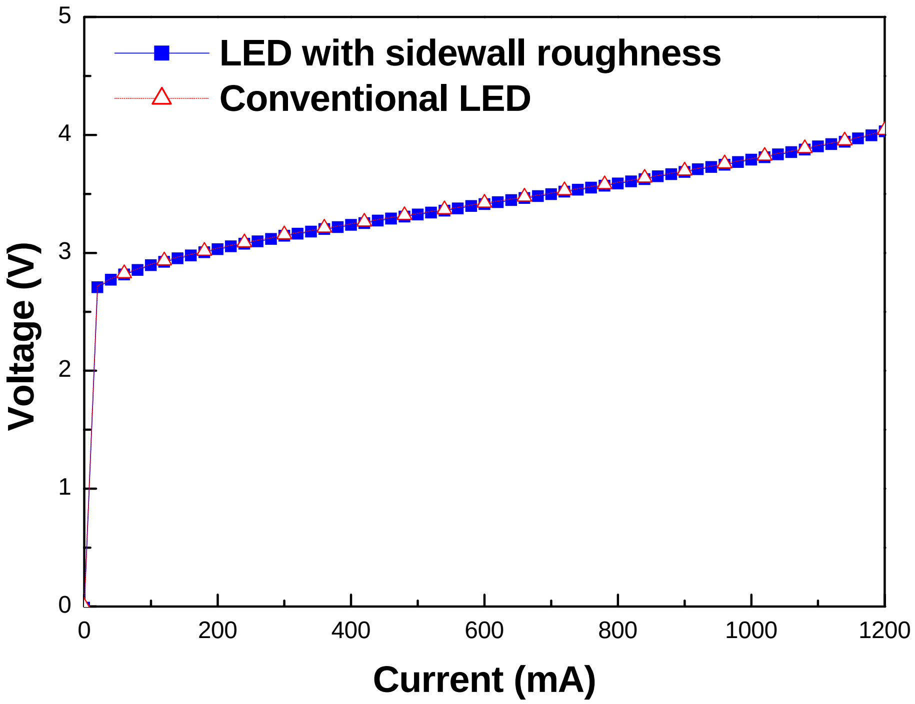

(a)

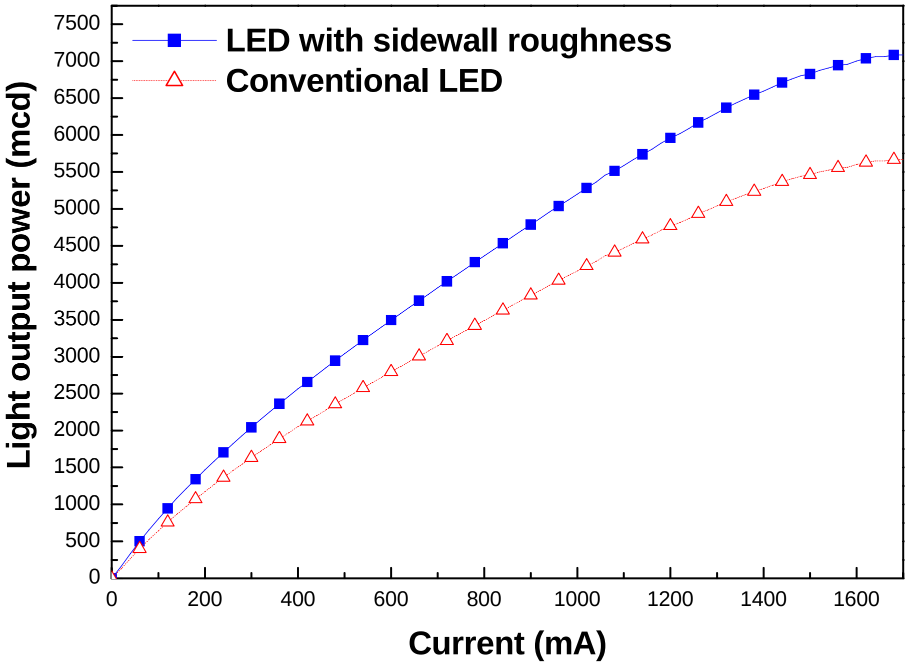

(b)

Fig. 3-8(a)Current-voltage (I-V) and (b)intensity–current (L–I) characteristics of conventional power chip LED and power chip LED with sidewall roughness fabricated in this investigation.

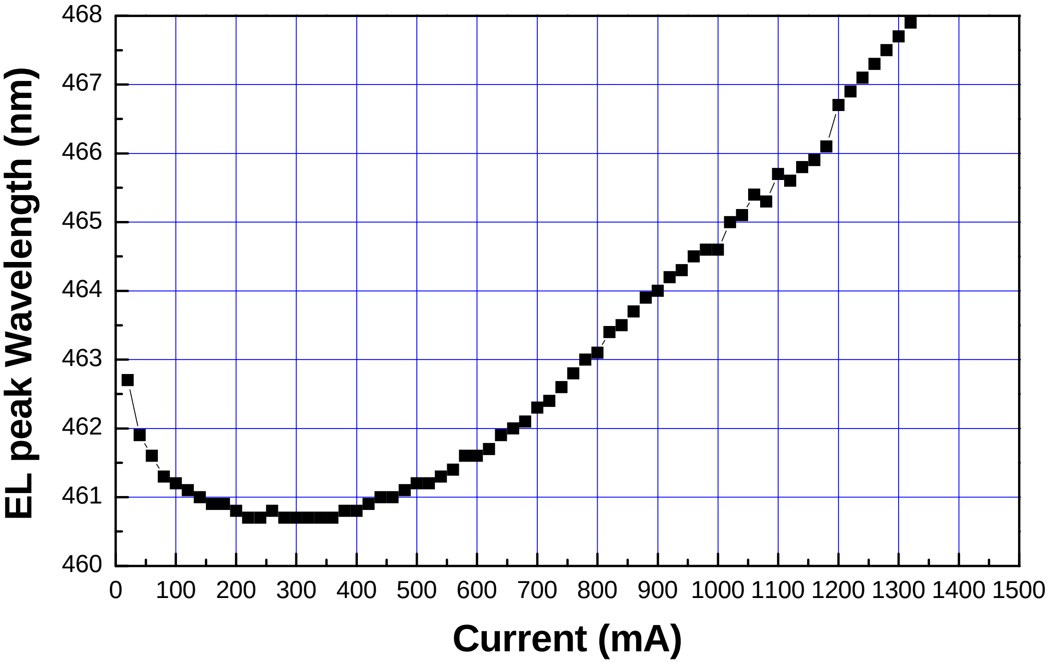

Fig. 3-9 Light output wavelength peak of the power chip LED with sidewall roughness.

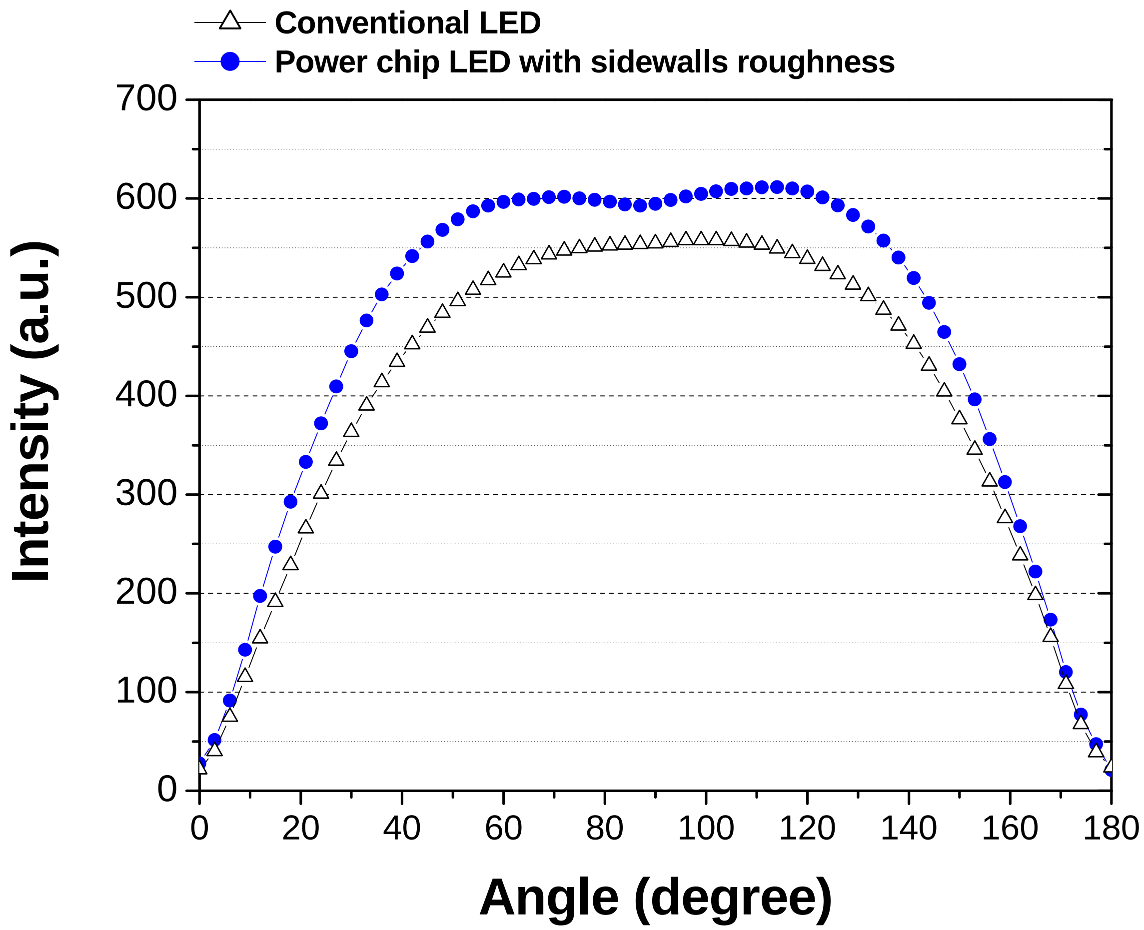

Fig. 3-10 Light output far-field patterns of the power-chip LED with sidewall roughness and the conventional LED.

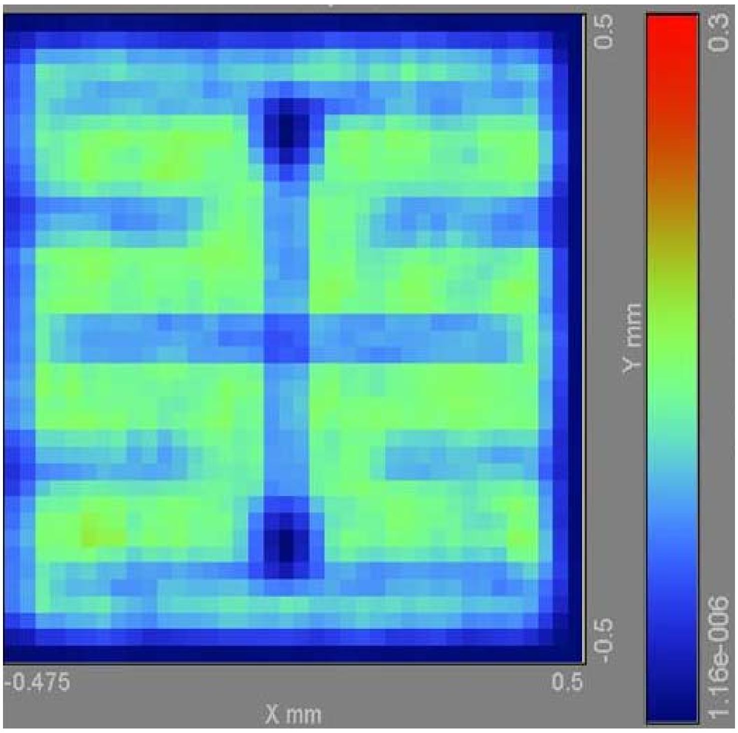

(a)

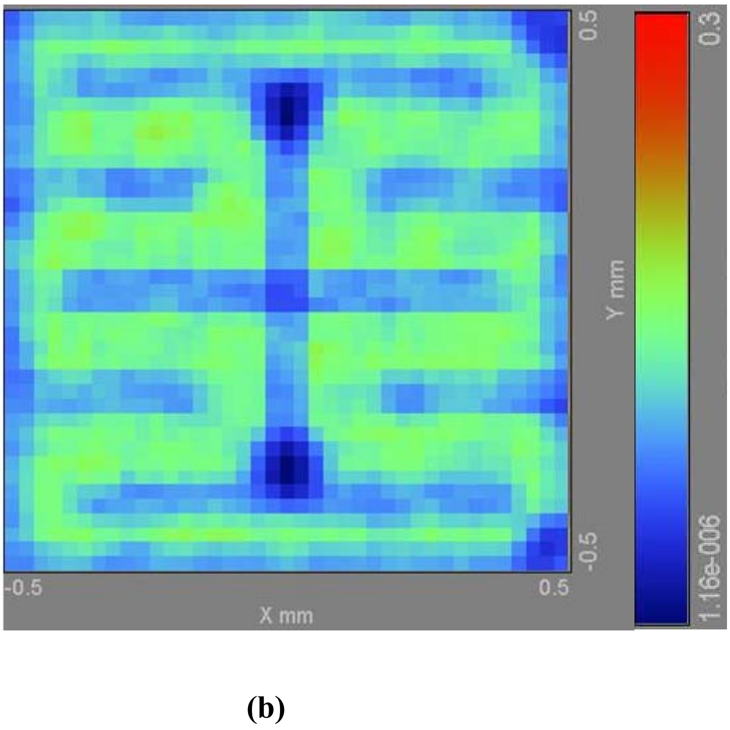

(b)

Fig. 3-11 Top-view ray tracing images of the (a) conventional power chip LED, and the (b) power chip LED with sidewall roughness.

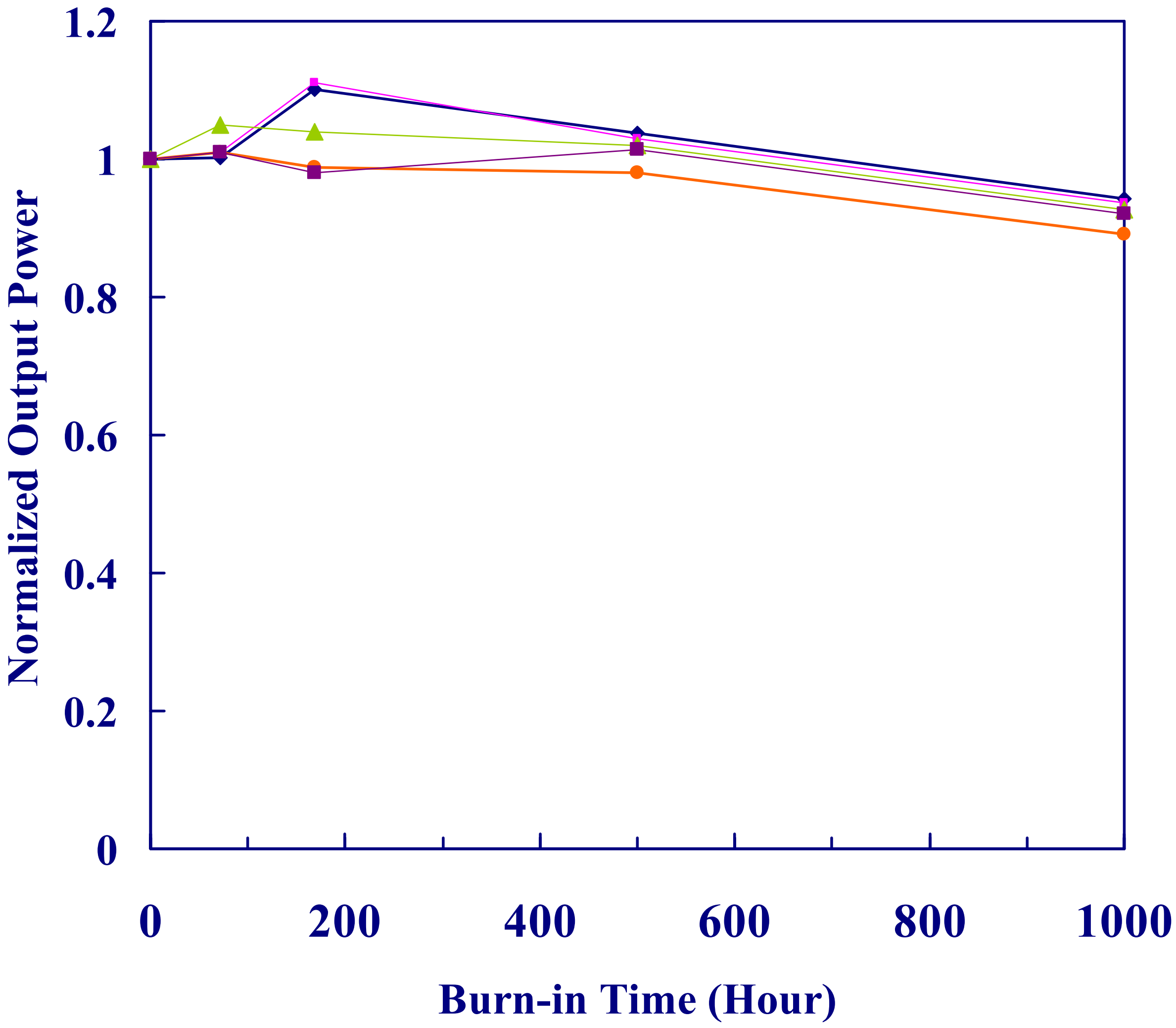

Fig. 3-12 Power chip LEDs with sidewall roughness were driven by 350 mA current injection at room temperature.

REFERENCE

[1] M. Koike, N. Shibata, H. Kato, and Y. Takahashi, IEEE J. Select. Topics Quantum Electron., Vol. 8, pp 271 (2002).

[2] M. R. Krames et al, Appl. Phys. Lett. Vol. 75, pp. 2365 (1999).

[3] C. Huh, K. S. Lee, E. J. Kang, and S. J. Park, J. Appl. Phys., Vol. 93, pp. 9383 (2003).

[4] S. M. Pan, R. C. Tu, Y. M. Fan, R. C. Yeh, and J. T. Hsu, IEEE Photo. Technol. Lett. Vol. 15, pp. 649 (2003).

[5] T. Fujii, Y. Gao, R. Sharma, E. L. Hu, S. P. DenBaars, and S. Nakamura, Appl. Phys. Lett., Vol. 84, pp. 855 (2004).

[6] Y. Gao, T. Fujii, R. Sharma, K. Fujito, S. P. Denbaars, S. Nakamura, and E. L. Hu, Jpn. J. Appl. Phys., Vol. 43, pp. 637 (2004).

[7] T. N. Oder, K. H. Kim, J. Y. Lin, and H. X. Jiang, Appl. Phys. Lett., Vol. 84, pp. 466 (2004).

[8] C. S. Chang, S. J. Chang, Y. K. Su, C. T. Lee, Y. C. Lin, W. C. Lai, S. C. Shei, J. C. Ke, and H. M. Lo, IEEE Photo. Technol. Lett., Vol. 16, pp. 750 (2004).

[9] H. W. Deckman and J. H. Dunsmuir, “Natural lithography”, Appl. Phys. Lett., Vol. 41, pp. 377 (1982).

[10] R. H. Horng and C. C. Yang J. Y. Wu S. H. Huang, C. E. Lee, and D. S. Wuu, Appl. Phys. Lett., Vol. 86, pp. 221101 (2005).

[11] H. W. Huang, J. T. Chu, C. C. Kao, T. H. Hsueh, C. C. Yu, H. C. Kuo, and S. C. Wang, Nanotechnology Vol. 16, pp. 1 (2005).

[12] H. W. Huang, C. C. Kao, J. T. Chu, C. C. Yu, H. C. Kuo, and S. C. Wang, *Member*, and IEEE Photo. Technol. Lett. Vol. 17, pp. 5 (2005).

[13] T. H. Hsueh, J. K. Sheu, H. W. Huang, J. Y. Chu, C. C. Kao, H. C. Kuo, and S. C. Wang, IEEE Photo. Technol. Lett. Vol. 17, pp.1163 (2005).

[14] C. F. Lin, Z. J. Yang, J. H. Zheng, and J. J. Dai, IEEE Photo. Technol. Lett. Vol. 17, pp. 2038 (2005).

[15] W. K. Wang, D. S. Wuu, S. H. Lin, P. H., R. H. Horng, T. C. Hsu, Donald T.C. Huo, M. J. Jou, Y. H. Yu, and A. Lin, IEEE J. of Quantum Electron., Vol. 41, pp. 1403 (2005).

[16] S. J. Kim, IEEE Photo. Technol. Lett. Vol. 17, pp. 1617 (2005).

[17] C. C. Kao, H. C. Kuo, H. W. Huang, J. T. Chu, Y. C. Peng, Y. L. Hsieh, C. Y. Luo, C. C. Yu, C. F. Lin, and S. C. Wang, *Member*, IEEE Photo. Technol. Lett. Vol. 17, pp. 19 (2005).

CHAPTER 4

InGaN/GaN nanorods fabricated by plasma etching with nanoscale nickel metal islands

4.1 Introduction

Wide-bandgap gallium nitride (GaN) and other group III-nitrides based semiconductors have been successfully employed to realize short-wavelength light emitting diodes (LEDs) and laser diodes [1-3]. Additionally, due to quantum confinement effects, fabrication and studies of nano-structure have recently attracted a great deal of interest for potential application on electronic and optoelectronic devices. Potential applications for nanorod LEDs include quantum cryptography and information processing. With the recent progress in semiconductor process technology, various nano-structure fabrication methods have been investigated such as e-beam lithography, and metal-catalyzed nano-structure synthesis by vapour-liquid-solid growth process on different materials [4-5]. For GaN-based materials, the fabrications and synthesizing of GaN nanowires and nanorods have been reported using various methods, for example carbon nanotube-confined reaction, metal-catalyzed growth assisted by laser ablation, and the high temperature pyrolysis approach and so on [6-11]. Furthermore, using photoenhanced wet etching technique to produce GaN whiskers [12-14] were also reported recently. However, all these reported methods are relatively complicated and mostly using synthesis approach with catalysts assist, and had no mention about the control of dimension and density for these fabricated GaN-based LEDs. We have been reported a method to fabricating controllable GaN-based structure dimension and density by ICP-RIE without mask [3], but the method caused GaN-based structure top-surface was etching and formation high resistance, so unable to fabricating GaN-based light emitting devices. The study of the self-assemble nanometer-sized metal or semiconductor islands has became particularly important recently as it is an attractive method for producing intrinsic nanoscale devices without the need for expensive lithography. In this chapter, we report a novel technique to fabricate GaN-based nanorod LEDs with controllable dimension and density using self-assemble nickel nano-mask and inductively coupled plasma reactive ion etching (ICP-RIE). Structural and optical properties were examined with field-emission scanning electron microscopy (FESEM), transmission electron microscopy (TEM), photoluminescence (PL), and time-resolved photoluminescence (TRPL) measurements.

4.2 Fabrication of InGaN/GaN MQWs nanorods

These LED samples using Ni metal nano-mask were separated into two sets for different process procedures. As shown in Fig. 4.1(a), the first set of samples was deposited thin Ni layer with a thickness of 150 Å directly on top of the GaN LED film using an electron-beam evaporation. As shown in Fig. 4.1(b), the second set of samples was deposited a 3000 Å Si_3N_4 thin film layer on GaN-based LED film, followed by the deposition of a Ni layer with the thickness ranging from 50 to 150 Å. All samples were subsequently rapid thermal annealing (RTA) under flowing N_2 at temperatures 800 to 900℃ for 1min to form various nanometer-sized Ni clusters (nano-masks). Finally, all GaN-based LED samples (first and second sets of samples) with various Ni nano-masks were than etched using a planar type ICP-RIE system (SAMCO ICP-RIE 101iPH) at the ICP power and bias power source with RF frequency of 13.56 MHz. The ICP has a reactor chamber which is connected to a load-lock chamber. The etchant gases of Cl_2 and Ar gases were introduced into the reactor chamber through independent electronic mass flow controllers (MFCs) that can control the flow rate of each gas with an accuracy of about 1 sccm. An automatic pressure controller (APC) is placed near the exhaust end of the chamber to control the chamber pressure. The etching rate is about 4000 Å/min under a gas mixture condition of $Cl_2/Ar = 50 / 20$ standard cubic centimeter min (sccm) with the ICP source power, bias power set at 400 / 100 W and chamber pressure of 5mTorr for 3 min of etching time. After the etching process, the dimension and density of the nanorods were estimated by the scanning electron microscope (SEM) (Hitachi FE-SEM S-5000).

(a) Effect of Si_3N_4 film under Ni layer

As shown Fig. 4.2(a) is the SEM image of Ni/Si_3N_4 nano-mask image, the Ni /Si_3N_4 mask dimension size were about 200/150 nm and Ni clusters height was about 100 nm. Fig. 4.2(b), (c) show the first and second set SEM images with the same Ni thickness 150 Å, at the RTA condition of 850°C for 1min and ICP-RIE etching process to form the GaN-based nanorod LEDs. As shown in Fig. 4.2(b), (c), the second set GaN-based nanorod LEDs with the dimension of about 130 ~ 190 nm was more uniform and narrower than that of the first set with the dimension of about 200 ~ 300 nm. This can be explained by the strain effect. The room temperature lattice constant of Ni was about 0.352 nm and that of the corresponding crystalline GaN (first set) surface to be 0.318 nm in *a* direction and 0.518 nm in *c* direction. This gives the room temperature strains were $\varepsilon_{a(GaN/Ni)}$= 10% and $\varepsilon_{c(GaN/Ni)}$=-32%, however

Si_3N_4 (second set) surface to be 0.761 nm in the *a* direction and 0.291 nm in the *c* direction gives the room temperature strains as $\varepsilon_{a(Si3N4/Ni)}$= -53% and $\varepsilon_{c(Si3N4/Ni)}$ =21% respectively. This means that the deposition of Ni on Si_3N_4 result in a higher compressive strains in *a* direction, and resultant Ni nano clusters size is smaller and more uniform than that of the first set of samples [15]. The dimension of the second set of nanorods shows more uniform and narrower than first set of nanorods due to the Ni nano-mask dimension was more uniform and smaller, and additionally undercut effect on nano-masks Si_3N_4 underlayer after RIE etching.

(b)Effect of temperature

We estimate the mean dimension and density of the GaN-based nanorod LEDs as a function of the Ni nano-mask RTA temperature. The RTA temperature need to be chosen above 700℃ to form the Ni self assemble nano-masks. Shown in Fig. 4.3, the nanorods density can be estimated about 2 ~ $3x10^9$ cm^{-2} as the Ni nano-mask RTA temperatures between 800 and 900℃ for 1 min at fixed Ni film thickness 150 Å on the first and second set samples. The dimension of the GaN-based LED nanorods on the first set was about 160 ~ 380 nm as the RTA temperature from 800 to 900℃ for 1min, while the second set was about 120 ~ 220 nm. The Ni nano-masks formed under RTA temperature condition at 850℃ for 1min showed more uniform distributed dimension with smaller standard deviation error bar. Therefore, we performed RTA at 850℃ for 1 min on the later experiments.

(c) Effect of thickness of the Ni film

It is known that the thickness of the Ni film can play an important role in determining Ni nanometer clusters at a given temperature. We have examined the influence of using various Ni initial layer thickness from 50 to 150 Å deposited on Si_3N_4/GaN LED film (second set) to investigate this effect at 850℃ RTA process for 1 min. The nanorod LEDs were then formed using various Ni/Si_3N_4 nano-masks and ICP-RIE. Fig. 4.4 shows the mean dimension and density of GaN-based nanorod LEDs as a function of Ni-mask initial layer thickness from 50 to 150 Å. The nanorod densities increase form $2.2x10^9$ to $3x10^{10}$ cm^{-2} and the dimension decrease from 150 to 60 nm as the Ni film thickness decrease from 150 to 50 Å. Under the same annealing condition, the Ni cluster get larger and dispersed resulting in bigger and dispersed nanorod LEDs. On the other hand, as the Ni initial thickness decrease, it is more easily for Ni migration and Ni clusters dimension size became smaller and denser at the same annealed condition [15].

The transmission electron microscopy (TEM) (JEOL, JEM-200CX) image of the InGaN/GaN MQW nanorod LEDs fabricated by Ni/Si_3N_4 nano-mask (50Å Ni and 850℃ RTA) and ICP-RIE as illustrated in Fig. 4.5 shows that the diameter of the GaN nanorods is approximately 80 nm and the etching depth is about 1 μm. and five pair InGaN/GaN MQWs embedded within the straight nanorod LEDs can be clearly observed. Many TEM images demonstrate that the diameter distribution of the GaN nanorods is average at 60-80 nm.

4.3 Optical properties of the InGaN/GaN MQWs nanorods

The samples were grown by metal-organic chemical vapor deposition with a rotating-disk reactor on a c-axis sapphire (0001) substrate at the growth pressure of 200 mbar. The structure consists of a 50-nm-thick GaN nucleation layer, a 3 μm-thick Si-doped n-GaN buffer layer, an unintentionally doped $In_{0.3}Ga_{0.7}N$/GaN MQW active region, and a 0.1-μm-thick Mg-doped p-GaN. The MQW active region consists of eight periods of 7-nm/15-nm-thick $In_{0.3}Ga_{0.7}N$/GaN well layers and barrier layers. A schematic diagram of $In_{0.3}Ga_{0.7}N$/GaN MQWs nanorods is shown in Fig. 4.6(a). The detailed process conditions of nanorods have been reported elsewhere [16]. The dimension and density of the $In_{0.3}Ga_{0.7}N$/GaN MQWs nanorods were measured by the FESEM (Hitachi, FE-SEM S-5000), TEM (JEOL, JEM-200CX). The density and mean diameter of the $In_{0.3}Ga_{0.7}N$/GaN green emission nanorods as shown in Fig. 4.6(b) of tilted 45° SEM image were estimated to be around 3×10^9 cm^{-2} and 100 nm, respectively. Figure 4.6(c) shows that TEM image of the $In_{0.3}Ga_{0.7}N$/GaN MQW nanorods and the etching depth is about 0.6 μm. In Fig. 4.6(c) eight pairs $In_{0.3}Ga_{0.7}N$/GaN MQWs of 7-nm/15-nm-thick $In_{0.3}Ga_{0.7}N$/GaN well layers and barrier layers embedded within the green emission nanorod can be clearly observed. The In percentage of the QWs was identified by the fitting results in X-ray measurement. The optical properties were studied by PL at temperature between 20 and 300K and by TRPL at 10K and 300K. For the PL measurement, the samples were excited by a 325-nm He-Cd laser line with an excitation power of 25 mW and the emitted luminescence light was collected through a

0.32-m spectrometer with a charge-coupled device detector. The TRPL measurements were carried out using a second-harmonic pulsed Ti:sapphire laser at a wavelength of 400 nm and the time-correlated single photon counting detection system.

a. Photoluminescence measurement

Figure 4.7(a) shows Arrhenius plot of an integrated PL intensity obtained from the $In_{0.3}Ga_{0.7}N$/GaN MQWs active layer emission for the as-grown and nanorod samples over a temperature range from 20 to 300 K. The PL intensity in the green emission nanorods is enhanced by a factor of approximately 3.5 over the as-grown sample emission at room temperature as shown in Fig. 4.7(a). The large emission enhancement could result from improvement either in internal quantum efficiency or external extraction efficiency. In addition, the temperature dependent data in Fig. 4.7(a) were fitted with the following formula: $I_T = I_0/[1+A\ \exp(-E_a/kT)+B\ \exp(-E_b/kT)]$, where the I_T, I_0 are integrated PL intensity for T and 0 K, A and B are constant, k is Boltzmann constant, T is temperature, and E_a is the activation energy for PL quenching, and E_b is generally associated to the free exciton binding energy [17]. The energy E_b of as-grown and nanorods were approximately 6.2 and 7.8 meV, which was similar to the previous report [18]. However, the activation energy E_a of as-grown and nanorod samples were 35 and 79 meV, respectively. Though the high surface ratio around the peripheral of the nanorods could provide many non-radiative recombination paths, the larger activation energy of the green nanorod structure we obtained still demonstrated higher potential barriers for carriers easily localized in the effective potential minima in the nanorod structures [19]. Figure 4.7(b) compares the PL peak energy from the as-grown sample and nanorod samples measured from 20 to 300K. The PL emission peaks were 506.1 nm for the as-grown sample and 499.5 nm for green emission nanorods measured at 300 K. The blue-shift phenomenon of the emission peak from a nanorod structure could be caused by a partial reduction of the piezoelectric field since the 100-nm diameter of the nanorod is too large to result in the quantum confinement effect. Since the blue-shift of 6.6 nm (32.5 meV) corresponds to the reduction in the piezoelectric field caused by the partial strain release, the reduction of the internal field in a quantum well was obtained to be around 32.5 meV/7 nm = 0.05 MV/cm, where 7 nm is the well thickness. The reduction of the internal field could account for part of the reasons in the larger activation energy and emission efficiency due to the better wave-function overlapping between electrons and holes in the nanorod MQWs.

b. TRPL measurement

Figure 4.8 shows the carrier lifetime from the as-grown and green nanorods measured by TRPL at 10K and 300K. Since a purely radiative recombination at T = 10 K can be assumed [20], the radiative lifetime of the nanorod sample is similar to the as-grown sample as approximately 54 ns, indicating that the internal field reduction plays minimal role in emission enhancement. As the temperature increased to 300K, the carrier lifetime were further shortened to 8.7 ns and 16.5 ns for the nanorod and as-grown samples due to the increase of the non-radiative recombination rate. The relatively larger non-radiative recombination rate at room temperature for the nanorod sample was probably due to the increasing surface recombination around the peripheral of nanorods. As a result, the internal quantum efficiency of the nanorod sample at room temperature was not improved, indicating that the total PL intensity enhancement observed from the nanorod samples could result from the increased emission surface providing by the nanorod structures.

We further used a commercially advanced physical model of semiconductor devices (APSYS) software to calculate the spontaneous emission rate from the InGaN quantum well with different internal fields [21] In the gain model, material gain and loss for both bulk and QW as functions of wavelength and carrier density are computed, and the gain spectral function are widened by including many body Coulomb interaction. For this specific simulation, the material dependent parameters are taken from Ref. [22] and the default database values given in the APSYS material macro file [21]. The calculation of the interface charge density including spontaneous and piezoelectric polarization in the ternary III-nitride material as a function of composition and microscopic structure is by the use of ab initio density-functional techniques and Berry phase method [23]. During the simulation, a simple structure that consists of a single 7-nm-thick $In_{0.3}Ga_{0.7}N$ QW and two 15-nm-thick GaN barrier, which are sandwiched between 2-μm-thick n-type GaN and 100-nm-thick p-type GaN, is assumed for the discussion of the strain relaxation effect. The band tiling of the QW may have strong consequences on carrier distribution and affects the output device characteristics. Figure 4.9 shows the radiative recombination rates of the structures with the two different polarization charges in the special location of single-QW. In this calculation, we assumed that the charges at single-QW were with partial 33% screening and partial 20% screening, representing the QW conditions in simulated nanorod and as-grown samples, respectively. The carrier density in the simulated as-grown and nanorod MQW structure was $1.7*10^{18}$ cm^{-3}, which is similar to the carrier density generated in our optical pumping experiment. The calculation results show that the spontaneous emissions at 502 and 510 nm for simulated nanorod and as-grown samples were of similar magnitude, which is the same as the low temperature TRPL result, since this simulation did not take into account the non-radiative recombination. This calculation indicates that the internal field existing in such a 7-nm-thick $In_{0.3}Ga_{0.7}N$ QW was relatively large that partial relaxation by formation of nanorods did not improve radiative recombination rate to a significant extent. As a result, the enhanced PL intensity of the nanorod sample measured at room temperature shown in Fig. 4.9 could be mainly resulted from the increased light extraction efficiency from the large emission surface areas and the multiple scattering paths between nanorods.

In conclusion, we have demonstrated enhanced emission from the green emission nanorods. The enhancement factor is 3.5 from the large emission surface areas and the multiple scattering paths between nanorods. The blue-shift phenomenon of the emission peak from a nanorod structure could be caused by a partial reduction of the piezoelectric field. As the temperature increased to 300K, the carrier lifetime were further shortened to 8.7 ns and 16.5 ns for the nanorod and as-grown samples due to the increase of the non-radiative recombination rate.

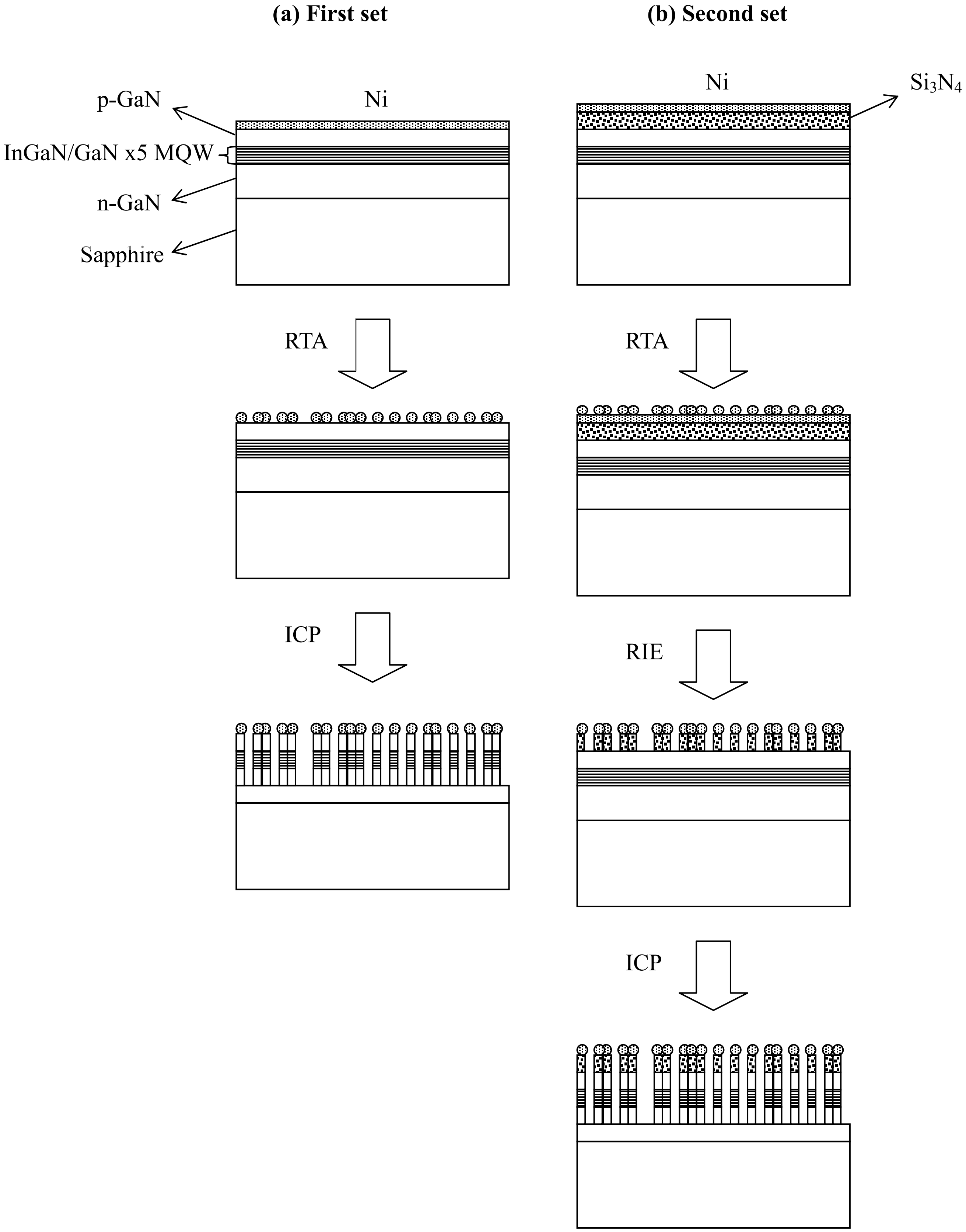

Fig 4.1 Schematic illustration of GaN-based nanorod LEDs' process: using (a) Ni (first set) and (b) Ni/Si_3N_4 (second set) as nano-masks formation. The reaction products after RTA and ICP-RIE etching, leading to the formation of GaN-based nanorod LEDs.

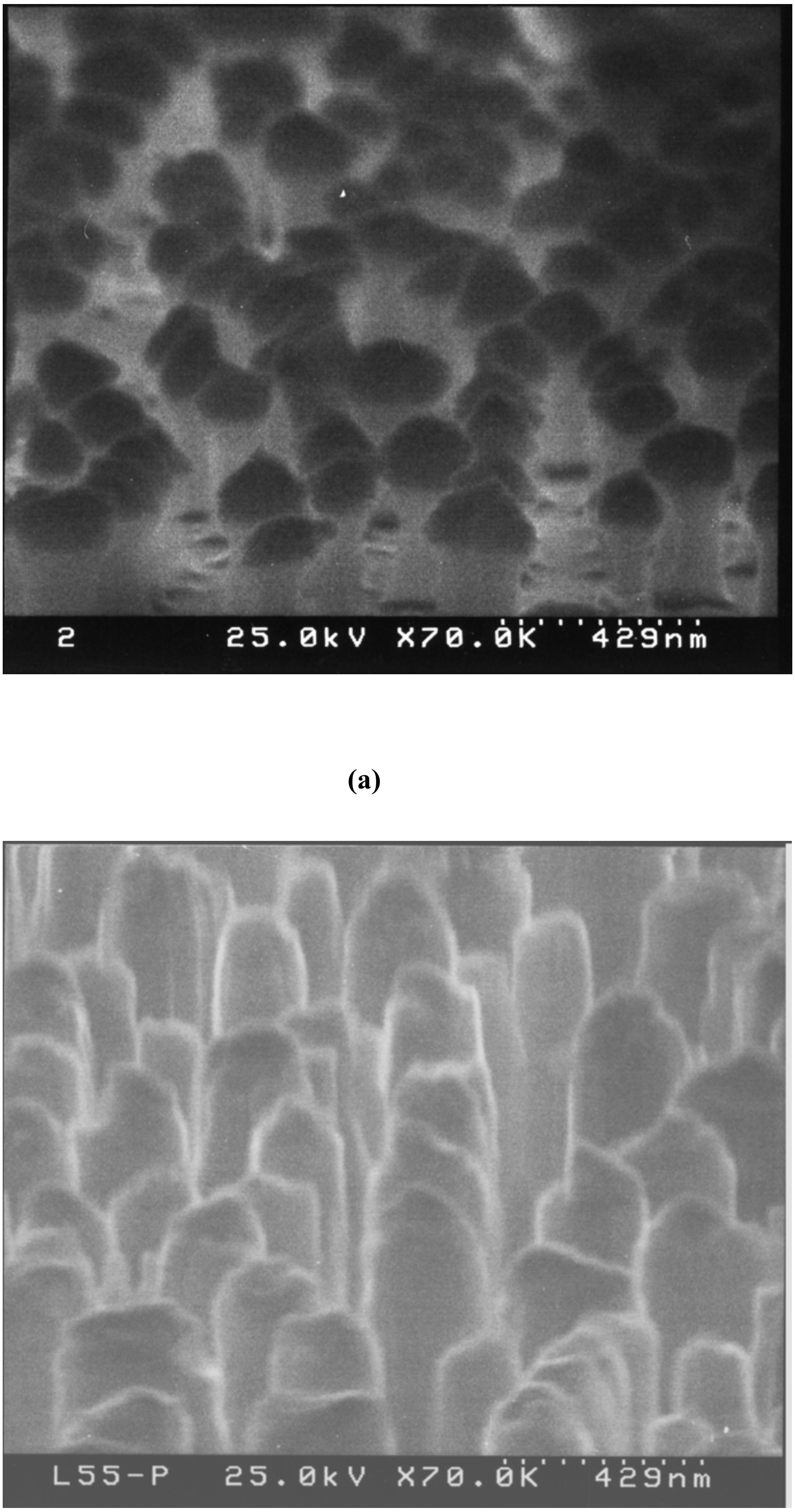

(a)

(b)

Fig. 4.2 The SEM images of GaN-based nanorod LEDs samples: (a) only Ni/Si_3N_4 nano-masks, (b) etching first set sample.

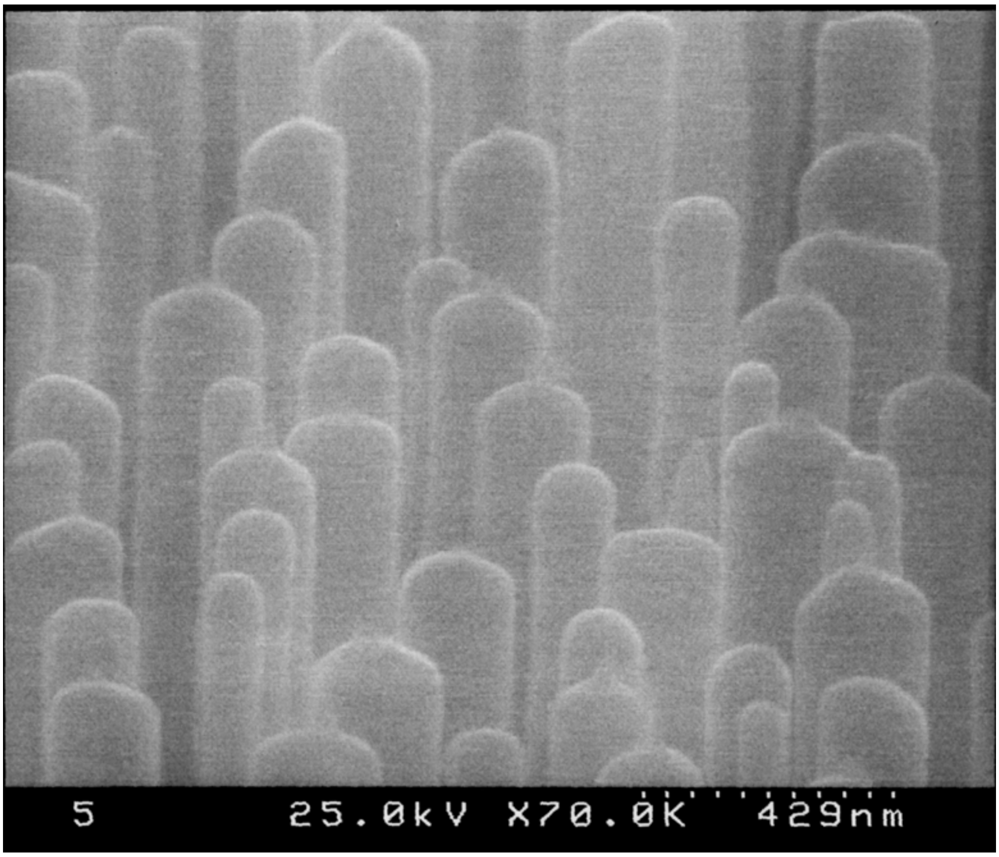

(c)

Fig. 4.2 The SEM image (c) etching second set sample at fixed the same RTA temperature 850^{o}C, annealing time 1min, Cl_2/Ar flow rate of 50/20 sccm, ICP/Bias power of 400/100 W, and chamber pressure of 5mTorr for 3 min of etching time.

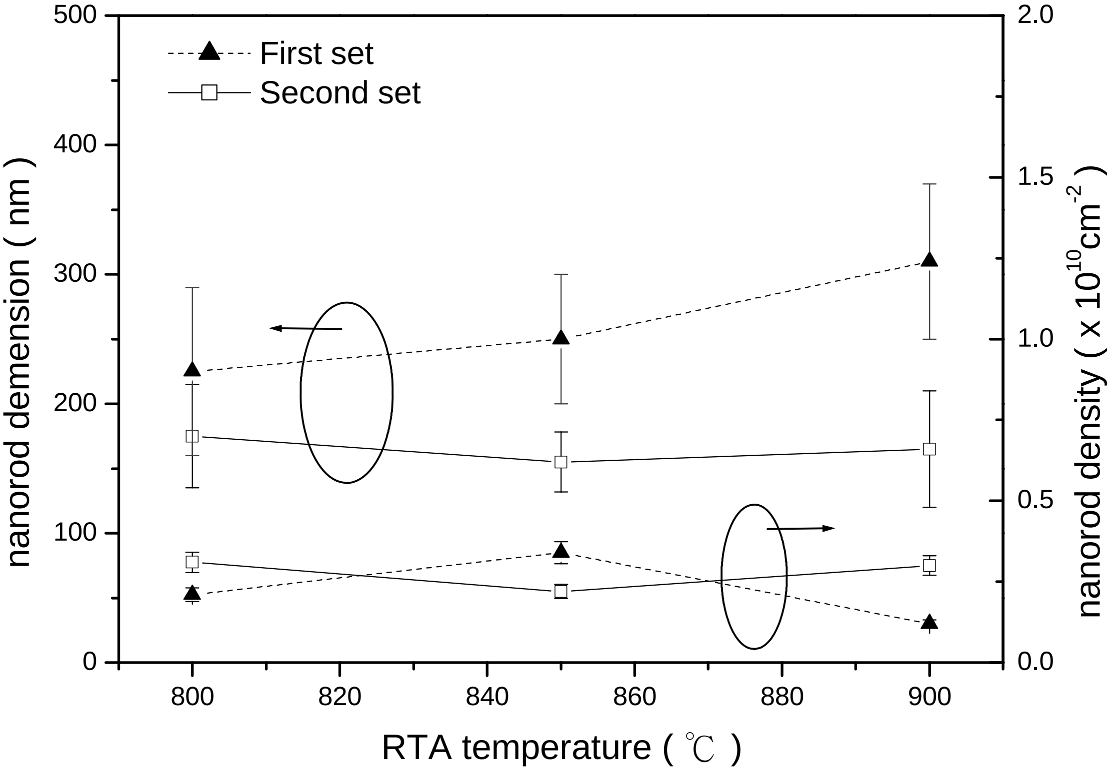

Fig. 4.3 The mean dimension and density of GaN-based nanorod LEDs on first and second set samples as a function of the RTA temperature varies from 800 to 900℃ for 1min with Cl_2/Ar flow rate of 50/20 sccm, ICP/Bias power of 400/100 W, and chamber pressure of 5mTorr for 3 min of etching time.

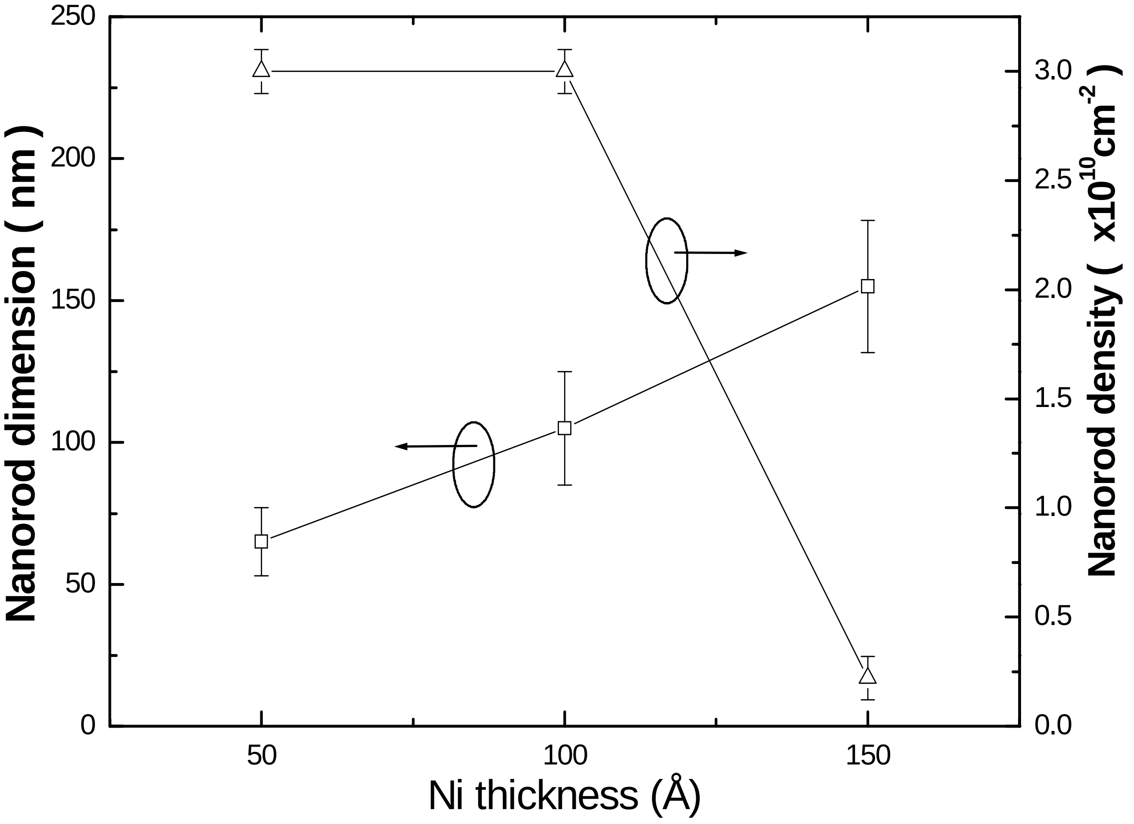

Fig. 4.4 The mean dimension and density of GaN-based nanorod LEDs on second set samples as a function of the Ni film thickness varies from 50 to 150 Å at the same RTA 850℃ for 1min with Cl_2/Ar flow rate of 50/20 sccm, ICP/Bias power of 400/100 W, and chamber pressure of 5mTorr for 3 min of etching time.

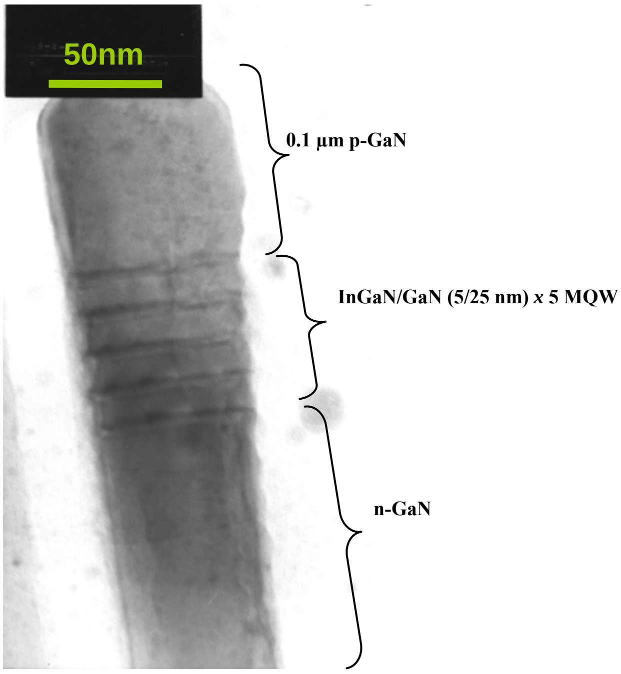

Fig. 4.5 TEM image of a single InGaN/GaN MQW nanorod.

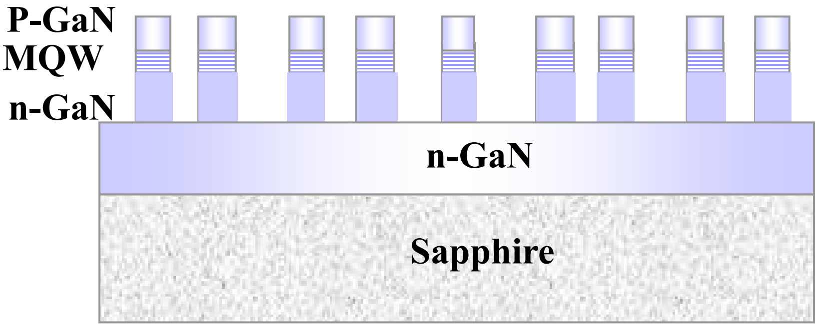

(a)

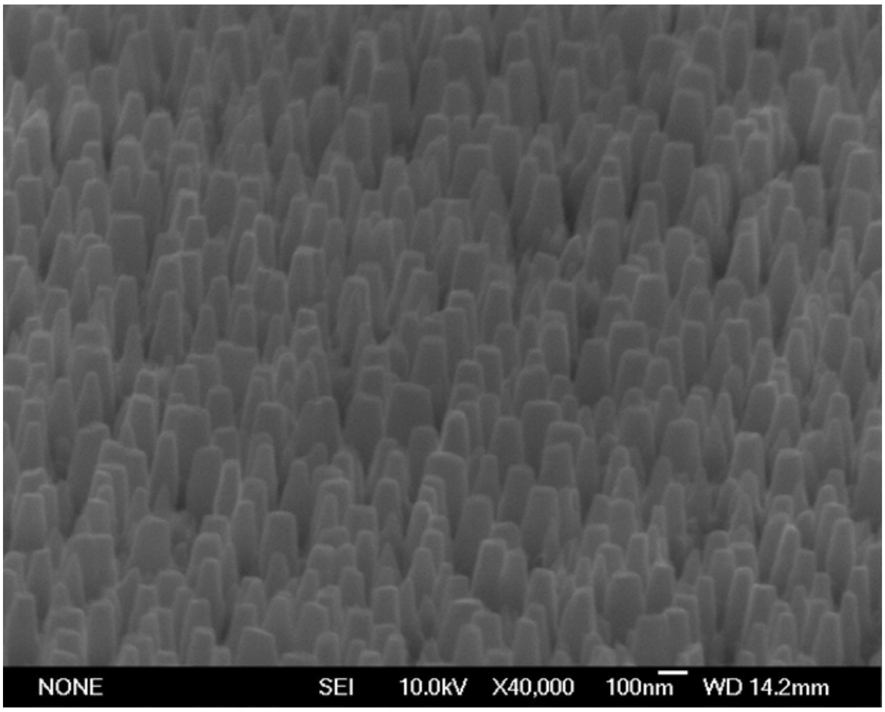

(b)

Fig. 4.6 (a) A schematic diagram of $In_{0.3}Ga_{0.7}N$/GaN MQWs green emission nanorods structure. (b) Tilted 45° SEM image of $In_{0.3}Ga_{0.7}N$/GaN MQWs green emission nanorods.

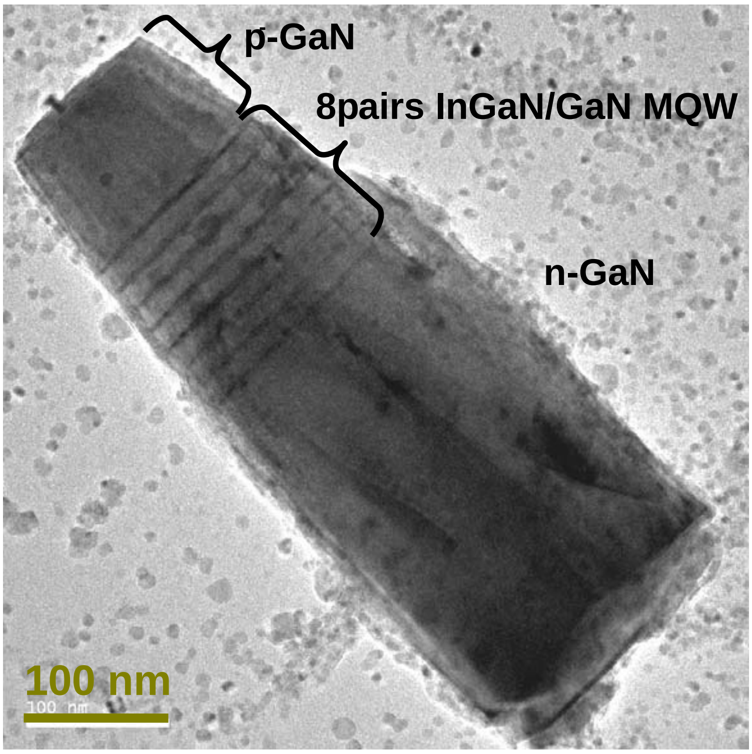

(c)

Fig. 4.6 (c) TEM images of $In_{0.3}Ga_{0.7}N$/GaN MQWs green emission nanorods.

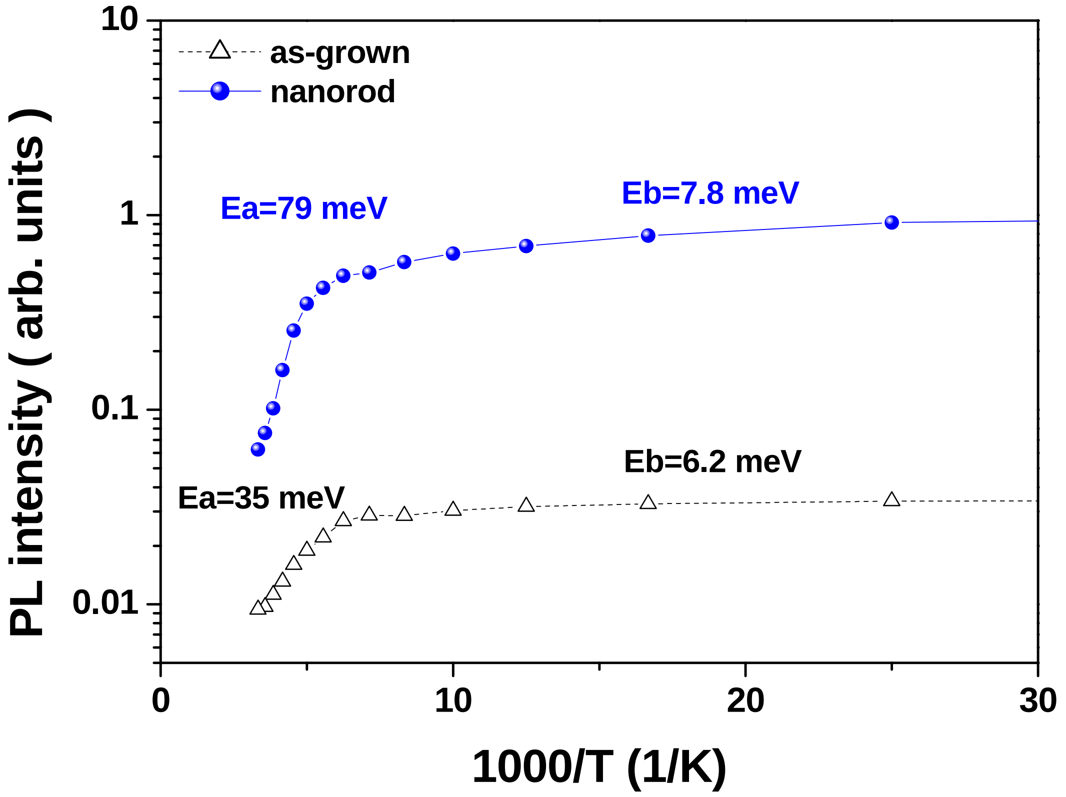

(a)

Fig. 4.7(a) The Arrhenius plot of an integrated PL intensity obtained from the $In_{0.3}Ga_{0.7}N/GaN$ MQWs active layer emission over a temperature range from 20 to 300 K.

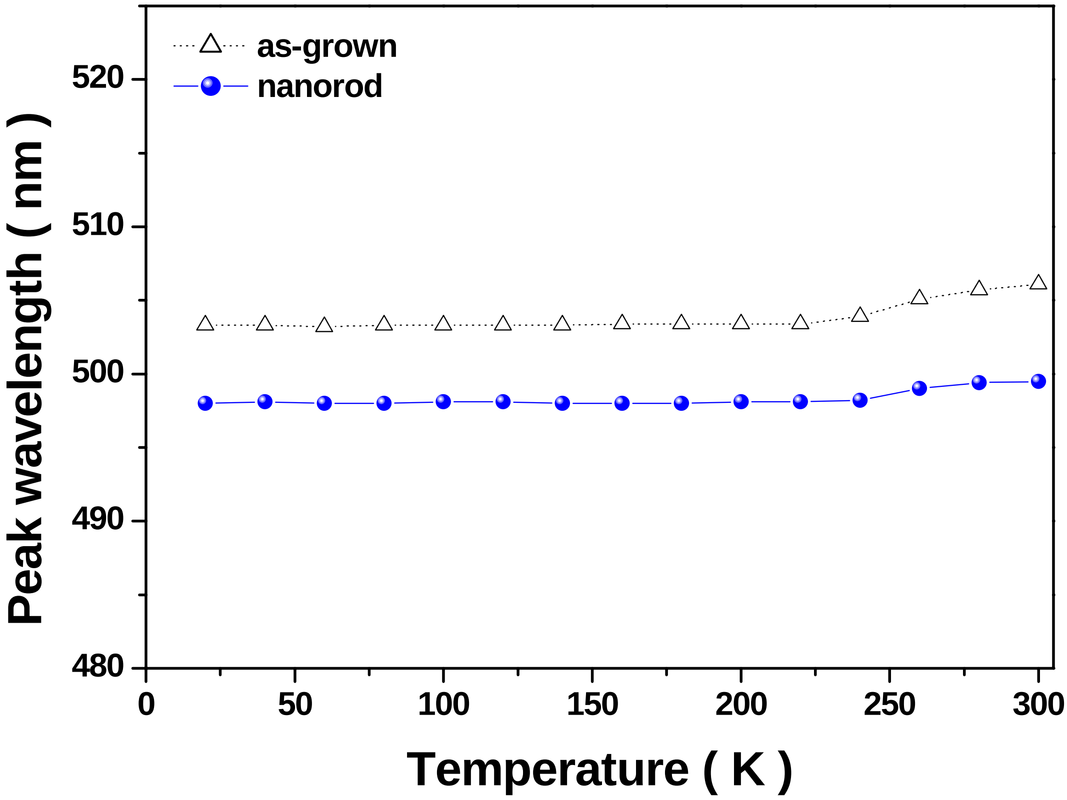

(b)

Fig. 4.7(b) Comparing the PL spectra from as-grown and green emission nanorods of excited by a 325 nm He-Cd laser from 20 to 300K.

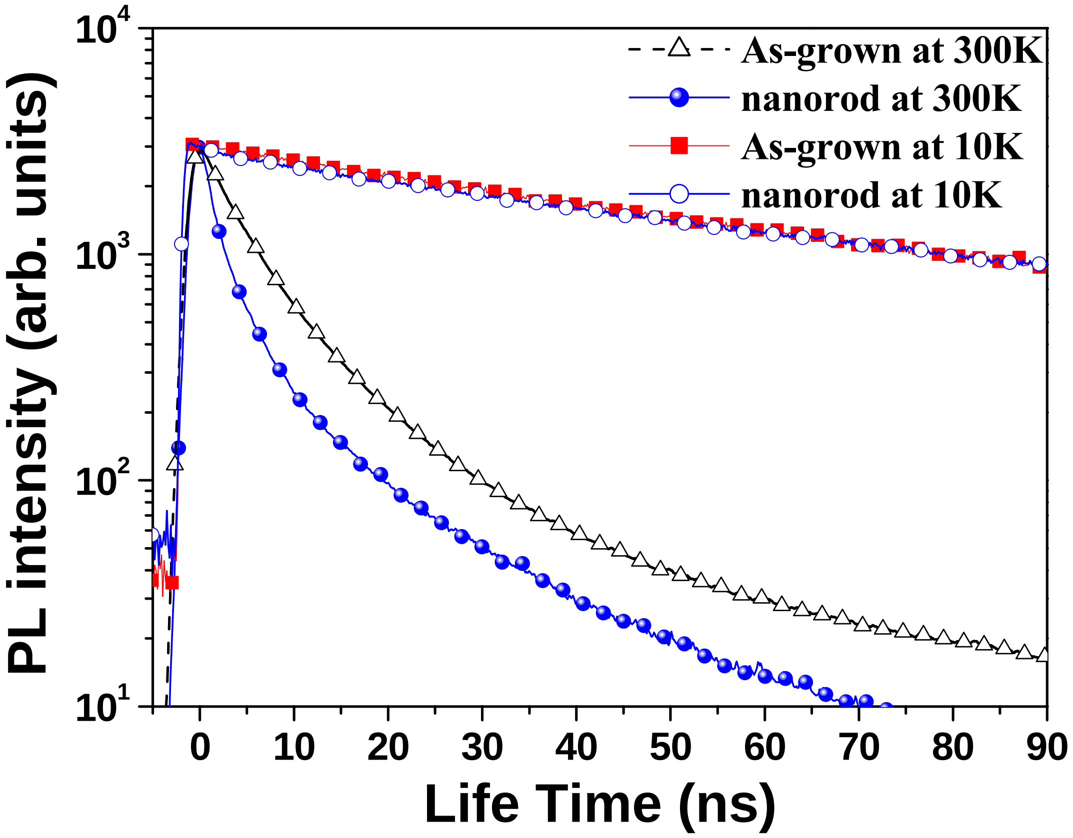

Fig. 4.8 TRPL life time curves of the $In_{0.3}Ga_{0.7}N$/GaN MQW as-grown and green emission nanorod samples for the main InGaN emission peak measured at 10K and 300K.

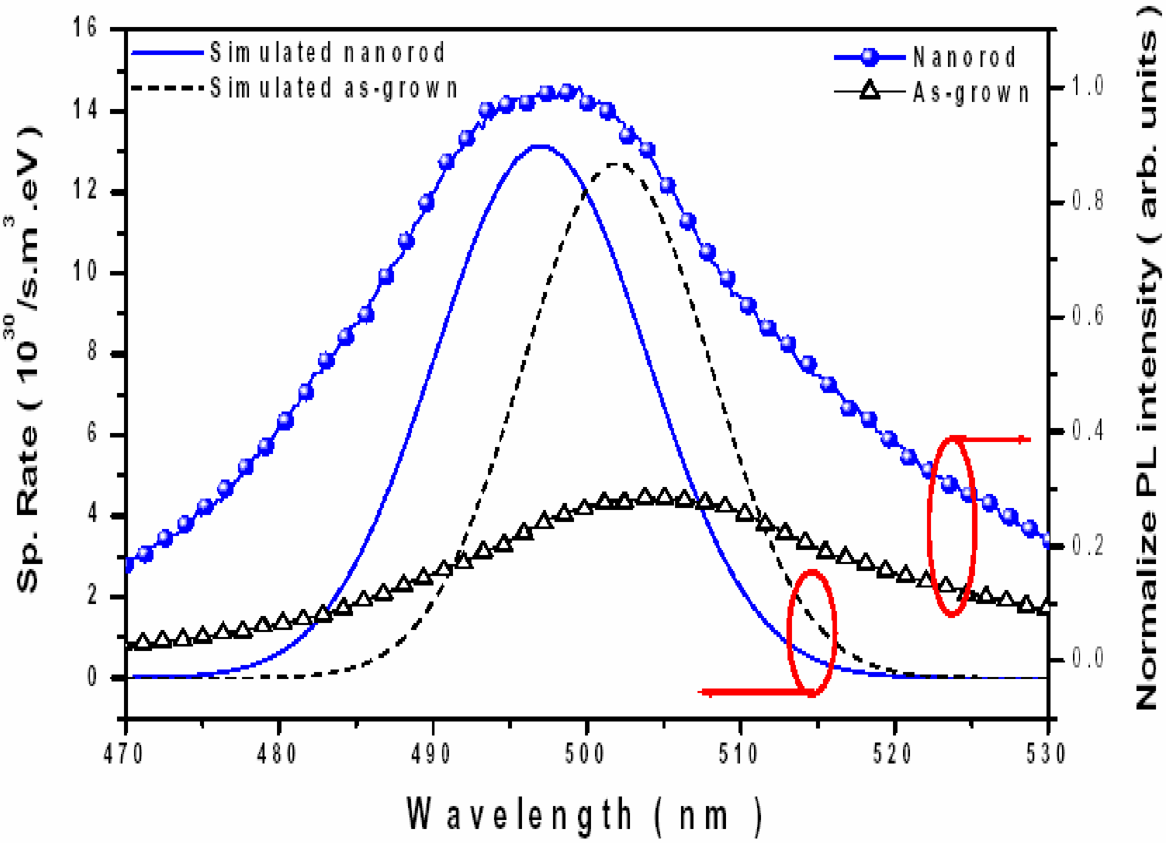

Fig. 4.9 Radiative recombination rates of the structures with the two different polarization charges in the special location of single-QW.

REFERENCE

[1] S. Nakamura, M. Senoh, N. Iwasa and S. Nagahama : Jpn. J. Appl. Phys., 34, L797 (1995).

[2] S. Nakamura, T. Mokia and M. Senoh : Appl. Phys. Lett. 64, 1689 (1994).

[3] C. C. Yu, C. F. Chu, J. Y. Tsai, H. W. Huang, T. H. Hsueh, C. F. Lin and S. C. Wang : Jpn. J. Appl. Phys., 41, L910 (2002).

[4] M. T. Bjork, B. J. Ohisson, T. Sass, A. I. Persson, C. Thelander, M. H. Magnusson, K. Deppert, L. R. Wallenberg and L. Samuelson : Appl. Phys. Lett. 80, 1058 (2002).

[5] M. S. Gudiksen, L. J. Lauhon, J. Wang, D. C. Smith and C. M. Lieber : Nature 415, 617 (2002).

[6] W. Han, S. Fan, Q. Li and Y. Hu : Science 277, 1287 (1997).

[7] G. S. Cheng, L. D. Zhang, Y. Zhu, G. T. Fei, L. Li, C. M. Mo and Y. Q. Mao : Appl. Phys. Lett. 75, 2455 (1999).

[8] C. C. Tang, S. S. Fan, M. L. de la Chapelle and P. Li : Chem. Phys. Lett. 333, 12 (2001).

[9] X. Duan and C. Lieber : J. Am. Chem. Soc. 122, 188 (2000).

[10] H. Peng, X. Zhou, N. Wang, Y. Zheng, L. Liao, W. Shi, C. Lee and S. Lee : Chem. Phys. Lett. 327, 263 (2000).

[11] W. Q Han and A. Zettl : Appl. Phys. Lett. 80, 303 (2002).

[12] C. Youtesy, L. T. Romano and I. Adesida : Appl. Phys. Lett. 73, 797 (1998).

[13] C. Youtesy, L. T. Romano, R. J. Molnar and I. Adesida : Appl. Phys. Lett. 74, 3537 (1999).

[14] P. Visconti, K. M. Jones, M. A. Reshchikov, R. Cingolani, R. J. Molnar and H. Morkoc : Appl. Phys. Lett. 77, 3532 (2000).

[15] J. D. Carey, L. L. Ong and S. R. P. Silva . Nanotechnology 14, 1223 (2003).

[16] H. W. Huang, C. C. Kao, T. H. Hsueh, C. C. Yu, C. F. Lin, J. T. Chu, H. C. Kuo, and S. C. Wang, Mater. Sci. & Eng. B 113, 125 (2004).

[17] C. C. Yu, C. F. Chu, J. Y. Tsai, C. F. Lin, S. C. Wang, J. Appl. Phys. 92, 1881 (2002).

[18] Y. L. Lai and C. P. Liu, Y. H. Lin and R. M. Lin, D. Y. Lyu, Z. X. Peng, and T. Y. Lin, Appl. Phys. Lett. 89, 151906 (2006).

[19] Y. H. Cho, S. K. Lee, H. S. Kwack, J. Y. Kim, and K. S. Lim H. M. Kim, T. W. Kang S. N. Lee, M. S. Seon, O. H. Nam, and Y. J. Park Appl. Phys. Lett. 83, 2578 (2003).

[20] E. Deleporte, J. Martinez-Pastor, A. Filoramo, D. Batovski, Ph. Roussignol, C. Delalande, C. Morhain, E. Tournié, and J. P. Faurie, IL NUOVO CIMENTO 17 , 1436 (1995).

[21] APSYS User’s Manual Crosslight Inc. Software, Canada. Available online at web page

http://www.crosslight.ca.

[22] Y. A. Chang, S. H. Yen, T. C. Wang, H. C. Kuo, Y. K. Kuo, T. C. Lu, and S. C. Wang, Semicond. Sci. Technol. 21, 598 (2006).

[23] Bernardini F and Fiorentini V, Phys. Stat. Sol. (a) 190, 65 (2002).

CHAPTER 5

Fabrication of InGaN/GaN nanorod light emitting diodes with self-assembled Ni metal islands

5.1 Introduction

Direct wide-bandgap gallium nitride (GaN) and other Ⅲ-nitride based semiconductors have attracted much attention for potential applications such as blue, green, and ultraviolet (UV) light emitting diodes (LEDs) and blue laser diodes [1-3]. Additionally, it has been widely proposed that fabricating nano-structures on the LEDs can enhance the performance effectively due to the quantum confinement and strain releasing effect [4]. For GaN-based nanoscale structures, so far, the GaN nanorods have been produced by various fabrication methods, such as growth of InGaN/GaN multiple quantum nanocolumns/nanorods on Si substrate by RF plasma-assisted molecular-beam epitaxy [5-6] or growth of single crystal GaN nanorods by hybrid vapor phase epitaxy [7], synthesis using carbon nanotube as templates [8], inductively coupled plasma reactive ion etching (ICP-RIE) without masks [9] or via E-Beam patterned [10] nanorods, all along with relatively complicated process. To simplify the patterning process, it is possible to produce nanoscale self-assembled nickel (Ni) islands by choosing the correct Ni layer thickness, annealing time and annealing temperature on the top of the LED surface [11]. Nevertheless, it was believed that a large leakage current existed in nanorod structures because the rough sidewall of nanorods etched by ICP-RIE could result in poor electrical properties. In this paper, we introduce a novel method combining ICP-RIE and photo-enhanced chemical (PEC) wet oxidation process with self-assembled Ni metal islands to fabricate InGaN/GaN nanorod LEDs. After the process of nanorod formation, the sidewall of the nanorods and ICP etched layers were oxidized to produce Ga_2O_3 layers, which can isolate nanorods electrically. Structural and optical properties of the nanorod LEDs were examined with field-emission scanning electron microscope (FESEM), photoluminescence (PL) and electroluminescence (EL) measurements.

5.2 Experiments

The GaN-based LED layer structures were grown by metal-organic chemical vapor deposition (MOCVD) with a rotating-disk reactor (Emcore D75^{TM}) on a c-axis sapphire (0001) substrate at the growth pressure of 200 mbar. Trimethylgallium (TMG), Trimethylaluminum (TMA), ammonia, CP_2Mg and Si_2H_6 were used as sources of Ga, Al, N, Mg and Si. The LED structure includes a 50 nm-thick GaN nucleation buffer layer grown at 550 ^{o}C, a 3.0 μm-thick highly conductive Si-doped GaN layer grown at 1050^{o}C, an active region of undoped multiple quantum wells (MQW) consisting five periods of 3/7 nm-thick $In_{0.21}Ga_{0.79}N$/GaN multiple quantum wells grown at 770^{o}C, a 50 nm-thick Mg-doped AlGaN layer grown at 1050^{o}C and a 0.25 μm-thick Mg-doped GaN grown at 1050^{o}C. The process flowchart for the nanorod LED with PEC oxidation process was shown in Fig. 5.1. First, a 100 Å Ni layer was deposited on the top of LED samples by E-gun evaporator. The Ni-coated LED samples were subsequently sent for rapid temperature annealing (RTA) under the N_2 atmosphere of 5 standard litres per minute (SLPM) at temperature of 850^{o}C for 1 min to form self-assembled Ni metal clusters.[4, 12] Then, the LED samples were etched down to the n-type GaN layer by ICP-RIE system (SAMCO ICP-RIE 101iPH) operated at 13.56 MHz. The etching conditions are listed as followed: a gas mixture condition of Cl2/Ar=50/20sccm with a ICP power, bias power set at 400/100W, and a chamber pressure of 5mTorr, and the etching time is 2 min to etch the LED samples down to the n-type GaN layer to form nanorods consisted of InGaN/GaN MQWs. Then, the samples were dipped into a nitric acid solution (HNO_3) at temperatures of 100^{o}C for 5 min to remove the Ni nano-masks followed by the PEC oxidation process. An 800 W Hg lamp was used as the illumination source in the PEC oxidation process. Unstirred deionized

(DI) water was used as the solution during the PEC process. An external dc bias fixed at positive 20 V was applied to the n-type GaN layer surface as the anode contact and platinum (Pt) as the cathode for 10 min as the exposure time. Positive charges (holes) occurred on the GaN:Si layer that attracted OH^- ions in the DI water. Light power density was fixed at 2.5 W/cm^2 from the front-side of LED samples. Then, the Ga_2O_3 layer, which was identified by the energy dispersive X-ray spectra analysis, was formed at the nanorods sidewall and the ICP etched n-type GaN layer. The p-type layer was nearly unoxidized because the conductivity of p-type layer is lower than the n-type layer. Most of the positive charges (holes) were accumulated at the n-type surface to attract the OH^- ions in the DI water under the positive bias applied on the n-type surface [13]. Finally, a 20/500 nm-thick Ni/Au layer was deposited on the entire surface of the PEC nanorods LED to form a connection with the p-type ohmic contacts of each individual nanorods. Finally, 20/800 nm-thick Cr/Au was deposited onto the p and n bonding layer electrode.

After all processes of nanorod LEDs were done, the dimensions and density of the nanorods LED with and without PEC oxidation process samples were estimated by the FESEM (JEOL-7000). Figure 5.2 shows the (a) SEM image of the Ni nanomasks on the p-GaN surface of a LED sample. The SEM image in Fig. 5.2(a) shows that the size and density of the self-assembled Ni masks were approximately 250 nm and $3x10^9$ cm^{-2}, and the height of the Ni clusters was approximately 125 nm when the original Ni thickness was 10 nm under RTA conditions of 850^oC for 1 min. The InGaN/GaN MQW nanorods density was estimated to be approximately 3×10^9 cm^{-2}, and the diameter of nanorods was about 140 nm and the etching depth was about 0.5 μm. The SEM image of in Fig. 5.2(c) shows the InGaN/GaN MQW nanorods LED after PEC process, left side shows the nanorods with PEC process and right side shows ICP-RIE etching surface after PEC process. The SEM image of in Fig. 5.2(d) shows the Ni/Au contact metal deposited on InGaN/GaN MQW nanorods to form connections with the p-type ohmic contacts for each individual nanorod.

The optical properties were studied by PL and EL measurement at room temperature. All LED samples were excited by a 325 nm He-Cd laser with an excitation power of 25 mW for PL spectrum measurement. The as-grown LED and nanorod LED samples with PEC oxidation process were excited under applying 1 mA driving current for EL spectrum measurement. Both the excited lights were collected through a 0.32 m spectrometer with a charge-coupled device (CCD) detector.

5.3 Photoluminescence measurement

Fig. 5.3 shows the normalized PL spectrum of the as-grown LED sample, nanorods LED samples with and without PEC process, all measured at room temperature. The energy of the excitation light was 3.82 eV (325 nm) and the power density was 1.5 W/cm^2 in all cases. The PL emission peaks of the InGaN/GaN active layer were observed at 449.0 nm (2.76 eV) for as-grown samples, 445.2 nm (2.78 eV) for nanorods samples without PEC oxidation process and 440.4 nm (2.81 eV) for the nanorods samples with PEC oxidation process. The PL peak intensities of InGaN/GaN MQW active layers in samples with and without PEC oxidation process were enhanced by factors of approximately six and five times compared with as-grown LED samples. The blue-shift phenomena were observed both at the nanorod LED samples with and without PEC oxidation process and the blue-shift values were 3.8 nm (20 meV) and 8.6 nm (50 meV), respectively. The blue-shift might be caused by the partial reduction of the piezoelectric field by the strain release in the nanorod structures. The peak shifts can be translated to the reduction of the piezoelectric field at around 20 meV / 3 nm = 66.7 KV / cm and 50 meV / 3 nm = 166.7 KV / cm, for LED samples with and without PEC oxidation process, respectively (3 nm is the well thickness). In addition, the PL intensity was enhanced by a factor of five of the nanorods without PEC and of six of the nanorods with PEC oxidation process. The PL enhancement could be resulted from the side-wall scattering in the nanorod structures. In addition, the enhancement of the PL intensity could be explained by the increased wave-function overlap of the electron and the hole band structure of the InGaN/GaN MQWs with the partially reduced piezoelectric field in InGaN/GaN active layers. One can see that the nanorods with PEC oxidation process have a higher PL intensity and a larger piezoelectric reduction due to the smaller nanorods diameters by the PEC oxidation process. It shows that the PEC oxidation process not only can form an oxidation layer to isolate the individual nanorod electrically, also can reduce the diameter of the nanorods for a stronger strain relaxation effect [10, 15].

5.4 Electroluminescence measurement

Fig. 5.4 shows the normalized EL spectrum of the as-grown LED and nanorod LED samples with PEC process at room temperature at an injection current of 1 mA. The inset of Fig. 5.4 was taken from the top of the InGaN/GaN MQW nanorod LED under a biased condition of about 1 mA. It shows that the PEC oxidation process can effectively form oxidation layers to isolate nanorods and can facilitate contact formation more easily and cost effectively. The EL intensity from nanorods LED with PEC was about 1.76 times that of as-grown LED. The EL MQW emission peaks of the InGaN/GaN active layer were observed at 467.9 nm (2.65 eV) for as-grown samples, 457.4 nm (2.71 eV) for nanorods samples with PEC oxidation process. The blue-shift effect was again observed at the nanorods LED samples with PEC oxidation process with the blue-shift value of 10.5 nm (60 meV), which was similar to the observation in the PL measurement. The inset Fig. 5.4 shows a top-view photograph image taken from the top of nanorod LED with PEC on sapphire substrate at 1mA DC driving current.

In summary, we successful fabricated the InGaN/GaN nanorod LED using self-assembled Ni nano-masks, ICP-RIE etching and PEC process. The PEC process produced Ga_2O_3 oxidation layers surrounding nanorods to provide a better isolation for nanorods to bring p-type GaN nanorods in contact with p-type electrodes more easily. The enhancement by factors of six and five times in photoluminescence intensities of nanorods with and without PEC process compared to that of as-grown structures were observed. The peak wavelength observed from PL measurement showed a blue shift of 3.8 nm of the nanorods without PEC oxidation process and 8.6 nm of the nanorods with PEC oxidation process compared to that of the as-grown LED sample. The blue shift might be attributed to the strain relaxation in the wells for nanorod LEDs. Also, the EL spectrum showed a 10.5 nm blue shift of the nanorods with PEC from that of the as-grown LED sample.

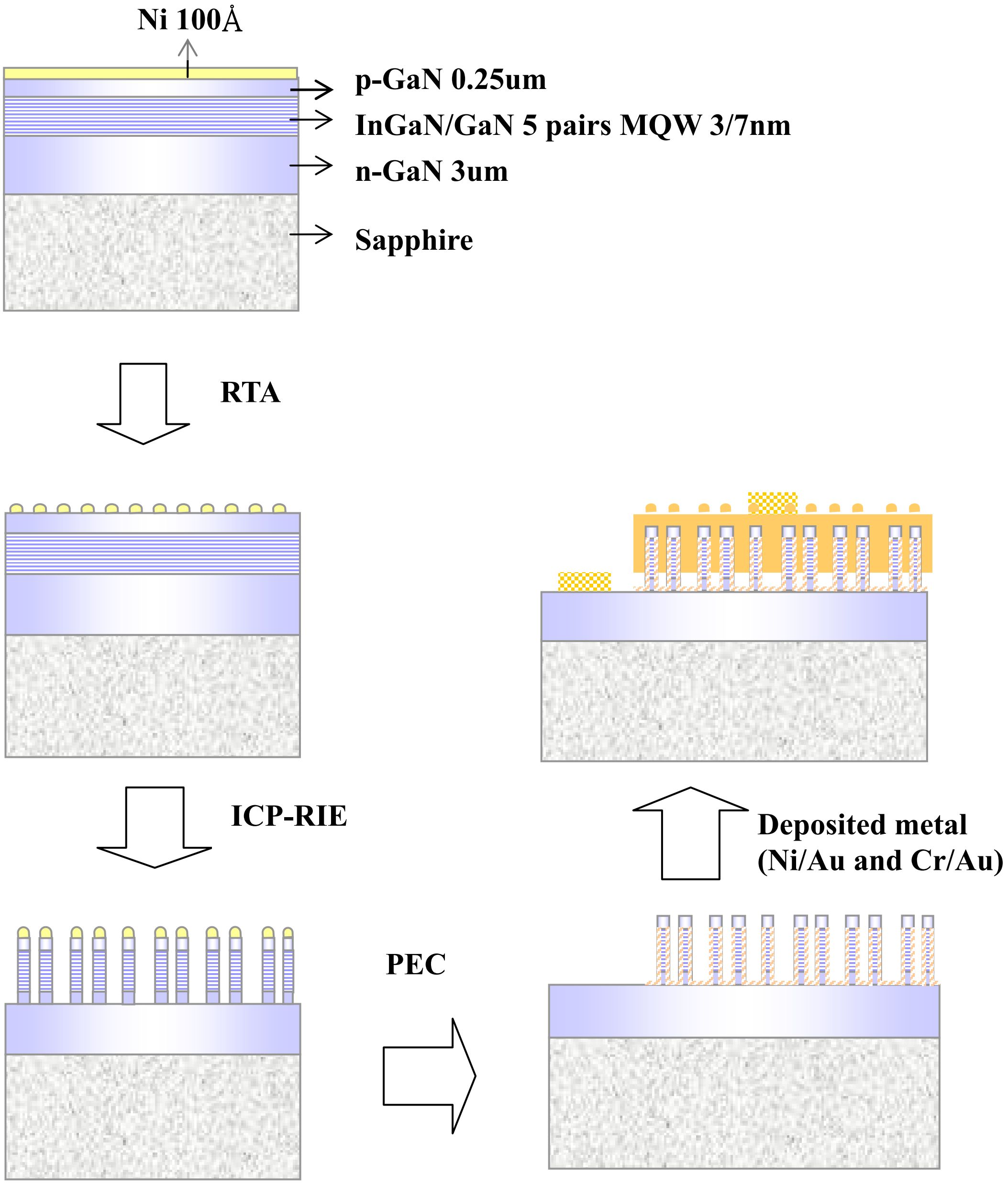

Fig. 5.1 Schematic illustration of process flowchart for InGaN/GaN MQW nanorods LED.

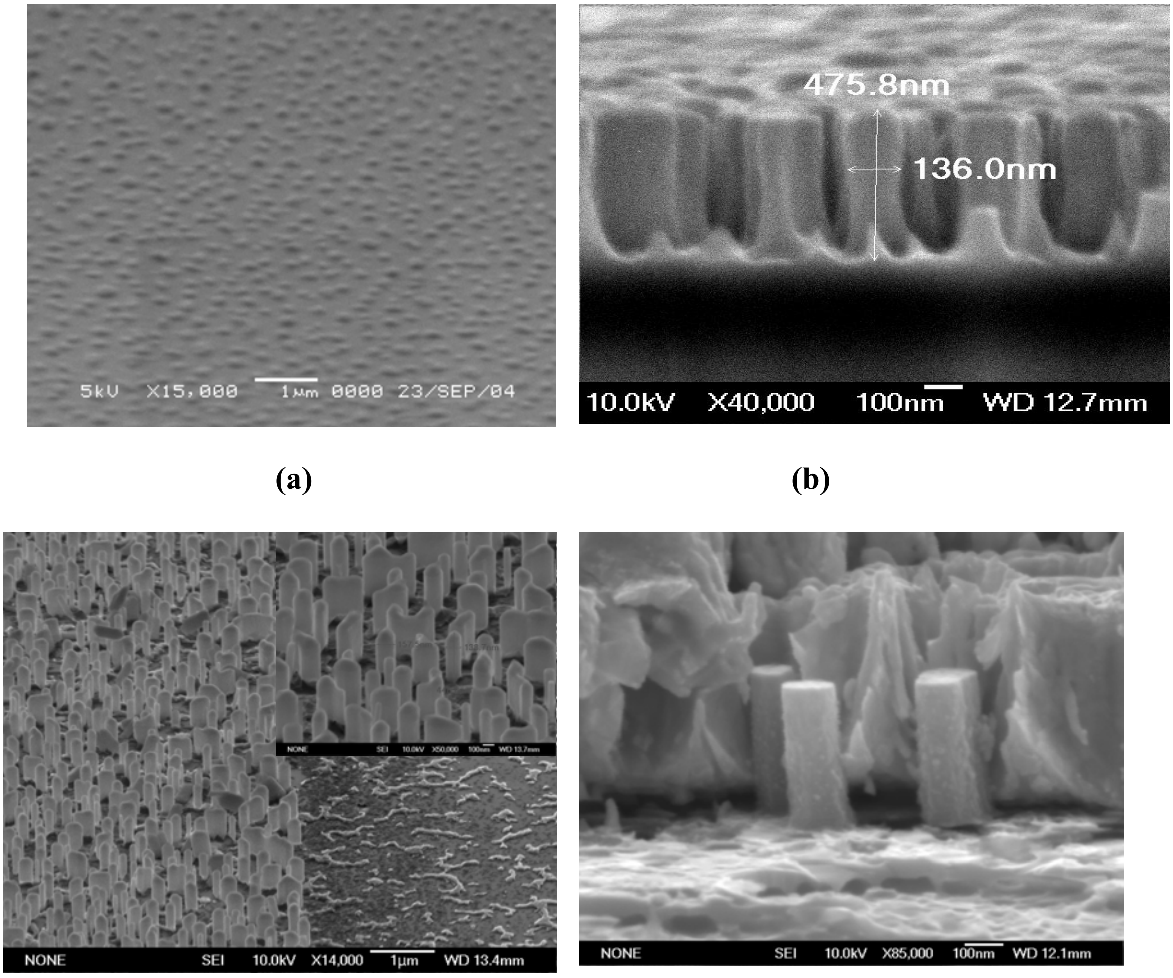

(a) (b)

(c) (d)

Fig. 5.2 the SEM images of (a) Ni nano-masks on p-GaN top surface after RTA process, (b) InGaN/GaN MQW nanorods LED after ICP-RIE etching. (c) InGaN/GaN MQW nanorods LED after PEC process. (d) InGaN/GaN MQW nanorods LED after deposited contact metal.

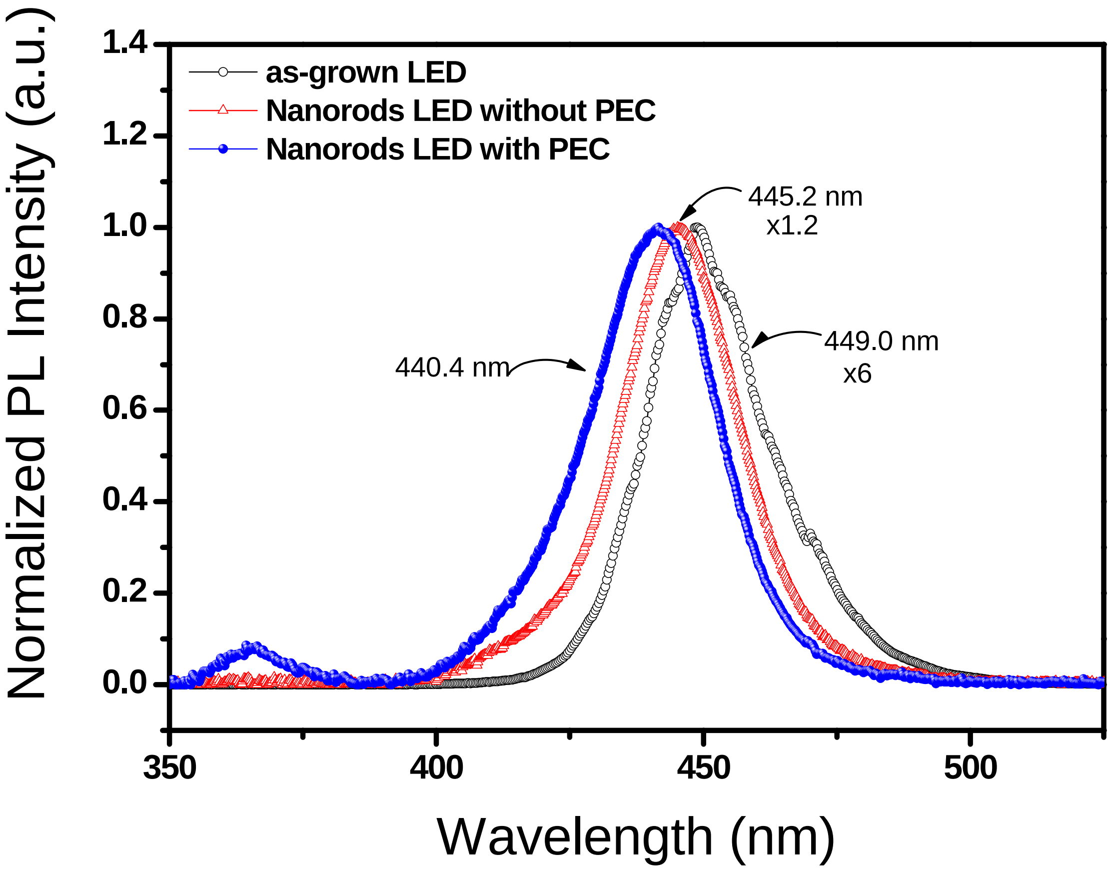

Fig. 5.3 Normalized PL intensity spectra for as-grown LED and nanorods LED with/without PEC at room temperature.

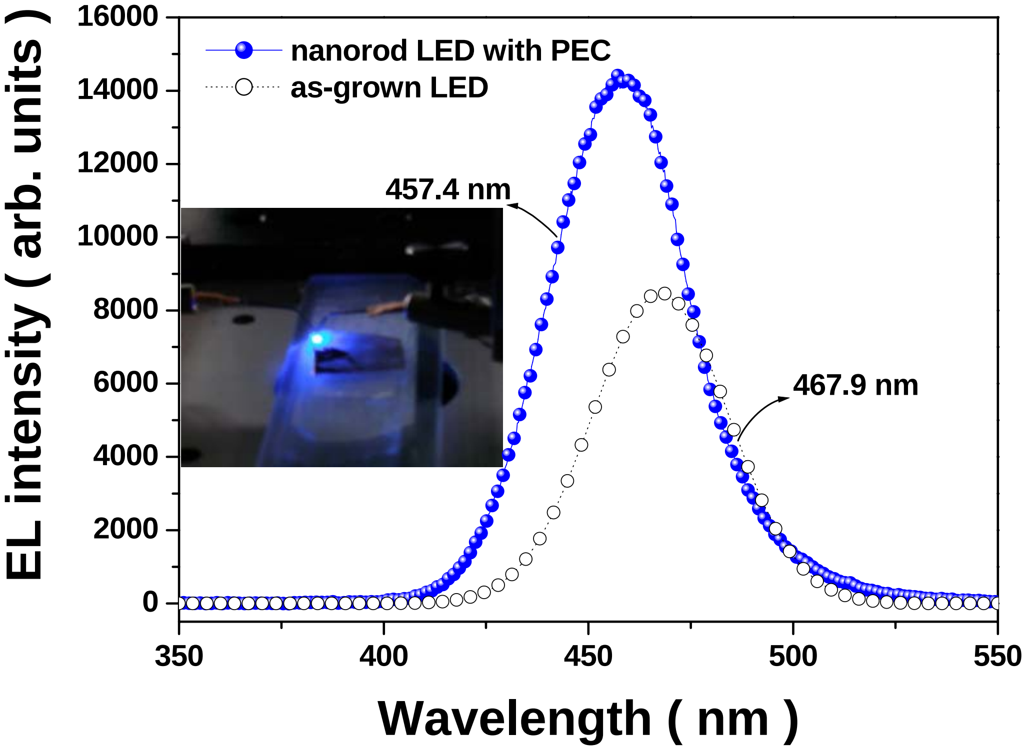

Fig. 5.4 Normalized EL intensity spectra for as-grown LED and nanorods LED with PEC at room temperature. Insets show the top-view photograph image of a blue emission from InGaN/GaN MQW nanorods LED at 1 mA dc current. The inset shows the top-view photograph image of nanorod LED with PEC.

Reference

[1] T. Mukai, M. Yamada, and S. Nakamura, *Jpn. J. Appl. Phys.*38, 3976 (1999).

[2] S. Nakamura, M. Senoh, S. Nagahama, N. Iwasa, T. Yamada, T. Matsushita, H. Kiyoku, and Y. Sugimoto, *Jpn. J. Appl. Phys.* 35, L74 (1996).

[3] I. Akasaki, S. Sota, H. H. Sakai, T. Tanaka, M. Koike, and H. Amano, *Electron. Lett.* 32, 1105 (1996).

[4] T. H. Hsueh, H. W. Huang, C. C. Kao, Y. H. Chang, M. C. Ou-Yang, H. C. Kuo and S. C. Wang, *Jpn. J. Appl. Phys*. 44, 2661 (2005).

[5] T. Kouno, A. Kikuchi, K. Kishino, E. Callja, M. A. S. Garcia, F. J. Sanchez, F. Calle, F. B. Naranjo, E. Munoz, S. I. Molina, A. M. Sanchez, F. J. Pacheco and R. Garcia, 1999 201/202 *J. Cryst. Growt, 201/202,* 296 (1999).

[6] Akihiko Kikuchi, Mizue Kawai, Makoto Tada and Katsumi Kishino, *Jpn. J. Appl. Phys*. 43, L1524 (2004).

[7] H. M. Kim, D. S. Kim, T. W. Kang, Y. H. Cho and K. S. Chung, *Appl. Phys. Lett.* 81, 2193 (2002).

[8] W. Q. Han, S. S. Fan, Q. Q. Li and Y. D. Hu, *Science* 277, 1287 (1997).

[9] C. C. Yu, C. F. Chu, J. Y. Tsai, H. W. Huang, T. H. Hsueh, C. F Lin and S. C. Wang, *Jpn. J. Appl. Phys*. 41, L910 (2002).

[10] H. S. Chen, D. M. Yeh, Y. C. Lu, C. Y. Chen, C. F. Huang, T. Y. Tang, C. C. Yang, C. S. Wu and C. D. Chen, *Nanotechnology* 17, 1454 (2006).

[11] J. D. Carey, L. L. Ong and S. R. P. Silva, *Nanotechnology* 14, 1223 (2003).

[12] H. W. Huang, J. T. Chu, T. H. Hsueh, M. C. Ou-Yang, H. C. Kuo, and S. C. Wang, *J. Vac. Sci. & Tech.* B 24, 1909 (2006).

[13] C. F. Lin, Z. J. Yang, J. H. Z and J. J Dai, *Phot. Tech. Lett*. 17, 2038 (2005).

[14] C. F. Lin, J. H. Zheng, Z. J. Yang, J. J. Dai, D. Y. Lin, C. Y. Chang, Z. X. Lai, and C. S. Hong, *Appl. Phys. Lett.* 88, 083121 (2006).

CHAPTER 6

Summary

In summary, in this dissertation we have studied the nano-structure of GaN-based materials and devices, including their fabrication, electrical and optical phenomena. In the case of surface roughened nano-structure, the enhancement in light output of the InGaN/GaN MQWs nano-roughened LEDs were simultaneously examined with the ASAP simulation. The electrical characteristics of the InGaN/GaN LED was reduced from 3.54 to 3.27V at 20 mA on laser energy was 300mJ/cm^2 and the series resistance was reduced by 32% by the increase in the contact area of the nano-roughened surface. The light output from the nano-roughened LEDs has increased the maximum light output and wall-plug efficiency of 55% and 68% respectively over the conventional InGaN/GaN LEDs at 20 mA when the energy of laser etching was 300 mJ/cm^2.

In the case of InGaN/GaN LEDs with nano-scale textured sidewalls have been fabricated. By using PSs as the etching mask and ICP-etched the epitaxial layers of LEDs to achieve nano-scale textured sidewalls. The electrical characteristics of the 300 μm x 300 μm LED devices are similar to those of conventional LEDs. The LED with nano-scale textured sidewalls increased the output power of the InGaN/GaN MQW LEDs by a factor of 1.3 at 20 mA, indicating that the 300 μm x 300 μm LED with nano-scale textured sidewalls had larger light extraction efficiency. The wall-plug efficiency of nitride-based LED was increased by 30% with textured sidewalls.

The LED with sidewalls roughness increased the light output intensity of the InGaN/GaN MQW LEDs by a factor of 1.26, indicating that the power chip (1mm x 1mm) LED with sidewalls roughness had larger light extraction efficiency at an injection current of 350 mA. The wall-plug efficiency of GaN-based power chip LED was increased by 26.5% with sidewalls roughness at an injection current of 350 mA. After 1000 h life test, it was found that normalized output intensity of power chip LED with sidewall roughness only decreased by 7-11%.

In the case of nano-rods structure, the fabrication and characterization of InGaN/GaN MQWs embedded within nanorods with diameters of about 50 to 250 nm were investigated. Two fabrication technologies of the nanomasks were presented, including with the self-assembled only Ni and Ni/SiN nanomasks. Their optical properties showed that PL and TRPL optical emission spectra from the InGaN/GaN MQWs nanorods, observed by photoluminescence measurement at 300K, reveal a large blueshift of about 32.5 meV and over 3.5 times enhancement in photoluminescence intensity-density compared with that of the as-grown wafer under the same excitation power density. Partial reduction of the piezoelectric field in the etched InGaN/GaN MQWs nanorods was considered to be one of the origins of the blueshift in the photoluminescence spectra. As the temperature increased to 300K of TRPL, the carrier lifetime were further shortened to 8.7 ns and 16.5 ns for the nanorod and as-grown samples due to the increase of the non-radiative recombination rate.

In the case of nano-rods structure, we successful fabricated the InGaN/GaN nanorod LED using self-assembled Ni nano-masks, ICP-RIE etching and PEC process. The enhancement by factors of six and five times in photoluminescence intensities of nanorods with and without PEC process compared to that of as-grown structures were observed. The peak wavelength observed from PL measurement showed a blue-shift of 3.8 nm of the nanorods without PEC oxidation process and 8.6 nm of the nanorods with PEC oxidation process compared to that of the as-grown LED sample. The blue-shift might be attributed to the strain relaxation in the wells for nanorod LEDs. Also, the EL spectrum showed a 10.5 nm blue shift of the nanorods with PEC from that of the as-grown LED sample.

Publication List

(A) Journal Papers :

1. C. C. Yu, C. F. Chu, J. Y. Tsai, **H. W. Huang**, T. H. Hsueh, C. f. Lin, and S. C. Wang, **Japanese Journal of Applied Physics** 41, L910 (2002).

2. **H. W. Huang**, C. C. Kao, T. H. Hsueh, C. C. Yu, C. F. Lin, J. T. Chu, H. C. Kuo, and S. C. Wang, **Materials Science and Engineering B** 113,125 (2004).

3. **H. W. Huang**, C.C. Kao, J.T. Chu, C.C. Yu, C.F. Lin, H.C. Kuo, and S.C. Wang, **Materials Science and Engineering B** 113, 19 (2004).

4. **H. W. Huang**, C.C. Kao, J.Y. Tsai, C.C. Yu, C.F. Chu, J.Y. Lee, S.Y. Kuo, C.F. Lin, H.C. Kuo, and S.C. Wang, **Materials Science and Engineering B** 107, 237 (2004).

5. C. C. Kao, **H. W. Huang**, J. Y. Tsai, C. C. Yu, C. F. Lin, H. C. Kuo, and S. C. Wang, **Materials Science and Engineering B**107, 283 (2004).

6. F. I. Lai, Y. H. Chang, T. H. Hsueh, **H. W. Huang**, L. H. Lai, H. C. Kuo, S. C. Wang, and T. C. Gung, **Materials Science and Engineering B** 113, 203 (2004).

7. T. H. Hsueh, J. K. Sheu, **H. W. Huang**, Y. H. Chang, M. C. Ou-Yang, J. K. Sheu, H. C. Kuo, and S. C. Wang, **Japanese Journal of Applied Physics** part 1, 44, 7723 (2005).

8. **H. W. Huang**, C. C. Kao, J. T. Chu, C. C. Yu, H. C. Kuo, and S. C. Wang, **IEEE Photonics Technology Letters** 17, 5, (2005).

9. T. H. Hsueh, J. K. Sheu, **H. W. Huang**, J. Y. Chu, C. C. Kao, H. C. Kuo, and S. C. Wang, **IEEE Photonics Technology Letters** 17, 1163 (2005).

10. J. T. Chu, **H. W. Huang**, C. C. Kao, W. D. Liang, F. I. Lai, C. F. Chu, H. C. Kuo, and S. C. Wang, **Japanese Journal of Applied Physics.,** 44, 2509 (2005).

11. J. T. Chu, C. C. Kao, **H. W. Huang**, W. D. Liang, C. F. Chu, T. C. Lu, H. C. Kuo, and S. C. Wang, **Japanese Journal of Applied Physics**, 44, 7910 (2005).

12. Y. H. Chang, T. H. Hsueh, F. I. Lai, C. W. Chang, C. C. Yu, **H. W. Huang**, C. F. Lin, H. C. Kuo, and S. C. Wang, **Japanese Journal of Applied Physics** 44, 2657 (2005).

13. C. C. Kao, Y. C. Peng, H. H. Yao, J. Y. Tsai, Y. H. Chang, J. T. Chu, **H. W. Huang**, T. T. Kao, T. C. Lu, H. C. Kuo, S. C. Wang, and C. F. Lin, **Appl. Phy. Lett.** 87, 081105 (2005).

14. T. H. Hsueh, **H. W. Huang**, C. C. Kao, Y. H. Chang, M-C O. Yang, H. C. Kuo and S. C. Wang, **Japanese Journal of Applied Physics** 44, 2661 (2005).

15. T. H. Hsueh, **H. W. Huang**, F. I. Lai, J. K. Sheu, Y. H. Chang, H. C. Kuo, and S. C. Wang, **Nanotechnology** 16, 448 (2005).

16. **H. W. Huang**, J. T. Chu, C. C. Kao, T. H. Hsueh, C. C. Yu, H. C. Kuo, and S. C. Wang, **Nanotechnology** 16, 1(2005).

17. C. C. Kao, H. C. Kuo, **H. W. Huang**, J. T. Chu, Y. C. Peng; C. C. Yu; C. F. Lin, and S. C. Wang, **IEEE Photonics Technology Letters** 17, 19, (2005).

18. C. C. Kao, T. C. Lu, **H. W. Huang**, J. T. Chu, Y. C. Peng, H. H. Yao, J. Y. Tsai, T. T. Kao, H. C. Kuo, S. C. Wang, and C. F. Lin, **IEEE Photonics Technology Letters**, 18, 877 (2006).

19. **H. W. Huang**, C.C. Kao, Y.A. Chang, H.C. Kuo ., L.H. Laih, and S.C. Wang, **Materials Chemistry and Physics** 97, 10 (2006).

20. F. I. Lai, S. Y. Kuo, Y. H. Chang, **H. W. Huang**, C. W. Chang, C. C. Yu, C. F. Lin, H. C. Kuo, and S. C. Wang, **J. Vac. Sci. Technol. B** 24, 1123 (2006).

21. **H. W. Huang**, J. T. Chu, T. H. Hsueh, M. C. Ou-Yang, H. C. Kuo, and S. C. Wang, **J. Vac. Sci. Technol. B** 24, 1909 (2006).

22. C. H. Lin, C. F. Lai, T. S. Ko, **H. W. Huang**, H. C. Kuo, Y. Y. Hung, K. M. Leung, C. C. Yu, R. J. Tsai, C. K. Lee, T. C. Lu, and S. C. Wang, **IEEE Photonics Technology Letters** 18, 2050 (2006).

23. **H. W. Huang**, H. C. Kuo, J. T. Chu, C. F. Lai, C.C. Kao, T. C. Lu, and S. C. Wang R. J. Tsai, C. C. Yu C. F. Lin, **Nanotechnology** 17, 1(2006).

24. **H. W. Huang**, J. T. Chu, C. C. Kao, T. H. Hsueh, T. C. Lu, H. C. Kuo, S. C. Wang, C. C. Yu, and S. Y. Kuo, **Japanese Journal of Applied Physics** 45 (4B), 3442 (2006).

25. Y. C. Peng, C. C. Kao, **H. W. Huang**, J. T. Chu, T. C. Lu, H. C. Kuo, S. C. Wang, and C. C. Yu, **Japanese Journal of Applied Physics.** 45 (4B), 3446 (2006).

26. C. C. Kao, T. C. Lu, **H. W. Huang**, J. T. Chu, Y. C. Peng, H. H. Yao, J. Y. Tsai, T. T. Kao,H. C. Kuo, S. C. Wang, and C. F. Lin, **IEEE Photonics Technology Letters** 18, 877 (2006).

27. **H. W. Huang**, C.C. Kao, J.T. Chu, W.D. Liang, H.C. Kuo, S.C. Wang, and C.C. Yu, **Materials Chemistry and Physics** 99, 414 (2006).

28. **H. W. Huang**, C. F. Lai, W. C. Wang, T. C. Lu, H. C. Kuo, S. C. Wang, R. J. Tsai, and C. C. Yu, **Electrochem. Solid-State Lett.** 10, H59 (2007).

29. **H. W. Huang**, C. C. Kao, J. T. Chu, W. C. Wang, T. C. Lu, H. C. Kuo, S. C. Wang C. C. Yu, and S. Y. Kuo, **Materials Science and Engineering B** 113, 19 (2007).
30. **H. W. Huang**, H. C. Kuo, C. F. Lai, C. E. Lee, C. W. Chiu; T. C. Lu, S. C. Wang, C. H. Lin, and K. M. Leung, **IEEE Photonics Technology Letters** 19, 565 (2007)

(B) Conference Papers:

1. C. C. Yu, C. F. Chu, J. Y. Tsai, **H. W. Huang**, T. H. Hsueh, C. f. Lin, and S. C. Wang, **International Symposium on Compound Semiconductors(ISCS 2002)**, Switzerland (2002).

2. **H. W. Huang**, C. C. Yu, J. Y. Tsai, T. H. Hsueh, C. F. Chu, C. F. Lin, and S. C. Wang, **2002 MRS Spring Meeting**, U.S.A. (2002).

3. T. H. Hsueh, **H. W. Huang**, C. C. Kao, Y. H. Chang, M. C. O-Yang, H. C. Kuo and S. C. Wang, **Solid State Devices and Materials** , Japan (2004).

4. T. H. Hsueh, **H. W. Huang**, C. C. Kao, Y. H. Chang, M. C. Ou-Yang, H. C. Kuo and S. C. Wang, **IUMRS**, Taiwan (2004).

5. T. H. Hsueh, **H. W. Huang**, C. C. Kao, Y. H. Chang, M. C. Ou-Yang, H. C. Kuo and S. C. Wang, **ICON**, Taipei (2004).

6. T. H. Hsueh, Y. S. Chang, F. Lai, **H. W. Huang**, M. C. Ou-yang, C. W. Chang, H. C. Kuo, S. C. Wang, J. K. Sheu, **CLEO** U.S.A. (2004).
7. C. C. Kao, J. T. Chu, **H. W. Huang**, Y. C. Peng, C. C. Yu, Y. L. Hsueh, C. F. Lin, H. C. Kuo, S. C. Wang, **LEOS**, (2004).

8. **H. W. Huang**, T. H. Hsueh, C. C. Kao, Y. H. Chang, M. C. O-Yang, H. C. Kuo and S. C. Wang, **LEOS** (2004).

9. **H. W. Huang**, T. H. Hsueh, J. K. Sheu, H. C. Kuo and S. C. Wang, **APWS**, HsinChu (2005).

10. H. Hsueh, J. K. Sheu, J. Y. Chu, **H. W. Huang**, C. C. Kao, H. C. Kuo and S. C. Wang, **APWS**, HsinChu (2005).

11. C. H. Chiu, **H. W. Huang**, H. C. Kuo, J. T. Chu, C. F. Lai, C. C. Kao, T. C. Lu, S. C. Wang, R. J. Tsai, C. C. Yu and C. F Lin, **Optics and Photonics Taiwan**, HsinChu (2006).

12. **H. W. Huang**, C. F. Lai, C. C. Kao, J. T. Chu, C. H. Chiu, T. C. Lu, H. C. Kuo, S. C. Wang, C. C. Yu, and T. H. Hsueh, **Optics and Photonics Taiwan**, HsinChu (2006).

Curriculum Vita

***Name*:** Mr. Hung-Wen Huang

***Place of Birth*:** Tainan, Taiwan

***Date of Birth*:** June 5, 1977

***Electronic Mail*:** stevinhuang737672@msn.com

Education:

Ph.D. 2003-2007, Electro-Optical Engineering, National Chiao Tung University, Taiwan

M.S. 2000-2002, Electro-Optical Engineering, National Chiao Tung University, Taiwan

B. S. 1997-2000, Physics, Tamkang University, Taiwan

***Areas of Special Interest*:**

Quantum optics, III-Nitride materials and optical devices, and Nanostructures.

Title of M.S. Thesis:

Research & Fabrication of GaN material dry etching
Research of the enhancement of p-type GaN carrier concentration using Be implantation

Title of Ph.D. Thesis:

Study of Nano-Processing Techniques for GaN-based Light Emitting Devices